3D Biomechanical Oropharyngeal Model for Training and Diagnosis of Dysphagia

by

Md Moshiur Rahman Farazi

B.Sc., Islamic University of Technology, 2011
M.Sc., Islamic University of Technology, 2013

A THESIS SUBMITTED IN PARTIAL FULFILLMENT OF
THE REQUIREMENTS FOR THE DEGREE OF

MASTER OF APPLIED SCIENCE

in

The Faculty of Graduate and Postdoctoral Studies

(Biomedical Engineering)

THE UNIVERSITY OF BRITISH COLUMBIA

(Vancouver)

December 2015

Abstract

Swallowing is a complex oropharyngeal process governed by intricate neuromuscular functions. Dysfunction in swallowing, clinically termed as dysphagia, can significantly reduce the quality of life. Modified barium swallow (MBS) studies are performed to produce vidoefluoroscopy (VF) for visualizing swallowing dynamics to diagnose dysphagia. To train the clinicians learning standardized dysphagia diagnosis, 2D animated videos coupled with VF are used. However, it is hypothesised that the physiologic components of the oral domain may benefit from extension of the training materials, such as inclusion of 3D models.

We develop a 3D biomechanical swallowing model of the oropharyngeal complex to extend the clinical dysphagia diagnosis training materials. Our approach incorporates realistic geometries and accurate timing of swallowing events derived from training animations that have been clinically validated. We develop rigid body models for the bony structures and finite element models (FEM) for the deformable soft structures, and drive our coupled biomechanical model kinematically with accurate timing of swallowing events. We implement an airway-skin mesh using a geometric skinning technique that unifies geometric blending for rigid body model with embedded surface for FEMs to incorporate the deformation of upper airway during a swallowing motion. We use smoothed particle hydrodynamics (SPH) technique to simulate a fluid bolus in the airway-skin mesh where the model dynamics drive the bolus to emulate bolus transport during a swallowing motion.

We validate this model in two phases. Firstly, we compare the simulated bolus movement with input data and match the swallowing kinematics identified in the standardized animations. Secondly, we extend existing training material for standardized dysphagia diagnosis with our 3D model. To test the usefulness of the extended training set using 3D visualizations, we conduct a pilot user study involving Speech Language Pathologists. The pilot data indicate that clinicians believe the additional 3D views are useful for identifying the salient features for differentiating between different swallowing

impairments, such as direction, strength and timing of the tongue motion, and could be a useful addition to the current standardized MBSImP™© training system.

Preface

Parts of this dissertation have been published elsewhere.

Full Length Paper

Versions of Chapter 3 and 4 have been published in

- **Farazi, M.R.**, Martin-Harris, B., Harandi, N., Fels, S. and Abugharbieh, R. "A 3D Dynamic Biomechanical Swallowing Model for Training and Diagnosis of Dysphagia", *International Symposium on Biomedical Imaging (ISBI)*, Brooklyn-USA, April Pages: 1385–1388, 2015.

MR Farazi was the main contributor of this paper under the supervision of Dr. Rafeef Abugharbieh and Dr. Sidney Fels. MR Farazi developed the 3D oropharyngeal model, performed simulations and analysis, generated figures and results, and prepared the manuscript for publication. Dr. Martin-Harris provided the VF and animation data, and helped to formulate the research question with clinical significance. N Harandi helped prepare the manuscript. Dr. Sidney Fels and Dr. Rafeef Abugharbieh carefully edited the manuscript and provided additional feedback.

Extended Abstracts

Some parts of Chapter 3 have been published as extended abstracts which are listed below:

- **Farazi, M.R.**, Martin-Harris, B., Abugharbieh, R. and Fels, S. "Development of a 3D Biomechanical Swallowing Model for Dysphagia Training", *International Symposium on Computer Methods in Biomechanics and Biomedical Engineering (CMBBE)*, Montreal-Canada, September 2015

- **Farazi, M.R.**, Martin-Harris, B., Abugharbieh, R. and Fels, S. "Swallowing Simulation Using an MBSImP-Based 3D Biomechanical Model", *International Symposium on Computer Methods in Biomechanics and Biomedical Engineering (CMBBE)*, Amsterdam-Netherlands, October 2014.

For both publications, MR Farazi was the primary author and main contributor to the design, implementation, and testing of the methods developed, under the supervision of Dr. Rafeef Abugharbieh and Dr. Sidney Fels. Dr. Martin-Harris provided the VF and animation data and helped with the analysis. M Farazi prepared the manuscript for the publication which was carefully reviewed and edited by Dr. Rafeef Abugharbieh and Dr. Sidney Fels.

Finally, a combination of Chapters 3, 4 and 5 will be submitted as a full journal article which is now under preparation.

Ethics Applications

This research met the minimal risk human ethics application criteria and thus an expedited review was conducted for both of the Behavioural Research Ethics Board (BREB) and Clinical Research Ethics Board (CREB) applications, required to conduct this research.

- The videofluoroscopic data used in this Thesis was provided by Dr. Bonnie Martin-Harris of Medical University of South Carolina (MUSC). This data sharing was approved by UBC Clinical Research Ethics Board (CREB) application number H15-02749.

- The user study conducted in this Thesis was approved by UBC Behavioural Research Ethics Board (BREB) application number H15-02665.

Conflict of Interest

The researchers and members of the thesis committee report no conflict of interest.

Table of Contents

Appendices

List of Tables

List of Figures

List of Abbreviations

DOF	Degree of Freedom
FDM	Finite-Difference Method
FEES	Fiberoptic Endoscopic Evaluation of Swallowing
FEM	Finite Element Method
SLP	Speech-Language Pathologist
SPH	Smoothed Particle Hydrodynamics
VF	Videofluoroscopy
VFSS	Videofluoroscopic Swallowing Study

Acknowledgements

I am thankful to Almighty Allah, most Gracious, who in His infinite mercy has guided me to complete this dissertation. Foremost, I would like to express my sincere gratitude to my supervisor Prof. Rafeef Abugharbieh, whose expertise, understanding and patience added considerably to my graduate experience. I would like to express my sincere gratitude to my co-supervisor Prof. Sidney Fels for his continuous support throughout my graduate study. His guidance, mentorship, patience and motivation helped me significantly duting this research and preparing this manuscript.

Beside my supervisors, I would like to thank our clinical collaborator Dr. Bonnie Martin-Harris of Medical University of South Carolina (MUSC), SC, USA for the productive collaboration over the past years. Her patience, enthusiasm, appreciation and immense knowledge motivated me to work harder. Without her support it would not have been possible to conduct this research.

I thank my fellow researchers at Biomedical Signal and Image Computing Laboratory (BiSICL) and Human Communication Technologies (HCT) Lab at UBC for all the stimulating discussions and for all the fun we have had in the last couple of years.

Finally, a heart felt thank-you to my parents and family members for providing me with a loving environment that let me learn and grow. I am grateful for their sacrifices, encouragement and support throughout my life.

Dedication

Dedicated to my parents and my family

Chapter 1

Introduction

1.1 Motivation

Swallowing is a physiologic process by which food travels from the mouth, through the pharynx and into the esophagus. Swallowing has two crucial biological features: food passage from the oral cavity to stomach and airway protection. Although it seems quite simple, swallowing is a very complex neuromuscular function involving voluntary and reflexive activities of more than 30 nerves and muscles[1]. Difficulty or inability to swallow is clinically termed as *dysphagia* which is derived from the Greek words *dys* meaning bad, disordered, impaired and the root *phag* meaning "eat". So dysphagia means difficulty or discomfort in swallowing.

Dysphagia can occur in any age but is most prevalent in the elderly population. Epidemiological data estimates that prevalence of dysphagia among people over 50 years can be as high as 22% [2; 3]. Dysphagia can lead to dehydration, malnutrition as it impedes the normal nutrition required in the body. As a result, patients suffering from dysphagia are at high risk of developing other medical conditions. In more severe cases of dysphagia, the airway protection mechanism fails and food enter the lungs through trachea rather than going to stomach through esophagus, which is called aspiration pneumonia. Aspiration pneumonia is a major cause leading to hospitalization for elderly people which causes costly care, and overall mortality rate ranges form 20% to 50% [4; 5; 6; 7], if not treated. Furthermore, dysphagia adds to the patients suffering as it has significant social and physiological impact [8]. For example, eating and drinking are most common social activity in almost every society. Often meals are the main activity of celebrations and gatherings. So dysphagia can sometimes cause social isolation, jeopardize ones social experience and degrade quality of life significantly.

Dysphagia can be a result of abnormalities related to neural control, muscle contraction, inflammation and commonly associated symptom of stroke, multiple sclerosis (MS), cancer and many other diseases that impede normal

Dentistry	Gastroenterology
General Surgery	Head and Neck surgery
Neurology	Neurosurgery
Nursing	Nutrition
Occupational Therapy	Oncology
Oral Surgery	Otolaryngology
Pediatrics	Physical Therapy
Pulmonary Medicine	Radiology
Rehabilitation	Rheumatology
Speech-Language Pathology	Thoracic Surgery

Table 1.1: Clinical specialties involved in the evaluation and management of swallowing disorders

functionalities of oropharyngeal nerves and muscles. Patients with dysphagia require a multidisciplinary approach to swallowing management. This may include swallow therapy, dietary modification and oral care. A large and diverse number of clinical specialties (see Table 1.1) are concerned with the evaluation and managements of dysphagia. Management and treatment of dysphagia can improve the patients nutrition. Improving patients care and offering them appropriate treatment could prevent the physiological damage and social isolation that could otherwise happen to the patient.

Simulating a swallowing motion itself is of interest of many disciplines (see Table 1.1) and the research is motivated by the application areas of the models. Some application that require simulation of swallowing motion are listed below:

Food texture modification

Patient suffering from dysphagia are in danger of aspiration pneumonia and the chances of death due to this is high for elderly patients [2; 3]. To improve the quality of life for dysphagiac patients, there is a need for development of oropharyngeal swallowing model for developing "safety food" by modifying the food texture [9]. Without a swallowing model, the determination of the safety food for dysphagic patients involved the testing of different food consistencies by trail and error. This method involves the risk of chocking or aspiration which is not desirable. As a result, research is going on for developing a swallowing model for understanding the action of food bolus

and corresponding oropharyngeal structures during the swallowing process. There are also some parallel research going on aiming to solve the same problem by developing robotic swallowing simulators using motors, actuators and muscular tube[10].

Surgical planning

Computer modeling of anatomical structures has proven to be useful in head and neck cancer management and otolaryngology. A significant number of patients undergoing head and neck surgery develop swallowing and speech related problems. Such computer models are built to predict anatomical and functional outcome during surgical planning and demonstrating the prognosis to a patient before the surgery. These models help reduce the treatment time significantly and help evaluate the risk of aspiration and other swallow related complexities. For addressing these issues, research is going on for developing patient specific computer models of oropharyngeal complex for predicting functional mastication and swallowing outcome.

Obstructive sleep apnea (OSA)

Obstructive sleep apnea (OSA) is a symptom characterized by partial or completed obstruction of the airway during sleep. Such obstruction causes narrowing of the pharynx, which decrease the tone of the pharyngeal dilator muscle [11] and cause snoring. Some studies [12; 13; 14] suggest that the neurogenic lesions in the pharynx and soft palate are triggered by vibrations produced by snoring. The pharynx and soft palate are two major oropharyngeal structures that contribute to the propagation of food bolus and such lesions impair their sensitivity and functionality. It is hypothesized that patients with OSA may have subclinical swallowing abnormalities due to low frequency vibrations, and negative intrathoracic pressure during apnoea [14]. To explore this cause and effect relationship between OSA and dysphagia, computer models of the oropharangeal complex are developed to simulate OSA. The application of such model include condition by developing oral appliance for OSA patients and so on.

Therefore, there exists a need for a biomechanical oropharyngeal swallowing model in dysphagia research. The application of such biomechanical model include but are not limited to, standardized dysphagia training, post–operative rehabilitation, treatment planning. A survey conducted by

American Speech-language Hearing Association (ASHA) reported that 92% and 100% speech-language pathologists (SLPs) working respectively in hospital settings and residential health-care setting such as nursing home or care facilities, regularly serve individuals with swallowing disorders [15]. The degree and type of training in diagnosis and evaluation of dysphagia are highly varied and sparse [16]. Contribution towards the clinician training to evaluate and diagnose dysphagia would have tremendous impact on dysphagia research. So in this Thesis, we developed a biomechanical swallowing model to help clinician training for dysphagia diagnosis.

1.2 Problem Statement and Scope

Clinician training is instrumental to establish a standardized diagnostic protocol. Such training ensures that clinicians across institutions can score reliably and communicate the test results across the continuum of care. In this Thesis, a biomechanical modeling approach is investigated in order to assist clinicians in standardized training of dysphagia using a 3D biomechanical swallowing model. The model geometries are built from geometries and clinically validates timings of swallowing event. The model is built using realistic geometries and kinematic information derived from clinical training data used in MBSImP™© [17]. With such physics driven models, the clinicians would be able to alter the timing of swallowing movements and visualize the effect of these simulated interventions on bolus clearance and airway protection. By interactively changing views and altering timing of swallowing movements, we anticipate that clinicians will gain deeper understanding of the complex dynamics involved in swallowing, especially as it relates to different patients, to facilitate diagnosis and treatment planning.

1.3 Physiology of a Normal Swallowing

As stated earlier, swallowing is a very complex synchronized action undertaken by oral, pharyngeal and laryngeal muscles and structures (see Figure 1.1). During a normal swallow, the bolus is propelled from the mouth through the oral cavity, pharynx and esophagus by the positive pressure applied to the bolus tail. At the beginning of swallowing, the tongue holds the bolus at the oral cavity by having the tongue tip and base elevated against the front

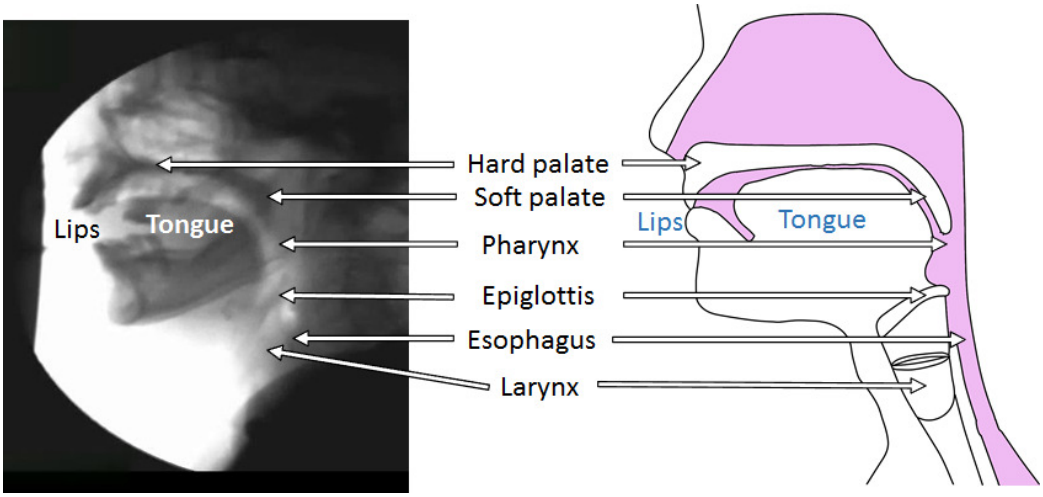

Figure 1.1: Mid-sagittal VF and illustration of oropharyngeal complex. VF image reproduced from MBSImP™© training module, with permission.

teeth and soft palate respectively. Following the holding motion, the tongue tip moves along the roof of the mouth and the base separates from the soft plate allowing the bolus to flow from the oral cavity into the pharynx. Afterwords the bolus passes the upper esophageal sphincter (UES) and through the esophagus to the stomach for digestion.

Swallowing is historically divided in to four phases [18] namely (see Figure 1.2):

1. Oral preparatory phase,
2. Oral phase,
3. Pharyngeal phase and
4. Esophageal phase.

The first two phases are modulated primarily by voluntary control however last two are governed by involuntary control. Martin-Harris et al. [19] reported that oropharyngeal swallow events do not segment into discrete oral and pharyngeal phases and there is a overlap between the initiation of oral and pharyngeal phase of swallow. Some studies [20; 21; 22] investigated the swallowing physiology with manometric and videofluoroscopic analysis and demonstrated that physiologic events during swallowing are inter-dependent,

which means, one event impacts another. These findings contradict the traditional description of swallowing mechanism which is based on visual observations and temporal measurement of structural movements and bolus flow throughout the upper aerodigestive tract from lateral videofluoroscopic recordings. However, having the complex swallowing mechanism divided into discrete phases and discussing about physiological characteristics individual to that particular phase, makes it easier to differentiate between normal and impaired swallow. For this reason following subsections discuss about different phase of swallowion mottion even if these phase are not independent and may be overlapping.

1.3.1 Oral preparatory phase

During the oral preparatory phase the food is tasted, broken down by mastication and prepared for swallowing. At first the lips are closed off and muscles are activated to contain the liquid and/or the food inside the oral cavity. The lip closure ensures the seal at the anterior part. On the other hand, the soft palate touches the tongue base to seal off the oral cavity posteriorly . The posterior seal is an important airway protection mechanism as it prevents premature slippage of food or liquid into the oropharynx [23]. Mastication takes place once the bolus containment is achieved and the jaw performs a lateral circular or rotary motion to crush the food into small pieces. During mastication of a solid bolus, tongue is moved laterally and vertically to position the food between the teeth and the bolus is mixed with saliva. Without normal range of tongue movement and muscle control, tongue mobility cannot be achieved which is the most important activity during oral preparatory phase.

1.3.2 Oral phase

After the bolus is prepared at the oral preparatory stage, the oral phase (sometimes in literature referred as oral transport stage) begins. The newly formed cohesive bolus is propelled through the oral cavity to be transported into the oropharynx. The tongue propels the bolus posteriorly with a upward and backward rolling motion while the soft palate is elevated to seal off the nasopharynx. The oral- and nasopharangeal seal is important as they create closed pressure system within the oral cavity to facilitate the bolus transport. This wavelike motion is both centripetal and centrifugal in nature. It

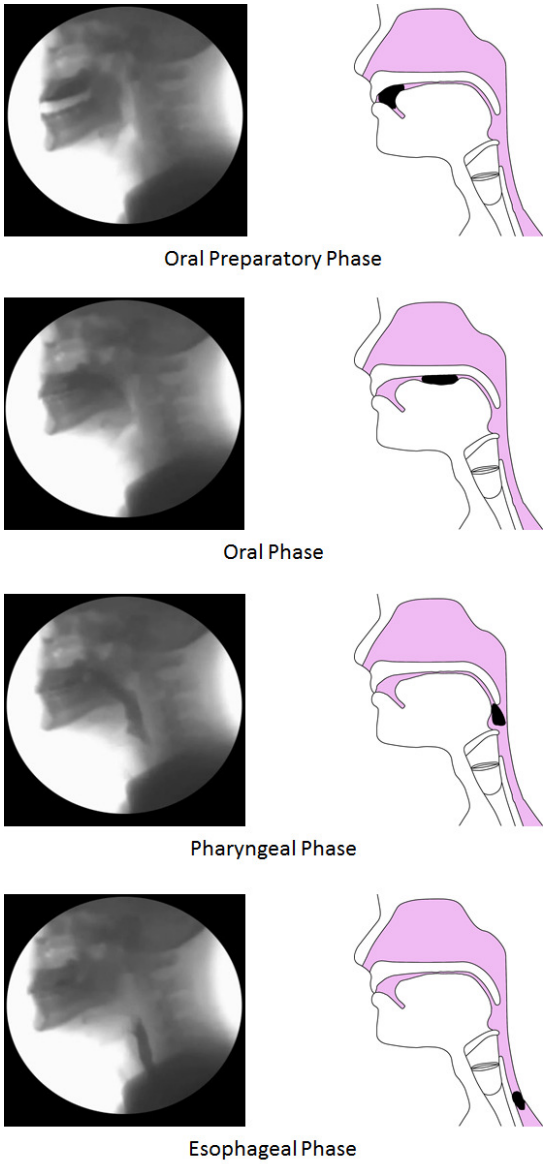

Figure 1.2: Lateral view of a healthy swallow during an modified barium swallow (MBS) exam showing different phases of swallowing motion. VF image reproduced from MBS video used in MBSImP™© training, with permission.

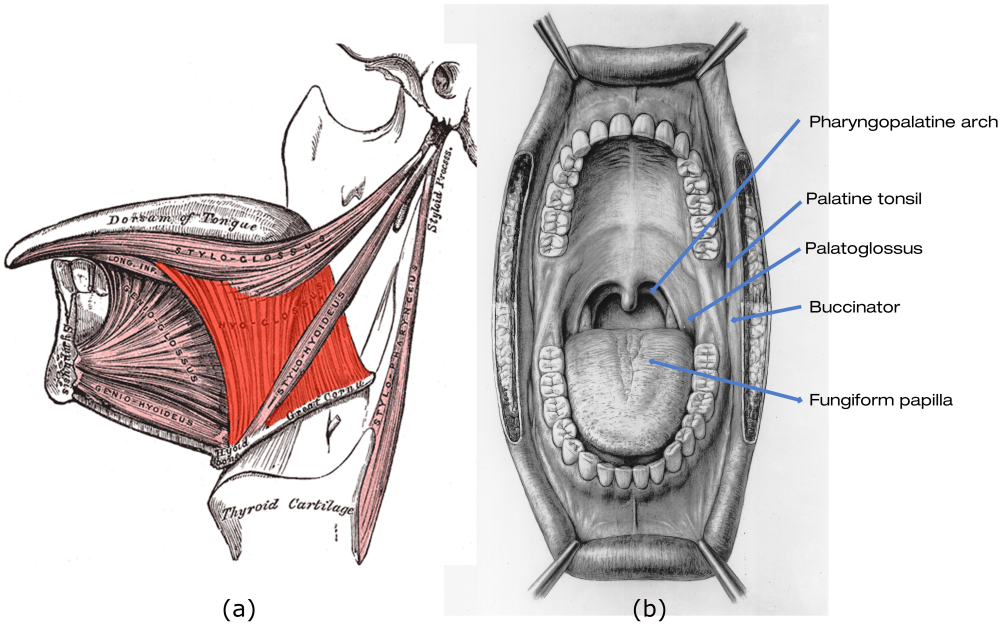

Figure 1.3: (a) Lateral and (b) anterior view of the extrinsic tongue muscles that insert into the tongue from outside origins and allow the tongue to move in different directions. Images (a) and (b) are adapted respectively from [26] and [27] licence via Wikimedia Commons.

occurs as a result of activity within the intrinsic and extrinsic tongue muscles (see Figure 1.3) of the tongue i.e. genioglossus, hyoglossus, styloglossus, palatoglossus, superior longitudinal [24]. The extrinsic tongue muscle names have the root word "glossus" = tongue at the end and at the beginning has the name of the origin. For example, genioglossus from "genio" = chin, styloglossus from styloaid bone, palatoglossus from soft palate, hyoglossus from hyoid bone. The intrinsic muscles originates within the tongue and allow the tongue to change its shape. The bolus enters into the oropharynx by depression of the posterior tongue while the soft palate is elevated. This oral phase of swallow in terminated when the swallowing reflex is triggered. The normal duration of this phase is around 1s and it is not varied significantly with bolus consistency, age, sex of people [25].

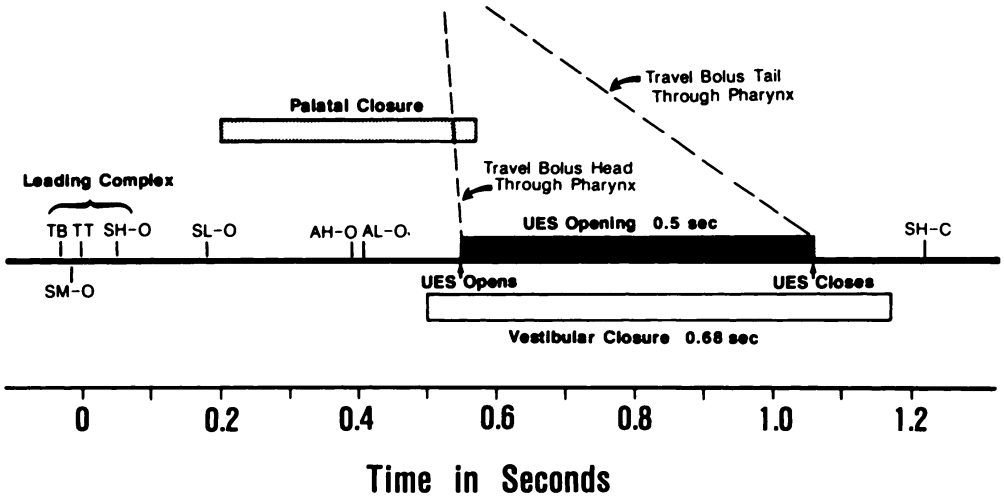

Figure 1.4: Time line showing timing of events for the oral and pharyngeal phase of swallow for 5mL barium bolus swallow in normal subject. TB, tongue base movement; SM-O, onset of submental electric activity; TT, onset of propulsive tongue tip; SH-O, onset of superior hyoid movement; SL-O, onset of superior laryngeal movement; AH-O, onset of anterior hyoid movement; AL-O, onset of anterior laryngeal movement; SH-C, completion of superior hyoid movement. Image adapted from [32].

1.3.3 Pharyngeal phase

During the pharyngeal phase the bolus passes through the pharynx. This stage also lasts about 1s and despite its short duration it is the most complex of all swallowing phases. It requires quick and precise coordination of almost all swallowing musculature. The swallowing reflex is triggered by the glossopharyngeal nerve and it marks the beginning of the pharyngeal phase [28]. Bolus properties e.g. texture, taste, and volume can alter the timing of the involuntary "trigger" for the pharyngeal phase. For example, more viscous liquids may delay the pharyngeal trigger [29], on the other hand, sour foods might initiate an earlier trigger [30]. In addition, bolus size can also influence the timing of the trigger. For example, while drinking large amount of water in a continuous sequence, boluses may pass the faucial pillars and reach the valleculae before the trigger is initiated [31].

When the swallowing reflex is triggered some sequential neuromotor ac-

tivities occur. In literature, sometimes swallowing is quantified in a time–line (see Figure 1.4) to map the sequential and overlapping swallow related events with respect to time [32]. Firstly, when the bolus passes the opening onto the nasal cavity, velopharyngeal closure is achieved to ensure that the nasal cavity is closed and no bolus is entering the nose. This happens in a fraction of a second and respiration ceases during this period to ensure airway protection. Next, the pharyngeal muscles contract and the pharynx is elevated superiorly. The tongue base is retracted towards the posterior pharyngeal wall simultaneously and the pharyngeal constrictors are activated in a rostral-caudal direction [25]. As a result, pharyngeal constrictor contracts in a wavelike motion called pharyngeal peristalsis or the pharyngeal stripping wave because it strips along the tail of bolus and squeezing it through the pharynx and into the upper esophagus. The pharyngeal stripping wave generates an average pressure of 22 mmHg and an average force of 1.2 mmHg*s [33]. This wave descends inferiorly from the level of the nasopharynx to the level of the upper esophageal sphincter (UES) at a rate of between 9 and 25 cm/s [33].

Due to the elevation of the pharynx, the suprahyoid muscles contract to direct the hyoid bone superiorly and anteriorly [34]. Consequently, the thyrohyoid muscle contracts to move the larynx superiorly towards the hyoid bone. Anterior and superior movement of the larynx is important for a number of reasons. Firstly, these movements direct the larynx under the tongue base and inverting the epiglottis. It pushes the bolus away from the laryngeal inlet which is an important part of airway protection mechanism. Secondly, simultaneous elevation of larynx and hypopharynx creates a negative pressure below the level of the bolus. This pressure helps to guide the bolus inferiorly towards the esophagus. Finally, the elevation of larynx and pharynx creates a biomechanical force that helps to pull the cricoid cartilage up and away from the posterior pharyngeal wall. As a result, this force pulls open the cricopharyngeal muscle and the UES. The opening of the UES creates an additional suction force at the bolus for guiding it towards the esophagus. The combined effect and synergy of the suction force, tongue movement and pharyngeal stripping wave determines the efficiency of pharyngeal bolus transit.

1.3.4 Esophageal phase

The esophageal phase of swallowing begins when the bolus is passed through the UES. The biomechanical forces contributing to the opening of the UES

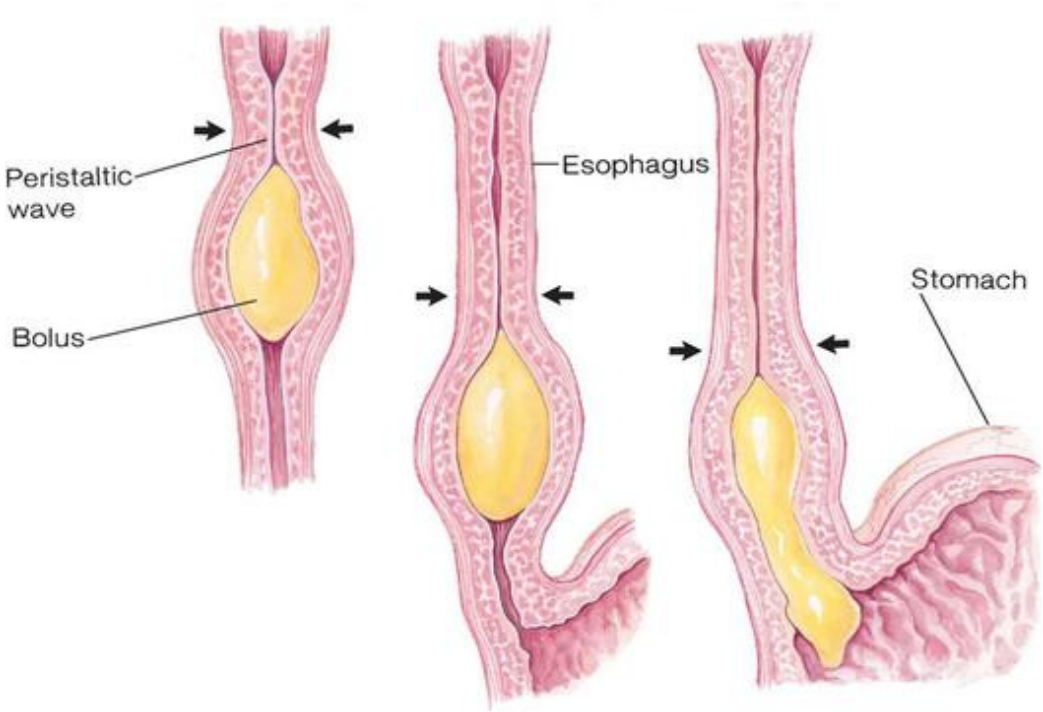

Figure 1.5: Esophagus contracts in an orderly sequence from top to bottom (peristalsis) in order to transport the swallowed bolus into the stomach. Adapted from [35] with ⓒ licence via Wikimedia Commons.

and relaxation of the cricopharyngeal muscle facilitates the UES opening. The relaxation lasts for about 0.5 to 1.2 seconds which is just enough time for the bolus to pass through the UES and into the esophagus. The cricopharyngeal muscle returns to its contracted state sealing off the esophagus once the bolus has successfully entered into the esophagus. This seal prevents any bolus that is directed backwards form entering the hypopharynx. Esophageal peristalsis (see Figure 1.5) is activated at this point and the bolus is pushed towards the lower esophageal sphincter (LES) and stomach. This esophageal peristaltic wave squeeze the bolus through the esophagus and travels at a rate approximately 3 to 4 cm/s [36]. Once the LES is triggered to relax, the peristaltic waves push and squeeze the bolus into the stomach which is followed by several secondary waves that can last up to an hour after the swallow. These secondary waves help to clear any remaining bolus residues in the esophagus [37]. Transit time during this phase is usually 8 to 13s,

however, this time can vary with age, bolus size and texture [38].

1.3.5 Airway protection mechanism

Airway protection is an important characteristic of a healthy and normal swallowing motion. People aspirate when airway protection mechanism fails and bolus enters the airway rather than going into the esophagus. Such aspiration, if untreated, can result in life threatening aspiration pneumonia. Proper coordination and timing of swallow events is crucial for ensuring airway protection as respiration and swallowing share similar anatomical pathways. Usually, when a person is starting to exhale, pharyngeal phase of swallow takes place [39; 40]. During swallowing, respiration ceases till the bolus has cleared the hypopharynx and entered the esophagus [39; 40].

Vocal folds and epiglottic deflection are important physiological activity that contributes to airway protection. Closure of the vocal fold is achieved just before the initiation of pharyngeal phase and it halts the respiration by closing off the airway. This seal prevents any misdirected foods bolus residue from entering the esophagus [41]. Further, during epiglottic deflection, the inferior surface of the epiglottic makes contact with the arytenoid cartilages which then directs the bolus past the airway and into the esophagus. As a result, vocal folds and epiglottic deflection acts as shields for the airway, preventing it against penetration and aspiration of liquid. Gag reflex has been historically regarded as a airway protection mechanism. However, absence of a gag reflex does not necessarily indicate that a patient is unable to swallow safely. Indeed, many individual with an absent gag reflex have normal swallowing, and some patients with dysphagia have a normal gag reflex. Some studies have also proven that reduced or absent gag reflex is not correlated with an increased risk for aspiration [42].

1.4 Diagnostic Evaluation of Dysphagia

Different swallowing assessment tools have been developed to diagnose and treat dysphagia. A swallowing assessment is a diagnostic procedure aimed to identify anatomy and physiology of all stages of the patients swallow accurately and detect any swallow related impairments. To identify swallowing abnormalities, it is important to perform a swallowing assessment, and to initiate early referral for diagnosis and treatment to minimize health risks. The

clinical tools to diagnose dysphagia can be broadly divided into 2 categories: (1) bedside and (2) instrumental assessment. If any sign of dysphagia is found during the bedside tests, which is a physiological assessment, the clinicians do a comprehensive instrumental assessment to observe the exact appearance and coordination of movement of the oropharyngeal structures and to evaluate aspiration. Instrumental evaluation include imaging techniques like videofluroscopy, fiberoptic endoscopy, ultrasound and nonimaging techniques like manometry to evaluate a swallowing motion. These tests provide additional information about the patients' swallowing mechanism to help the clinician diagnose the abnormality and devise treatment plan. Some widely used swallowing assessment techniques are listed in the following sections.

1.4.1 Clinical bedside swallow assessment

Bedside or initial swallowing assessment is usually the first swallowing assessment done when an individual is presented with swallowing discomfort. One study show that, 42% – 60% of acute stroke patients have been reported to have dysphagia on the basis of standardized clinical bedside within a median of 3 days from stroke [43]. This bedside test refers to a minimally invasive evaluation procedure of swallow motion that provides quick determination of the likelihood that dysphagia exists. Such screening is often performed to know if someones' swallowing ability has been compromised after a stroke or some other neurological diseases.

The first step of this bedside swallow assessment (often called a swallow screen) is to make sure that the patient can follow simple one step commands to be able to participate in the assessment. The patient is asked to open the mouth and the clinician, most often a Speech-Language Pathologist (SLP) with training in the area of evaluation and treatment of dysphagia, looks into the oral cavity for inspection. The patient is then asked to move the tongue sideways and up-and-down. The SLP looks for any sign of numbness or tingling in the face, cheeks or lips when the patient is following instructions. After that the SLP does a oral motor exam to test the strength of the muscles of the mouth. The SLPs hold a tongue depressor against the patients' tongue and the patient is asked to push the tongue depressor outward, lift it up and push it down. After the oral-motor exam the patient is asked to swallow water sequentially until the glass is empty. The SLP places his/her hand of the patients throat to feel the swallow. After the swallow is done, the SLP initiates a conversation with the patient to see if the voice is wet or gurgely.

Figure 1.6: A modern videofluoroscopy machine used to perform swallowing assessment. Adapted from [46] with licence via Wikimedia Commons.

If there were any water was stuck at the throat, the patient would have had a wet gurgely a voice. The clinician waits about a minute after the swallow to observe if there is any cough or chocking that might be caused by potential aspiration [44].

The bedside assessment is effective in identifying disorders in the oral preparatory and oral phase of swallowing. However, for evaluating pharyngeal aspects of swallowing, bedside assessment is not very useful because it is difficult to access if any bolus has entered the airway with a physical exam. Some patients suffering from neurological impairments may not cough or produce gargley voice even if bolus has entered the airway during a bedside exam[45]. Patients who show signs of dysphagia upon a bedside swallowing assessment are referred for comprehensive instrumental swallowing assessment.

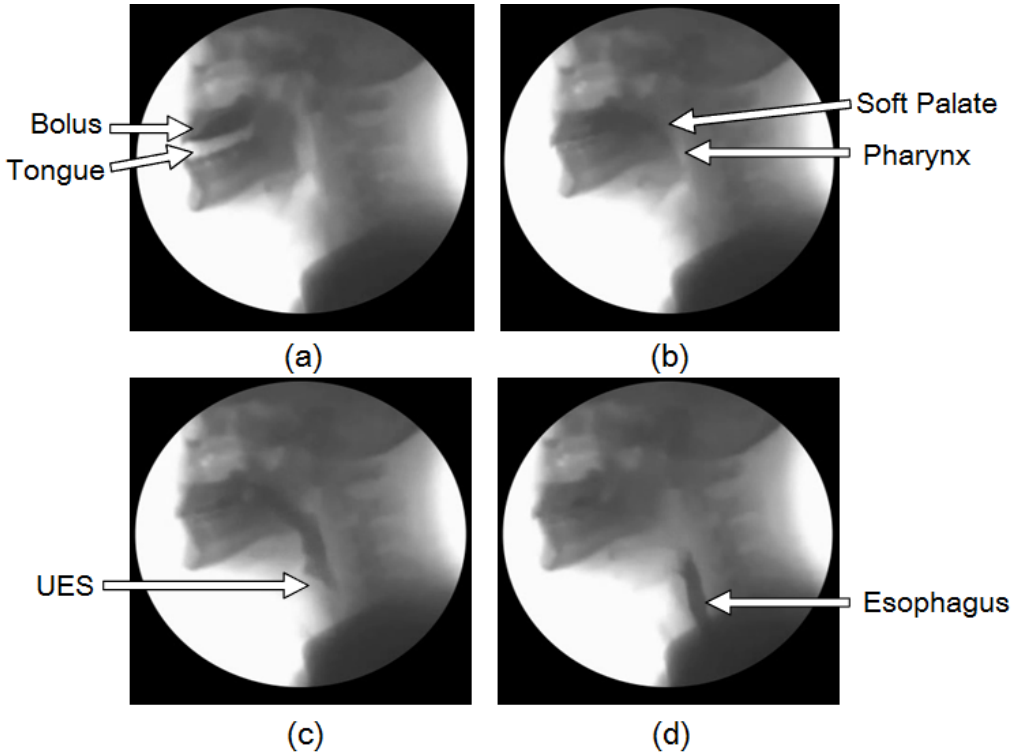

Figure 1.7: Lateral view of a health individual swallowing during an modified barium swallow (MBS) exam. (a) Oral preparatory phase, (b) oral phase, (c) pharyngeal phase and (d) esophageal phase. Created from normal swallow MBS video used in MBSImP™© training, with permission [17].

1.4.2 Modified Barium Swallow Study (MBSS)

The Modified Barium Swallow Study (MBSS), also known as video-fluoroscopic (VF) swallow study, is a common, standard procedure and has been historically reagarded as the gold standard for evaluating the swallowing mechanism [47; 48]. This test is often considered instrument of choice because it provides visualization of the bolus flow in relation to structural movement throughout upper aerodigestive tract. Such visualizations allow clinicians to robustly and consistently identify the nature and severity of swallowing impairment, and the presence and timing of aspiration.

The MBSS is usually conducted by a radiologist and a speech language pathologist (SLP). During a MBSS, the patient is seated inside a VF ma-

chine and presented with a bolus enhanced with barium to make the bolus visible in the fluoroscope (Figure 1.6). This swallowing assessment captures a sequences of videofluoroscopic images of bolus travelling through the oral cavity, pharynx and esophagus in real time. The patient swallow is initially viewed from lateral plane to evaluate the bolus transport during the oral and pharyngeal phase (Figure 1.7). This lateral view allows the clinician to measure the oral and pharyngeal transit times and presence of aspiration. The swallow can also be viewed from anterior-posterior plane to evaluate esophageal clearance. Boluses with different volume and consistencies are presented and clinical impressions of the presence and degree of swallowing impairment are obtained from the VF images [49; 50]. The clinicians also make judgment regarding the coordination and timing of the swallowing events based on the qualitative observation from the VF [51]. Furthermore, longitudinal MBSS is conducted to monitor any changes in swallowing function over time to track the progression of a disease or condition.

The disadvantage of MBSS is that it exposes the patient to a small amount of radiation. Although the dose of radiation is standard and may not pose any immediate threat, the clinician are cautious not to prolong the patients exposure to radiation. Moreover, VF is not readily available everywhere and may not be suitable for all patients e.g. patients with poor sitting posture, pregnant women, infants. Nevertheless, VF remains the standard swallowing assessment procedure and effective technique to evaluate level of aspiration.

1.4.3 Endoscopic Evaluation of Swallowing

The use of flexible laryngoscopy to evaluate oropharyngeal dysphagia was first published in 1988 [53]. This procedure, commonly known as Fiberoptic Endoscopic Evaluation of Swallowing (FEES), was developed as alternative procedure where it was not feasible for the patient to undergo a MBSS i.e. patients in ICU, care facility. FEES is one reliable method to assess the structural and functional status of the oropharynx and larynx, during the swallowing process. A thin, flexible tube, called a laryngoscope, is used that has a small camera on the end and is placed transnasally along the floor of the nose and advanced until end of the scope reaches the base of uvula. The scope is sometimes advanced to the tip of the epiglottis to get a better view of the pyriform sinuses and endolarynx, which is sometimes called protective"cup" that guides material around the airway until the swallow occurs. A FEES assessment provides a good view of the larynx and partial view

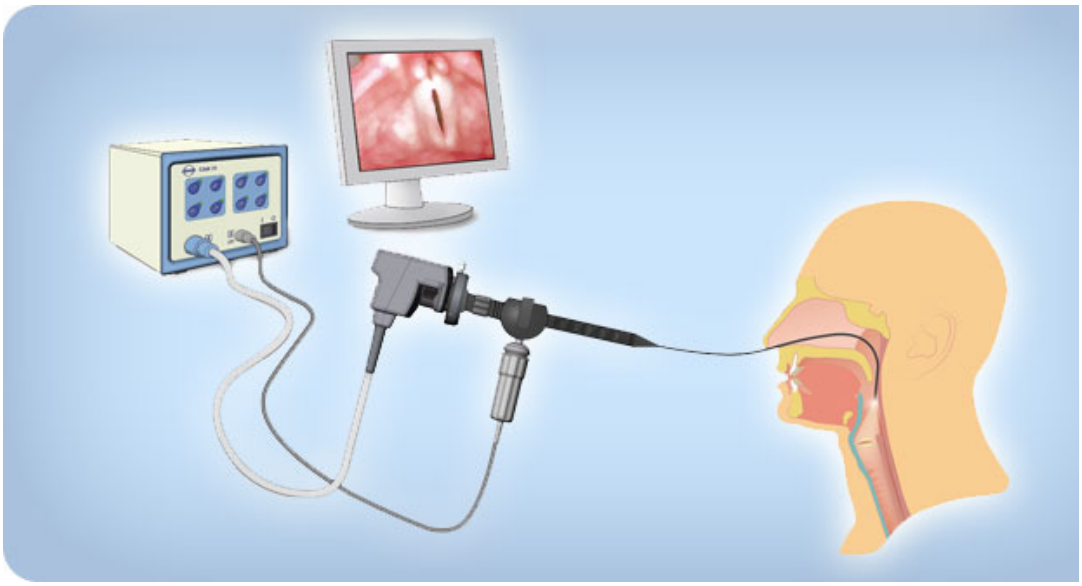

Figure 1.8: An illustration showing the flexible endoscopic tube placement behind the soft palate to view the pharyngeal movement during a swallowing motion. Adapted from [52] with ⓒ licence via Wikimedia Commons.

of nasopharynx, oropharynx and hypopharynx (see Figure 1.9). Hence, the oral phase of swallow can be partially evaluated by FEES. The laryngoscope cannot go beyond the UES opening into the esophagus, the esophageal phase of swallow cannot be accessed by the FEES examination.

An endoscopic evaluation can be divided into two major parts: observation and presentation of bolus. Once the scope is placed inside the nasal cavity the test begins. In the first phase the SLP assesses the anatomy of the patient to determine the potential of the patient to execute a normal swallow without presenting any bolus. The clinician take notes regarding the surface anatomy of nasopharynx, oropharynx, and hypopharynx. Any alteration in the anatomy from surgery, trauma can impair the normal swallowing physiology. The patient is referred to a otolaryngologist if there is a presence of any foreign bodies and masses. The SLP also assesses sensory physiology and may lightly touch the aryepiglottic fold or the tip of the epiglottis to induce a cough. These observation and tests help the clinician to focus the search to look for any particular dysphagic patterns that may present.

In the next part of the test, the patient is presented with a bolus to test

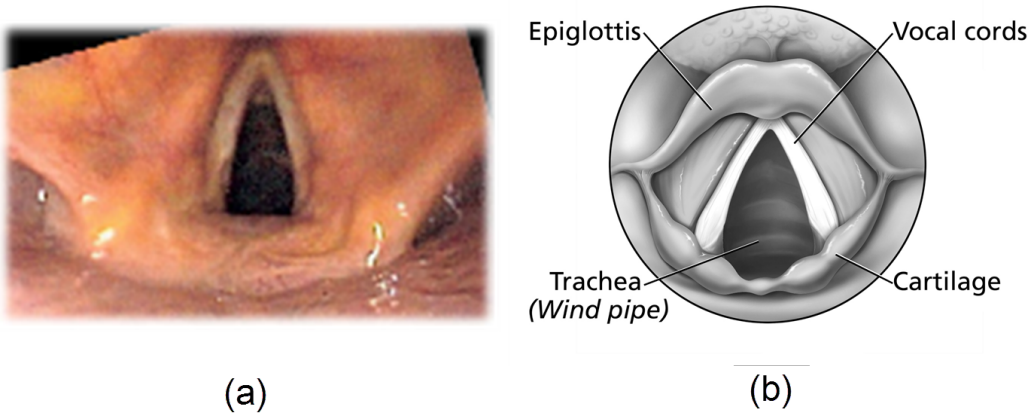

Figure 1.9: The view of larynx captured during a FEES assessment. (a) View of the glottis and vocal cords as seen during an endoscopic procedure. Adapted from [54] with licence via Wikimedia Commons. (b) A top view of the larynx: epiglottis, vocal cords, trachea, and cartilage are labeled. Adapted from [55] with licence via Wikimedia Commons.

the ability do a normal swallow. This is the major part of the test where the examiner directly assesses the patient swallowing of food or liquid with the endoscope placed inside the nasal cavity. It is recommended to use a small amount i.e. 5cc of a thin and/or thick liquid bolus and/or a bite of cracker [56]. With this test the SLP can evaluate and quantify bolus clearance, amount of aspiration and extent of airway closure. As an outcome of a endoscopic assessment of swallowing, the SLP formulates an accurate impression about the nature of the problem and makes realistic recommendations.

1.4.4 Manometry

Manometry is a test used to detect swallowing abnormalities after the bolus has entered into the pharynx and traveling towards stomach via esophagus. This test is used to measure pressures in the pharynx and/or esophagus during a swallowing motion. The measured pressure quantifies strength and muscle coordination of the pharynx and esophagus. MBS study can also be used simultaneously to observe indirect effects of pressure adequacy during swallowing.

During the manometry test, a small flexible tube is placed through the nose and into the pharynx and esophagus. Pressure sensors on the tube

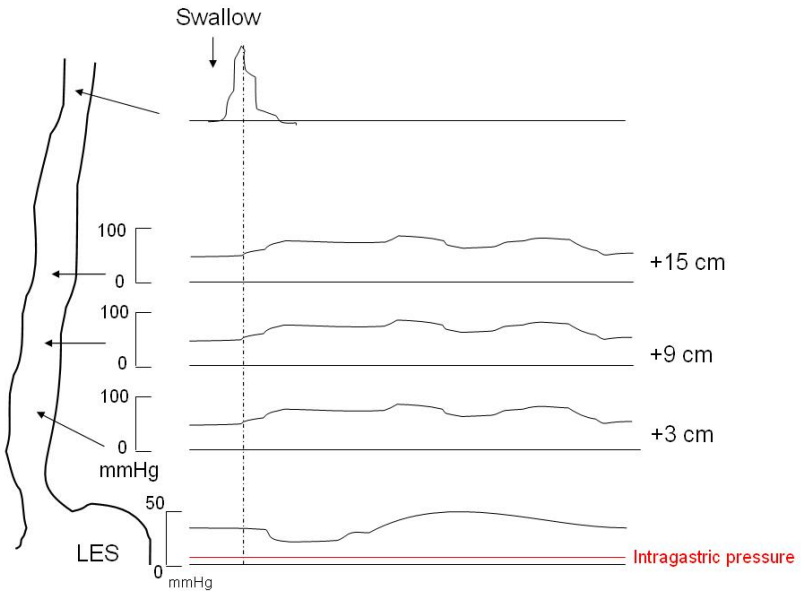

Figure 1.10: During manometry, a manometry catheter is passed through the nose, along the back of the throat, down the esophagus and into the stomach through the esophageal sphincter valves. This catheter records pressure for subsequent anatomical regions (shown in right). Adapted from [57] with licence via Wikimedia Commons.

records pressure throughout the swallow. If pressure is not adequate at any level of the pharynx, food will remain at that level, rather than being pushed along to the next level of the digestive tract. This test indicates how well the esophagus can perform peristalsis and allow the clinician to examine the muscular valve connecting the esophagus with the stomach called Lower Esophageal Sphincter (LES). LES relaxes to allow food and liquid to enter the stomach, and closes to prevent reverse flow of bolus moving out of the stomach and back up into the esophagus. Abnormalities with peristalsis and LES function may cause symptoms such as swallowing difficulty, heartburn, or chest pain [58]. Patients usually perceive this as food or fluid left over after their swallow. Figure 1.10 shows a schematic of manometry done for a patient diagnosed with achalasia. Achalasia is a condition in which the muscles of the lower part of the esophagus fail to relax, preventing food from passing into the stomach causing esophageal dysphagia. Figure 1.10 also shows that aperistaltic contractions, increased intra-esophageal pressure, and failure of

relaxation of the LES.

1.4.5 Ultrasound

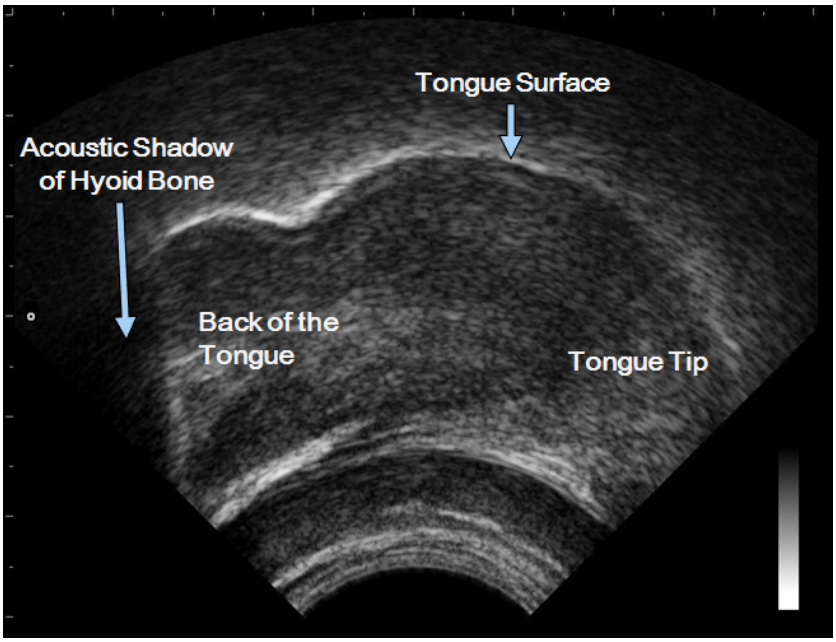

Figure 1.11: An ultrasound scan of oral complex during a swallow showing midline sagittal scan of the tongue from the tip to dorsum. The ultrasound transducer is held beneath the patients chin. Adapted from [59] with licence via Wikimedia Commons.

Ultrasound is an imaging modality that uses high-frequency sound waves to view the internal structures of the body. Unlike VF, no ionizing radiation exposure is associated with ultrasound imaging. Ultrasound is one of the most widely used imaging technologies found in medicine because it is portable, free of radiation risk, and relatively inexpensive when compared with other imaging modalities. Ultrasound has also been used to evaluate and access the swallowing process [60; 61]. Ultrasound is particularly useful in swallowing assessment of infants because it allows the clinicians to evaluate infants suck/suckle type feeding on breast or bottle. US evaluation for infants are preferred over other swallowing assessment techniques because it is non invasive and radiation free.

Newer ultrasound units are now capable of identifying normal and pathological oropharyngeal tissues and visualizing the coordinated movements of integrated structures within the oropharynx [62]. Sagittal sonography of the tongue makes it possible to evaluate the tongue at rest and during swallowing, and oral preparatory and oral phase of swallow can be clearly imaged with ultrasound. However, a limitation of ultrasound technique can is that sound wave cannot pass through air or bone, rather it will be completely reflected [63]. So ultrasound technique cannot visualize the trachea as it is an air-filled space. Although, ultrasound can detect pooling of secretion and residue in the valleculae [64], it is not able to detect penetration or aspiration of contents into the trachea. Another limitation is that the hard palate cannot be visualized as it is a bony structure, making it difficult to evaluate glossopalatal function and adequacy. These factors limits the use of ultrasound in assessment of pharyngeal phase of swallow [65]. Ultrasound is also useful for infants/children where repetition of the swallowing test may be essential and ultrasound scanning of the swallowing sequence can be repeated without any comparable radiation risk [66].

1.5 Clinical Decision Making: Which Swallowing Assessment is Indicated?

Different swallowing assessment provides different information about the swallowing physiology. Not one particular test can be used to evaluate swallowing abnormality rather different tests depending on the clinicians recommendation should be preformed to get a comprehensive picture of the abnormality for planning the treatment. For example, though MBS study is regarded as the gold standard [47; 48], repeated testing is not recommended due to the risk of redundant radiation exposure. On the other hand some studies have shown that FEES have a high level of agreement when one is trying to detect aspiration [67; 68; 69; 70], but this high level of agreement does not make the other test redundant. Furthermore, as discussed in section 1.4.3, endoscopic evaluation partially evaluate the oral preparatory and oral phase of swallow, and cannot evaluate esophageal phase of swallow. What it means is the indication towards a assessment technique are based on the nature of the suspected problem and the clinician should have all the procedures available so that the appropriate one can be used with each patient.

Some indication can also be logistic i.e. a FEES procedure requires a specialized equipment and skilled operator which may not be available at all settings.

1.6 Standardized Evaluation of Dysphagia Diagnosis

Standardized health care practices have been shown to improve clinical outcome by reducing ambiguous reporting and interpretation of test results [71]. Lack of such standardization in measurement methods produce ambiguous results when comparing results across heath care settings. Swallowing assessment using MBSS is a test of physiologic swallowing function and an indirect measure of sensory and motor functionalities that differentiates between a normal and impaired swallow. Variability in the MBSS result interpretation can result in inauspicious patient outcome and impact the overall health and well being of the patient.

Many swallowing screening and instrumental evaluation techniques have been developed for diagnosis of dysphagia (discussed in Section 1.4). These tools evaluate pressure, range, strength of structural movement, airway protection, sensation, bolus clearance and efficiency, and bolus flow patterns that characterizes a normal and impaired swallow [72]. During a swallow screening, the examiner looks for sings that could indicate dysphagia in a quick, efficient and safe manner. However, these screening tests does not give actual physiological information. Meanwhile, a swallowing assessment is more complex and sometime involve invasive measurement for providing providing quantitative and qualitative data about swallowing physiology. There are many studies in the literature conducted reviews to determine the effectiveness and feasibility of different screening and instrumental evaluation tests done to diagnose dysphagia [73; 74; 75]. Some research groups have compared similar findings from two studies and concluded that both have high level of agreement [67; 68; 69; 70]. So it is a subjective decision to choose the correct method of evaluation which depends on what the clinician is looking for and a single test cannot possibly provide the best assessment for every patient in every condition. Nonetheless, MBSS are preferred method by most of the clinicians to diagnose dysphagia and also used to monitor any changes in the swallowing function over time to tract the effectiveness of swallowing

treatment [72].

1.6.1 Modified Barium Swallow Impairment Profile

Martin-Harris et al. [17] established a protocol for standardizing MBSS called Modified Barium Swallow Impairment Profile (MBSImP ™©) which was developed during a five year study on over 300 dysphagic patients. This protocol establishes universally accepted terminology for describing swallowing motion and converts the clinical qualitative information into a quantifiable metric to diagnose swallowing impairment. MBSImP™© standardizes the volume, consistency and texture of the bolus administered during a videofluoroscopic evaluation. It includes 17 physiologic swallowing components grouped across three functional domains of swallowing (listed in Table 1.2) starting from lip closure to esophageal clearance. Each component is scored individually which uniquely contributes to judgement of overall swallowing impairment [17; 76]. A component is scored from 0 to 3,4,5 where a score of "0" for a particular component would mean normal functionality and higher number indicating a worse impairment (see Figure 1.12 for an example). Detailed component list, corresponding scores and score definitions defined in MBSImP™© are given in Appendix A.

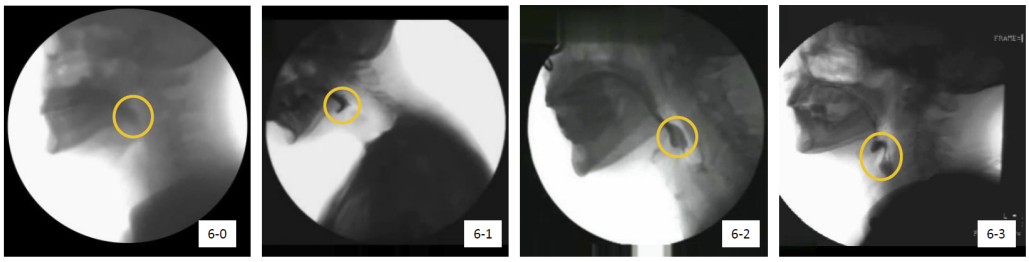

Figure 1.12: Operational definition used to score "Component 6 - Initiation of Pharyngeal Swallow". A score of 6-0 means bolus head (inside yellow circle) at posterior angle of ramus (first hyoid excursion), 6-1 means bolus head in valleculae, 6-2 means bolus head at posterior laryngeal surface of epiglottis and 6-3 means bolus head in pyriforms. A score of 6-4 (not shown in the figure) would mean no visible initiation at any location. Image sequence is created from MBSImP™© online training videos with permission.

Oral impairment domain		
(1)	Lip closure	(Lip C)
(2)	Hold position/tongue control	(HP)
(3)	Bolus preparation/mastication	(BP)
(4)	Bolus transport/lingual motion	(BT)
(5)	Oral residue	(OR)
(6)	Initiation of the pharyngeal swallow	(IPS)
Pharyngeal impairment domain		
(7)	Soft palate elevation	(SPE)
(8)	Laryngeal elevation	(LE)
(9)	Anterior hyoid motion	(HM)
(10)	Epiglottic movement	(EM)
(11)	Laryngeal closure	(LC)
(12)	Pharyngeal stripping wave	(PSW)
(13)	Pharyngeal contraction	(PC)
(14)	PES opening	(PESO)
(15)	Tongue base retraction	(TBE)
(16)	Pharyngeal residue	(PR)
Esophageal impairment domain		
(17)	Esophageal clearance in the upright position	(EC)

Table 1.2: List of physiologic swallowing components and corresponding acronyms used in MBSImP™© swallowing assessment.

1.6.2 Reliability training and testing

Inter-and intra rater reliability of MBSImP™© protocol is required to be 80% for blinded scores of modified barium swallow videos. In the training, if the concordance fell below 80%, the scores are reviewed and the training continued until the minimum of 80% concordance was achieved. The lower inter- and intra-rater variability of the training is, the better the clinicians can accurately and consistently score based on comparison to the standard. Specialized training including accuracy and reliability measurement is required to train clinicians to score each swallow in a standardized manner. To administer such training and ensure that the required reliability is maintained while scoring following MBSImP™© protocol, an online training platform has been developed [76]. The online training platform include standardized

training in swallowing physiology, skill development and reliability testing. The raining includes detailed animation derived from actual patient MBSS data for all 72 possible different scores. After completing the learning zone the trainee takes the reliability test.

1.7 Biomechanical Model in Standardized Dysphagia Training

The oropharyngeal anatomy is complex and composed of rigid structures including the cranium, jaw, and hyoid bone, highly deformable muscle activated tissues such as the tongue, soft palate, and pharynx, and larynx, an intricate arrangement of many muscles. These muscles and structures preform complicated and coordinated action like swallowing, mastication, chewing and speech. To understand such complicated motions and coordination to diagnose any dysfunction requires a sophisticated model that accounts for mechanics as well as dynamics of the oropharyngeal complex. Understanding of the swallowing motion requires 3D visualization of the swallowing motions which requires a 3D model representing the anatomical structures. So there is a need for a model that can provide 3D perspective visualization of the swallowing motion that can help understand the complex dynamics and help identify salient features of normal and impaired swallow. Furthermore, swallowing dynamics changes with the change in viscosity of the bolus that is being swallowed. So the model need to be able to simulate different consistencies of the bolus in order interactively learn how various bolus consistencies effect the swallowing dynamics.

1.8 Contributions

The contributions of this Thesis include creating a 3D biomechanical model of the oropharyngeal complex using realistic geometries and accurate timing of swallowing events (Chapter 3), simulating a stable bolus driven by model kinematics (Chapter 4) and extension of existing training material for standardized diagnosis of dysphagia (Chapter 5). The primary contributions of this dissertation are listed and summarized below:

Modeling of the oropharyngeal swallowing motion

i. **Built realistic 3D geometries of oropharyngeal complex.** We built realistic full 3D geometries of the oropharyngeal complex consisting of tongue, jaw, hard palate, soft palate, hyoid, pharynx, thyroid, cricoid, epiglottis and arytenoid from a animation model used in clinician training.

ii. **Extracted accurate timing of swallowing events.** We extracted accurate timing of swallowing events from video animations used in standardized clinician training for dysphagia diagnosis.

iii. **Created a coupled oropharyngeal swallowing model.** We generated rigid body and finite elements models from the surface geometries extracted earlier to create a coupled biomechanical model of the oropharyngeal complex.

iv. **Driving the model kinematically to emulate swallowing motion.** We used the kinematics derived earlier to drive our model usinng the accurate timing of swallowing events.

Fluid simulation to emulate bolus transport

i. **Incorporated the deformation of upper airway during swallow motion.** We used a airway-skin mesh for incorporating the deformation of the upper airway during a swallow motion.

ii. **Simulated stable bolus driven by model kinematics.** We simulated a stable fluid bolus in the airway-skin driven by model dynamics to emulate oropharyngeal swallowing motion in our model.

iii. **Validated simulation results with VF and animation video of normal swallow** We demonstrated that our model can simulate a bolus in a manner consistent with the VF and animated illustrations used in standardized clinician training for dysphagia diagnosis.

iv. **Simulated standardized bolus consistencies.** We also demonstrated that our model can simulate boluses with different viscosity by simulating standardized bolus consistencies used in clinical practice of dysphagia diagnosis.

Enhancing standardized training materials for dysphagia diagnosis

i. **Extension of training materials for most difficult physiologic swallowing component.** We interviewed the SLPs to find out if the additional 3D perspective visualization and flexibility of simulating fluid boluses with different consistencies can add value to their understanding of swallowing dynamics. With their feedback, we created 3D extension of existing training materials for standardized dysphagia diagnosis.

ii. **Conducted a user study involving SLPs.** The goal of the study was to investigate if additional 3D visualization adds value in standardized training. We built an interface similar to the existing MBSImP™© online training and added the training material afforded by our 3D model.

iii. **Concluded that our model can provide useful augmentation for standardized dysphagia training.** All the participating clinicians recommended with a high agreement score that the extension provided by our 3D model could be a useful addition for standardized dysphagia training.

1.9 Thesis Outline

The rest of the Thesis is organized as the following. First, an overview of the existing research in the relevant field is presented in Chapter 2. The full 3D oropharyngeal model development and driving the model with accurate timing of swallowing event is discussed in Chapter 3. Chapter 4 discusses about the development of the computational fluid simulation techniques used to simulate a bolus in the model and presents some qualitative and quantitative observation. Chapter 5 presents a user study conducted to evaluate the potential of extending standardized training materials for dysphagia diagnosis with our 3D model. Finally, the Thesis is concluded in Chapter 6 with a summary and some possible future directions.

Chapter 2

Related Work

The literature is dense with different models and simulation techniques aimed to emulate the oropharyngeal swallowing motion. Such models are intended to be used in different application starting from dysphagia research to modeling different food texture. In this chapter, the literature will be reviewed to find out about different approaches taken for simulating a swallow motion and discuss about the remaining challenges that still need to be addressed in order to develop a oropharyngeal swallowing for clinical training of dysphagia.

2.1 Resources Used for Clinical Education & Training

Physiological models that attempt to reproduce living anatomy or physiology are clinically called as "Simulator". 'Simulation" refers the application of such simulator to perform a particular task for education or training purpose. Simulation in some form has probably been used as a teaching strategy in education and training processes for clinicians in all domains for a long time. It is often said that the first time simulation was done when the first doctor tried to teach the first medical student how to perform a procedure properly. These simulators have a strong positive impact on health-care, as they lower the risk to patients of training and by providing a method of learning about care processes.

Illustrations of anatomic structures and animation of physiological process are also used for clinical training and they help explain a physiological process. Research is going on for developing more realistic, efficient, cheap and high-fidelity models to enhance such training materials. The following sections describe some clinical training models relevant to the scope of this Thesis.

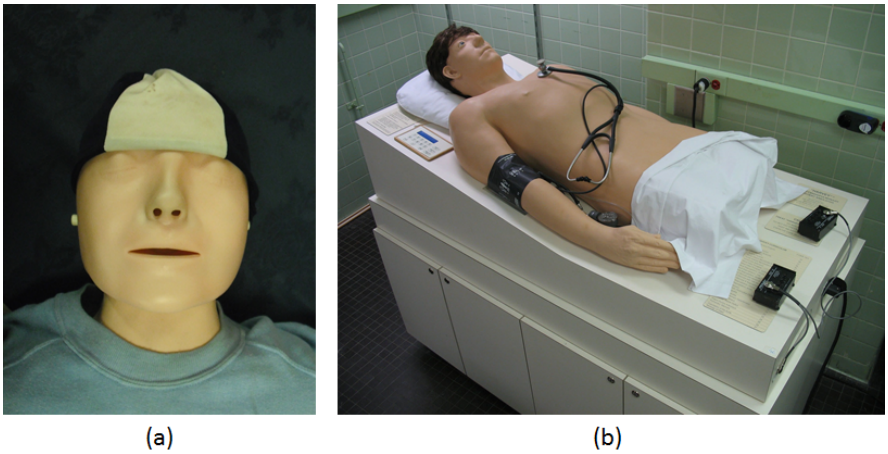

Figure 2.1: Two of the most recognised mannequin models. (a) Resusci-Anne and its later version are used for training CPR. Image adapted from [78]. (b) Harvey and its upgraded versions are used to simulate cardiopulmonary patient used mainly by medical students and cardiologists. Images (a) and (b) are adapted respectively from [78] and [79] licence via Wikimedia Commons.

2.2 Mannequin Simulator Models

Humanoid models for clinical education or training are often called mannequins simulators. Mannequin simulators have been developed over the years to be used for education, training and research purposes [77]. The application of such mannequin models are in cardiopulmonary resuscitation, cardiology skills, anaesthesia clinical skills, fiberoptic endoscopic evaluation of swallowing, crisis management and many others. Virtual patient models are also used for training clinicians about a specific procedure and the development of computational power has enabled higher fidelity, more realistic simulator of virtual patients. Both mannequin and virtual patient models are sometimes commercially available.

The mannequin simulators were invented due to almost independent developments that led to differences in technical approach in the early years. The first commercially available simulator model was "Resusci-Anne" (see Figure 2.1(a)) which was developed specifically for practicing a cardiopulmonary resuscitation (CPR) in early 1960s [80; 77]. Later on, higher fidelity models were developed in the 1990s with more anatomically correct airway

and simulator called SimMan [80]. Around the time when Resusci-Anne was created, Harvey [81] another mannequin simulator was created. "Harvey" was a full sized mannequin that simulates cardiac conditions (see Figure 2.1(b)). It was able to display various physical findings which included blood pressure, bilateral jugular venous pulse wave forms, arterial pulses and so on. Such historical milestones contributed significantly in the development of realistic mannequin simulators.

After the initial development of the mannequin simulators marked by "Resusci-Anne" and "Harvey" in the 1960s, simulation in health-care education and training started to gain acceptance. Mannequin simulators were first used for for teaching of swallowing examination in 1987 [82], for fiber-endoscopic training. For evaluating dysphagia fiberoptic endoscopic evaluation of swallowing (FEES) is becoming popular but one of the obstacle is to equip trainees with the transnasal endoscopy skills needed to perform the procedure. To help the trainees by providing necessary tools for learning, there are some head and neck mannequin models. However, training students with realistic simulation is costly. In addition to the purchase and maintenance costs of the endoscopy equipment, mannequins simulators range from $\$40,000$ for a basic mannequin to well over $\$95,000$ for a sophisticated mannequin [83]. Furthermore, it is also reported in [84] that there are no or little difference in pass time on volunteers between clinicians trained using mannequin simulators and clinicians trained on the non-lifelike tools, where both of the groups were faster and more confident when performing second endoscopy on a volunteer. So research is more focused on cost effective measures than developing more realistic and life-like simulator, when it comes to creating models for oropharyngeal complex.

There has been recent interest in the development of robotic devices for simulating human swallowing motion. Such models are mainly intended for modeling "safe food" for patient suffering from dysphagia. One of the therapies to improve swallowing efficiency is to recommend dietary modification [10]. For example, thicker boluses are easier to swallow than thin boluses for some dysphagia patients. So the SLPs suggest such modified diet to help the patients stay healthy and also improve the swallowing motion.

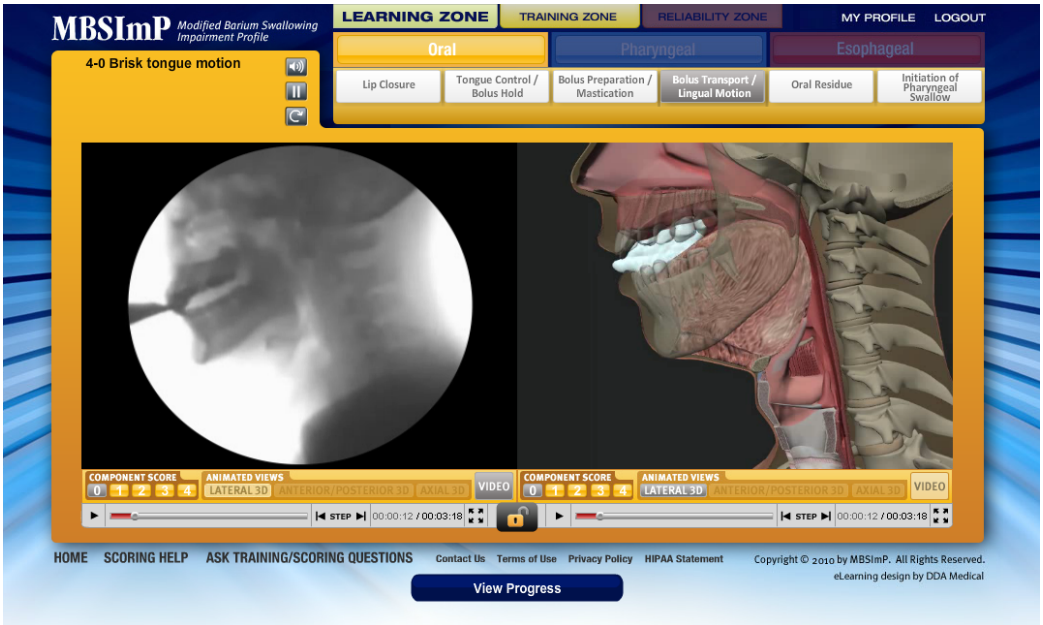

Figure 2.2: MBSImP™© online training platform includes both videofluoroscopic data and animated illustrations of the full range of standardized swallowing impairments. Image reproduced from MBSImP™© online training [76], with permission.

2.3 Animation Models

Development in the animation and rendering technology has enabled animated illustration of physiologic procedures to be used in clinical training. The earliest mention of computer based animation for oropharyngeal complex can be found in [85] where an animation routine was used to reconstruct oropharyngeal swallowing motion from biplane VF and dynamic CT images. This allowed somewhat more elaborate visualization of the mechanics of swallowing motion which was not possible with concurrent imaging technologies. Scholten et al [86] developed a multimedia program for teaching students about the swallowing dynamics which they called the "The Dynamic Swallow". It was a combination of different media including animations, video images, text, diagrams, and voice- overs and allowed some sort of interactive access to resources which was more effective than text-based material.

MBSImP™© protocol [17] uses animated videos side by side with VF

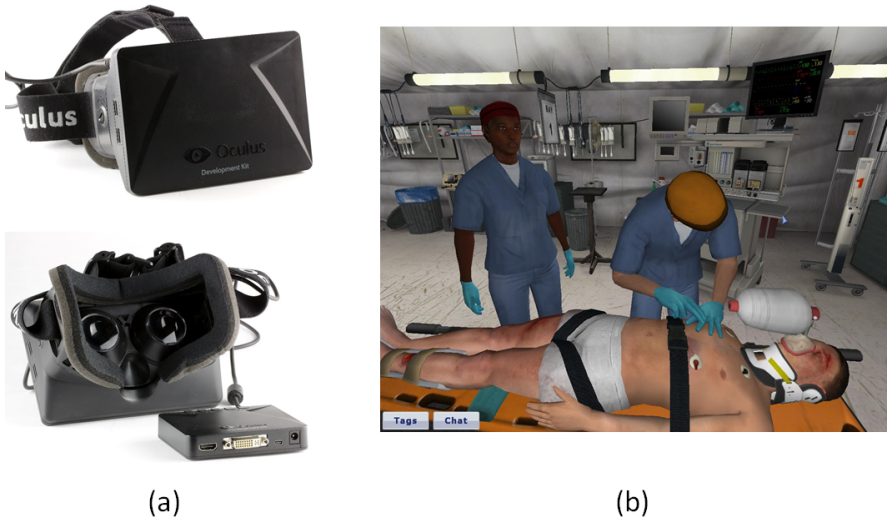

Figure 2.3: (a) Occuals rift, a virtual reality head-mounted display. The top picture shows the front view, and the bottom one the rear view and the control box [87]. (b) Application of such VR tools for assessment of students for clinical skills using 3DiTeams learner [88].

of patient swallow to help trainee clinicians understand the salient features of normal and different type of standardized dysphagic swallow (see Figure 2.2). This has been proven effective as the trainee clinicians needed to pass a reliability test with at least 80% or more reliability after the training was done. However, again, the additional visualizations provided with the VF are animated not generated using physics based simulation. So there is a lack of realism in animated motions.

Interactive models are an extension of the animated models and are afforded by technological advances in computational efficiency, image rendering and interface technology. Several limitations in developing mannequin model are discussed in the previous sections and it was suggested that training on standardized patients or volunteers is much more effective than training on a simulator. A standardized patient is a healthy person who is trained to act as real patient by accurately reproducing a history, physical and/or emotional medical scenario. However, there lies some obvious limitations concerning resources needed to have access to volunteers or standardized patients. This led to the development of VR simulation technology which has the following

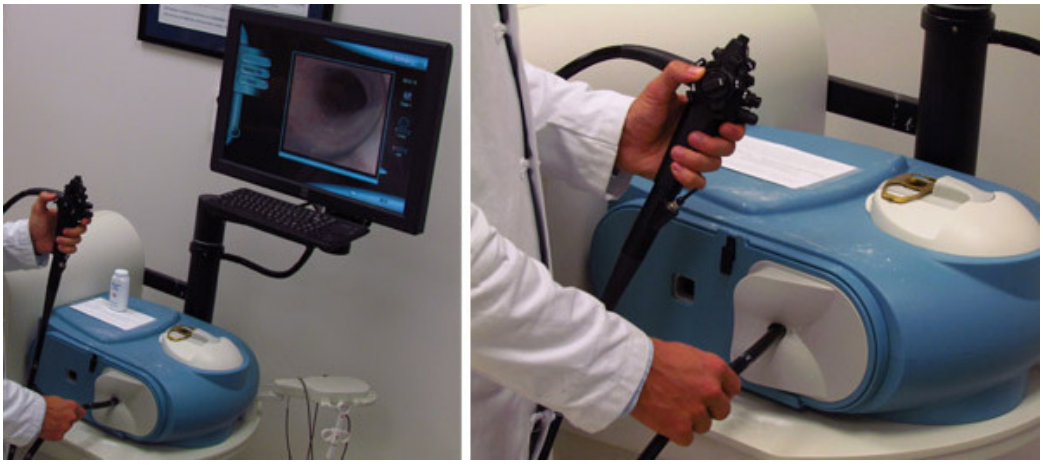

Figure 2.4: Flexible endoscopy training with the Simbionix GI Mentor™ [91].

advantages over mannequin model and volunteer models.

1. Standardized patients and sophisticated volunteers are expensive. VR can help reduce the cost significantly and allow for real life scenarios with highly interactive, artificially intelligent and natural language capable virtual human agents.

2. There are significant concurrent research going on for creating virtual reality headset like Oculus Rift [89] or Sony's Project Morpheus [90]. Such advance in VR technology is helping to create more realistic and interactive video technology that can be useful for training clinicians and medical students (see Figure 2.3).

3. Standardized patients and volunteers can characterize a limited diversity conditions and demographics. This is limited by the availability of human actors and their skills. This is even a greater problem when the actor needs to be a child, adolescent, elder, or when simulating a complex symptom presentation. Virtual patients can be tuned to mimic any demographic that may be necessary for the simulation.

Virtual reality devices give the trainee clinician more interactive learning experience than animated illustrations. However, all the illustration are

animated not simulated,the interaction with the model was limited by predefined set of activities and might not be suitable for simulating real clinical conditions. Computer models for endoscopic evaluation was first developed in 1980s [92]. Innovation in computational power helped computer models to be more effective and interactive. For an endoscopic training simulator (see Figure 2.4), endoscopic images from a real patients are stored. When the dummy endoscope in inserted in the model, the simulator records the movements of the endoscope. Corresponding images from the storage is displayed in response to the endoscopy being performed in real time. As technical advances continue, this capability is expected to have a significant impact on how clinical training is conducted in psychology and medicine. However, there is also a need for a cost analysis study to determine if such simulation can actually reduce the time of training.

2.4 Biomechanical Simulation Models

The traditional approach to biomechanical analysis involves recording observation of human movement and applying statistics to describe relationships within the observations. Such observational studies have generated a wealth of data regarding human motor physiology. The following steps are needed to for generating a biomechanical model of the oropharynx.

2.4.1 Oropharyngeal geometries

The quantitative analysis of the swallowing process may enable a systematic study of care foods that are safe and offer some degree of comfort to patients suffering from swallowing disorders. Few researchers have tackled the numerical simulation of swallowing in any detail. Movements of the esophagus and tongue have been discussed in relation to bolus transport and modeled mathematically. However, any discussion of dysphagia using the results of a numerical simulation must include the retroflexion of the epiglottis and laryngeal elevation because disorders relating to these movements are closely related to dysphagia. Thus the geometries of the oropharyngeal complex need to be realistic.

2.4.2 Simulation of bolus

The bolus motion is numerically solved in order to simulate swallowing motion in a coupled biomechanical model. Usually, numerical solution strategy starts from observing a physical phenomenon and defining characteristics that are relevant to the investigation. Some governing equations, initial or boundary conditions are defined to form a simplified mathematical model. The equations are numerically solved by discretizing the domain and obtaining a discrete representation of of the governing equations. Finally a set of ordinary differential equations are derived and translated into a computer code. Numerical solution for hydrodynamic equations involves similar steps and can broadly be divided into two major categories depending on the computational framework: (1) grid based methods and (2) meshfree methods.

2.4.3 Grid Based Methods

The **grid based methods** implement a computational model constructed by nodes through a predefined nodal connectivity. The accuracy of such numerical approximations significantly depend on mesh topology i.e. shape, size. To discretize the description of the fluid flow the partial differential equations are approximated. The partial derivatives can be approximated in different ways such as finite difference, finite volume, or finite element schemes using a computational mesh. This grid based techniques was first proposed by Harlow et al. [93] in 1965 called Marker and Cell (MAC) method. This method consists of markers which defines the position of the fluid and grid cells to reference the physical variables of the fluid such as velocity, pressure, temperature. This grid can be visualized as a computational mesh. This mesh can be fixed in space and cover the whole fluid domain, or it can be fixed with the fluid and move with the flow. The former approach is is called *Eulerian* method or spatial description and the latter is called *Lagrangian* method or material description. Both of the approaches are widely practiced in numerical methods with comparative advantages and disadvantages. Selection of any one approach depends on the problem description, thus are briefly discussed in the following sections.

Lagrangian Grid

The Lagrangian method describes the physical governing equations using material description and is usually represented by finite element method (FEM) [94]. In this method a mesh is fixed/attached to the fluid during the computation process. Due to such attachment, the mesh moves as the fluid flows. Since the mesh is fixed, the time history of all the field variables at a material point can be easily tracked for a moving fluid. Using an irregular mesh, a Lagrangian description can easily adapt to irregular and complex geometries and describes free or moving boundaries and material interfaces. Furthermore, there is no convective term in the related partial differential equation, whereas an Eulerian approach requires an computationally expensive convective term. Due to these features, such material description is useful in solving problems where the deformation is not large. However, if the motion of the fluid becomes geometrically complex, the mesh undergoes severe deformation; the underlying numerical methods become too unstable to compute a solution.

Eulerian Grid

On the other hand, an Eulerian approach describes the physical governing equations spatially which is typically represented by finite difference method (FDM)[95]. The computational mesh is fixed in space unlike the Lagrangian approach where the mesh is fixed with the fluid. As a result, the mesh points and cells remain spatially fixed during the computation while the fluid flows across the mesh. Physical quantities like velocity, energy, etc of the flow are calculated by simulating flux of mass, momentum and energy across mesh cell boundaries. As the Eulerian mesh is fixed in space large deformations in the fluid flow do not cause numerical problems like the Lagrangian grid-based methods. Hence, Eulerian methods are popular in computational fluid dynamics where the flow of the fluid is significant. However, it is difficult to track the time history of a field variable at a fixed point on the material. For complex geometries a complicated mesh generation process in required to convert the irregular geometry into computational domain. There also exists a trade off between the computational efficiency and resolution of the computational mesh as the Eulerian method requires a mesh over the whole computational domain. The coarser the mesh is the more computationally efficient the method becomes sacrificing accuracy and vice versa. Table 2.1

summarizes comparative features Lagrangian and Eulerian.

Grid	**(L)** Fixed with the material. **(E)** Fixed in space.
Tracking	**(L)** Movement of any point on materials. **(E)** Mass, momentum and energy flux across grid nodes and mesh cell boundary.
Time history	**(L)** Easy to obtain at a point attached on the material. **(E)** Difficult to obtain at a point attached on the material.
Moving boundary	**(L)** Easy to track. **(E)** Difficult to track.
Complex geometry	**(L)** Easy to model. **(E)** Difficult to model with good accuracy.
Large deformation	**(L)** Difficult to handle. **(E)** Easy to handle.

Table 2.1: Comparative features of Lagrangian(**L**) and Eulerian(**E**) grid based methods for solving hydrodynamic equations.

Combined Lagrangian and Eulerian grids

Both Lagrangian and Eulerian approach have comparative advantages and disadvantages. In literature, two hybrid methods are found to combine these two to benefit from the advantages and minimize limitations. They are the Coupled Eulerian Lagrangian (CEL) [96] and Arbitrary Lagrange Eulerian (ALE) [97; 98]. The CEL approach is often undertaken when there are two different types of materials with different level of deformation. The common practice is to discretize the one with little or no deformation, usually solid material, in a Lagrangian frame; and fluids or material have significant deformations using Eulerian frame. Both Lagrangian and Eulerian descriptions are setup in separate regions in the problem space and does not overlap. These independent regions interact with each other and exchange computational information between two set of grids. In Arbitrary Lagrange Eulerian (ALE) approach rezoning techniques for Lagrangian meshes are employed. Such rezoning aims to minimize mesh distortion when the Lagrangian mesh

is moved independently. In ALE the Lagrangian motion is computed at the beginning of each time step and is followed by rezoning step. During this rezoning step it is decided if the mesh is going to be rezoned to the original shape (Eulerian description), not rezoned (pure Lagrangian description) or some optimal shape (somewhere in between Lagrangian and Eulerian description). Many commercial solver i.e. LS-DYNA[99], MSC/Dytran[100] uses such hybrid approaches and has received much research interest. However, even with these hybrid approaches a severely distorted mesh causes errors in the numerical simulations [97; 98] and often causes termination of the computation process.

Limitations of the grid based methods

Grid based methods have been widely used in various areas of computational fluid dynamics(CFD) and computational solid mechanics (CSM). However, there are some inherent difficulties undertaking such grid based approaches which limit their application in many fluid simulation problem. For example, if taking a Eulerian approach like FDM, it is always challenging to construct a regular grid to accommodate complex geometry. This requires complex mathematical transformations which can be more expensive than the problem itself. Further, such approach has problems with tracking material properties, dealing with deformable boundaries and free surfaces as shown in Table 2.1. Meanwhile, Lagrangian FEM methods requires rezoning which is expensive and introduces additional inaccuracy to the solution. The limitations of grid based methods are more evident when considering large deformations, large inhomogeneities, moving material interfaces, deformable boundaries and free surfaces common in hydrodynamic phenomenon as explosion and high velocity impact (HVI). These limitations initiated the research on meshfree methods that is required to solve these problems.

2.4.4 Meshfree methods

The basic idea behind the **meshfree methods** is to discretize the continuum through a set of points which are not connected by a computational mesh.

Smoothed particle Hydrodynamics (SPH)

Smoothed Particle Hydrodynamics (SPH) is one of the most popular mesh-free representation methods for simulating free surface flows. SPH was first proposed independently by Gingold and Monaghan [101] and Lucy [102] in late seventies. It was developed to study astrophysical phenomena as the sheer scale of the astrophysical events deem experimental setups in a laboratory setting impossible for most of the cases. SPH has been used to study a range of astronomical events such as galaxy formation, star formation, supernovas, solar system formation and so on. SPH became popular in many other ares such as computational fluid simulation, solid mechanics and has various application in coastal engineering for modeling dam brake behaviours and plunging waves, virtual water simulation for video games or motion picture, virtual surgery, multifluid simulation and becoming increasingly popular [103]. As SPH defines a set of moving interpolation points which moves to represent the fluid flow; in a sense SPH is a *Lagrangian* motion even if the points are never linked via a computational mesh. The interpolation points assume values of dynamic fluid variables which are expressed as an integral interpolant using a smoothing kernel. The integral is approximated by a summation over the interpolation points. A detailed description about SPH fundamentals and formulation is given in Chapter B.

There are several advantages of the SPH method over the traditional grid based numerical methods [104]. By properly deploying SPH particles at the initial positions; the free surfaces, material interfaces and moving boundaries can be traced regardless of the complexity of the fluid movement which is very challenging to incorporate using Eulerian methods. Free surface representation of fluids allow a straightforward handling of very large deformations. This is because the computational mesh representing the fluid domain is not defined at the beginning rather the connectivity among the points is generated as a part of the computation at each time step. Furthermore, the accuracy can be controlled with flexibility and by adding more points (i.e. high resolution simulation) in the area of interest can give more accurate results when refinement is needed. Such characteristics makes SPH suitable for bio- and nano- engineering at micro and nano scale, and astrophysics at astronomic scale.

Upper airway model

A pure Lagrangian mesh representing a liquid bolus can be used to simulate the movement of bolus during a swallow. However, such meshing requires computationally expensive operation while simulating bolus merging and splitting bolus, requiring frequent remeshing. An Eulerian representation like Sonomura et al. [105] would require special handling of the irregular moving boundaries. Fluid simulation of swallowing is complex as it is depended on the irregular boundary motions provided by the anatomical structures of the oropharyngeal complex like tongue, soft palate and pharyngeal wall, which are subject to individual variation. In this thesis, SPH is used to simulate the bolus inside the oral cavity to emulate swallowing motion to take advantage of its mesh free formulation surface free representation. SPH has also been used to simulated both compressible[106] flow and incompressible flow[107; 108].

2.5 Summary

To summarize, human swallowing motion is very complex and hard to visualize even with the most state-of-the-art imaging technology. To comprehend the complex swallowing motion and investigate different swallowing impairment, realistic illustrations such as animations, 3D virtual models contributes significantly and helps clinicians learning. These illustration are primarily created from observation of the structural movements from medical images. However, the motion portrayed by the animators are plausible but sometimes not realistic as the anatomical structures are made to follow a certain motion that do not support the underlying kinematics causing it. As a result, this limits the interaction with the model limited and predefined where as real patient cases are more complex and specific.

Three areas of investigation were identified for generating biomechanical model of the oropharyngeal complex for simulating a swallowing motion.

First Getting realistic geometries of the oropharyngeal complex and accurate timing of swallowing events is challenging even with state-of-the-art structural and functional medical imaging data.

Second Stable fluid simulation techniques for incorporating deformable boundary condition are required to mimic the bolus transport of a swallowing motion in a biomechanical model.

Third The potential of a simulation based training model for being accepted at clinical practice largely depends on its effectiveness in clinical setting and its potential of improving the patient outcome.

In the following three chapters, the contribution of this Thesis towards these open research problems are described.

Chapter 3

Modeling of the Oropharyngeal Complex

This Chapter presents the process flow undertaken to create a 3D biomechanical model of the oropharyngeal complex for swallowing simulation. The first step towards getting the biomechanical model is building realistic geometries of oropharyngeal structures. In our process flow, the generation of a 3D biomechanical swallowing model involves several steps: building realistic geometries, formulating a biomechanical model with the derived geometries, addling accurate timing of swallowing events into the model, driving the model kinematically for a simulating a swallow. Each step of this process flow is explained in detail in the following sections of this chapter. While the process flow was developed for the purpose of generating a biomechanical model from swallowing animations, it can also be applied for creating general-purpose biomechanical models from animated illustration for other physiological process.

3.1 Building Geometries

Modeling the highly geometrically complex oropharyngeal structures are challenging because the oropharyngeal complex is made of soft tissues, muscles, bones and empty space in the airway. Such diversity makes it very difficult for any particular imaging modality to comprehend different type anatomical structures present in the oropharyngeal complex. Using realistic geometries for a biomechanical simulation is important, especially when the model is intended to be used for clinician training.

The MBSImP©™ training protocol include 72 videofluoroscopy segments, each combined with animation videos to illustrate 17 physiologic swallowing components and scores of the MBSImP©™ protocol. Appendix A lists the 17 physiologic swallowing components and consequent scoring of the components following MBSImP©™. The animations were created using an

underlying 2.5D geometric model (i.e. only a lateral side model is used) with shape changes specified over time for the animation. The geometries used to build the model were validated for clinical training of dysphagia by a team of expert clinicians. The animators consulted anatomy reference books, medical images i.e. CT, VF, MRI from patents data to build the geometries of the oropharyngeal complex. The geometries and timing of the swallowing events were iterated by the clinicians and animators until both were in an agreement that the animations exhibit the salient features of a swallowing motion. Leveraging the animators imagination guided by expert clinicians, the MBSImP©™ swallowing animations represent realistic geometries and validated timing of swallowing events. In this work, the animation model used to create MBSImP™© animation videos is leveraged to build our 3D biomechanical model. The kinematics from the animations are propagated to the biomechanical model to drive the model with clinically validated timing of swallowing events.

3.1.1 Generating full 3D model

The animation model(see Figure 3.1) for the was created in LightWave® 3D which is a registered trademark of NewTek Inc. It is a commercial software package extensively used to create visual effect, video games development and motion graphics. The surface geometries of the oropharyngeal complex were artistically designed in LightWave Modeler®. The model was designed in such a was that it would illustrate the oropharyngeal structures from mid sagittal cut plane. The model was designed in this half cut way because the animators wanted to render the videos from midsagittal cut plane to match the viewpoint of a usual MBS exam.

After the surface geometries were created, the animators used LightWave Layout® to arrange the 3D model and define shape changes into the surface geometries in key-frames to animate a swallowing motion. This is to be noted that the kinematics are also added artistically to the model to match the input VF data. After the animators and clinicians were in agreement the the kinematics exhibited by the model matched that of a real swallow, the animator then manually drew some line in rostral-caudal axis and animated some sort bolus like structures to follow that predefined bolus path. With the key frame animation to deform/move the oropharangeal structures, the bolus is moved in sync with the kinematics of the model to match a normal swallow. After the model was rendered to create a normal swallow, video was

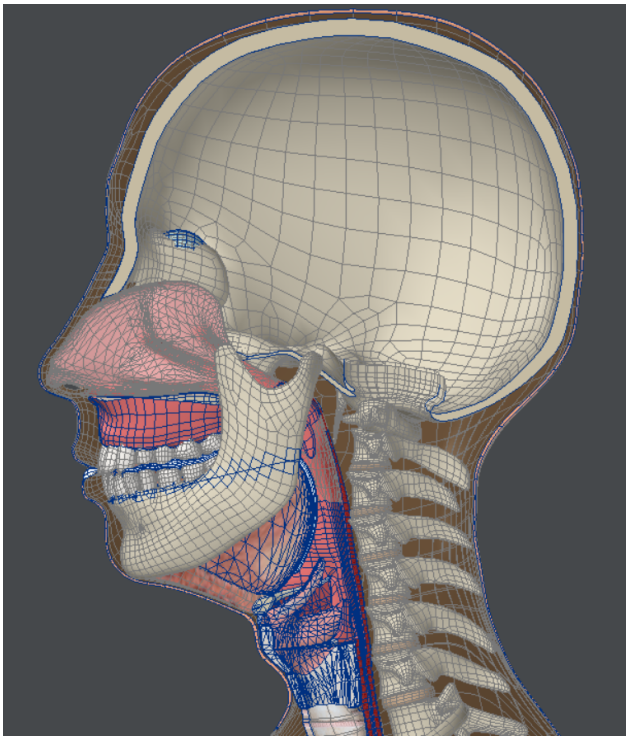

Figure 3.1: Animated swallowing model of the oropharyngeal built built using LightWave® 3D.

captured from mid sagittal cut plane to make the animated videos. Figure 3.2 show different instances of key-frame animation for a normal swallow and corresponding frame in the swallowing video. For creating videos of different impaired swallow, these steps are repeated starting from the key-frame animation. It is to be noted that the surface geometries are create once and different shape change controlled by key-frame animation enabled the animators to animate different types of swallowing impairment and render videos to be used in the MBSImP©™ training.

The half cut surface geometries are extracted from the LightWave Modeler® for building full 3D geometries. The animation model also included surface representation of human skeleton, eyeballs, lungs, hand and esophagus. However, for the scope of the this Thesis, 3D surface geometries of tongue, hard and soft palate, teeth , arytenoid, hyoid, jaw, thyroid, cricoid, epiglottis and trachea are built as the simulation of oropharyngeal swallow is of interest.

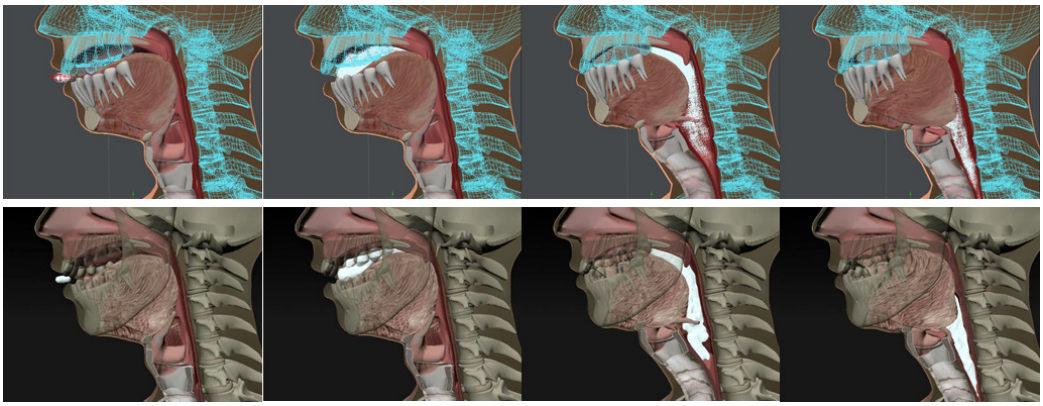

Figure 3.2: The top row shows instances of the animation model and the bottom row shows corresponding frame in the swallowing videos used in MBSImP©™ standardized training.

As mentioned earlier, the geometries are cut in half so there is a surface representing the mid sagittal cut plane. The first step for getting the 3D model is manually removing the vertices and faces of the mid sagittal plane. After the the surface mesh was mirrored with respect to mid-sagittal axis. To make the model close, the vertices new faces were defined to connect the half object from the left to right. This is to be noted that no new vertices were created or deleted in order to connect the two part rather only new faces were defined. This is very important not to introduce new vertices into the surface geometry. This is because in the future sections (Sections 3.2.1 and 3.2.3), when sequential meshes are generated to extract kinematics from the animation and use this kinematic information to drive the model, without one-to-one relation between the base mesh and sequential meshed the clinically validated kinematics could not be preserved. Figure 3.3 illiterates the steps undertaken to generate the 3D surface geometry for the tongue. This process is repeated for all the selected anatomies to be exported.

The hard palate, soft palate, uvula, pharyngeal wall and oropharynx is represented using one object in the animation model. However, such representation is problematic for building a biomechanical model because different part of this big object undergo different amount of deformation. For example, the hard palate is a bony structure exhibiting no deformation whereas the pharyngeal wall deforms significantly during a normal swallow motion. So the big object was divided into hard palate, soft palate, uvula and pharyngeal

wall depending on their anatomical location and level of deformations.

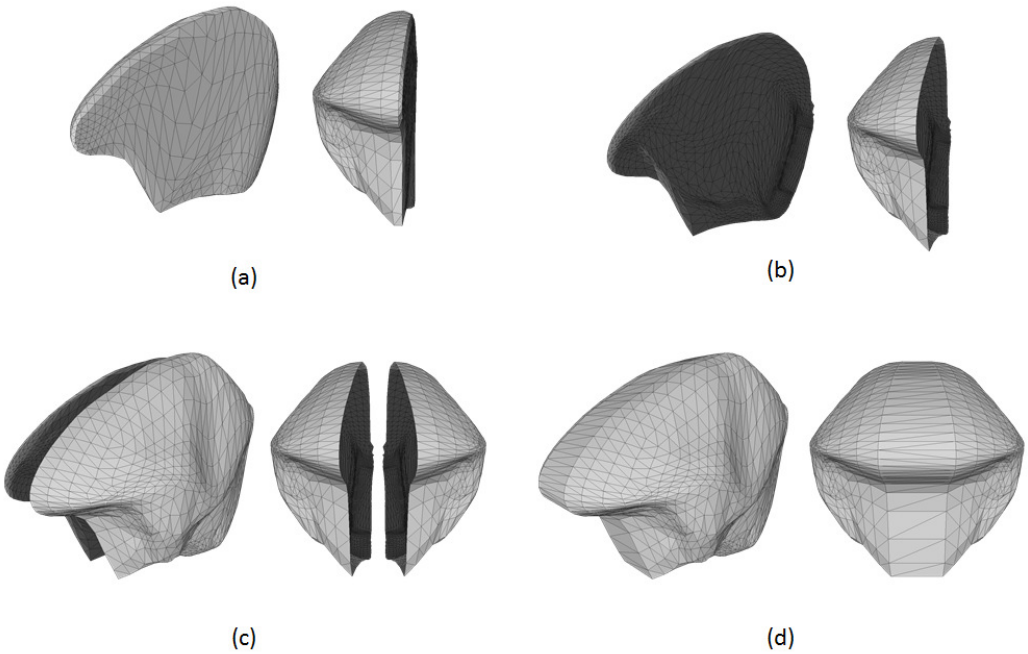

Figure 3.3: Steps for generating full 3D geometries of oropharyngeal complex, illustrated for tongue model. (a) The half cut object extracted from LightWave Modeler®. (b) First the mid sagittal cut plane surface is manually removed, afterwards (c) the object is mirrored and (d) the corresponding vertices are connected to create new faces and make the geometry bounded.

3.1.2 Realistic morphometry

After generating 3d surface model for the oropharyngeal complex the model is scaled to represent the dimension of average human oropharyngeal anatomy. Our model needs to be morphometrically realistic in order to produce meaningful clinical results. Having realistic shape and size enable a biomechanical model to generate clinically meaningful result. To make the model morphometrically realistic, the tongue was selected to the anatomy of reference. This is because, the tongue is of major interest to phoneticians, linguists, speech language pathologists and orthodontists. The size of the tongue is

highly variable between sex, age of the individual. Hopkin et al.[109] measured the dimension of 32 neonatal tongues (16 male, 16 female) and 30 adult tongue (14 male and 16 female) postmortem. The findings regrading mean dimension of neonatal and adult tongue from that study are reported in the following table.

	Neonatal ($N = 32$)			Adult ($N = 30$)		
	Mean	SD	SE	Mean	SD	SE
Length	39.91	4.25	0.76	79.83	7.57	1.40
Breadth	25.43	2.58	0.46	51.90	4.24	0.78
Thickness	8.76	0.98	0.17	16.13	2.51	0.46

Table 3.1: Mean dimension in mm of neonatal and adult tongue reported by [109]. SD and SE stands for Standard Deviation and Standard Error of mean respectively.

The above table shows that mean dimension of an adult tongue are about double of a that of a neonatal. As the aim of this Thesis is to generate a model for clinician training and offer a generic representation of the population, adult tongue dimension was considered to in order to scale the model. Among the three attributes of tongue dimension reported, the one with the least standard deviation should be selected. Tongue length was measured from the tip of the epiglottis to the apex of the tongue. The breadth was measured at the widest part of the tongue and the thickness was measured at the free edge of the tongue at its widest part. In Table 3.4, it can be seen that tongue thickness has the least standard deviation. However, the free edge of the widest part of the tongue is not clearly defined and hard to measure in the model. The tongue length has higher standard deviation than tongue breadth, so tongue breadth was selected to calculate the scaling factor for making our model morphometrically realistic. It can be seen from Table 3.4 that the mean tongue breadth for adults was found to be 51.9mm. For calculating the scaling factor, the widest part of the tongue model was scaled to have 51.9mm in breadth (Figure 3.4). The same scaling factor is then used to scale the whole model. By doing so, we make our model morphometrically realistic.

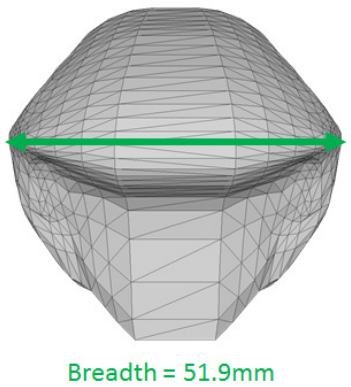

Figure 3.4: Average tongue breadth simulated in the model to match the dimensions reported in [109]

3.2 Building the biomechanical model

The MBSImP©™ animations exhibit accurate timings of the swallowing events which is validated for clinician training and this accurate timing of swallowing events are incorporated in the biomechanical model. This section will discuss about extracting the kinematics from the animation, building a coupled biomechanical model with the full surface geometries and deriving the coupled biomechanical with the kinematics extracted from the animation.

3.2.1 Extracting kinematics from animation

To build our biomechanical swallowing model, the full 3d geometries derived in the previous section (Section 3.1) are driven with the kinematics extracted from the animation. This animation is introduced and rendered by LightWave Layout® software to create videos for MBSImP©™ swallowing animations. 109 frames starting from 0th the 108th time instant was animated to render the 3 second animations illustrating a normal swallow. The vertices position of the each surface mesh representing an object in the animation scene was recorded from time instance 0 to 108 to capture the shape change of the object over the duration of the swallowing motion. In other words, to capture accurate timing of swallowing events, a surface mesh representing the object was exported for 0 to 108 time instant producing 109 surface meshes. As one surface meshes represent the same object at a

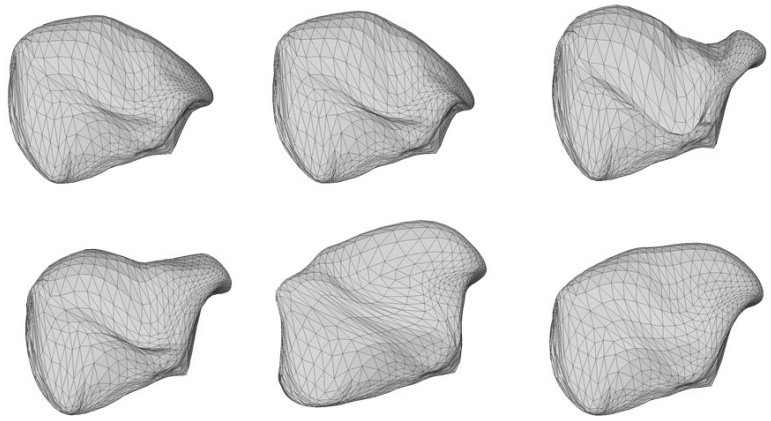

Figure 3.5: Sequential meshes extracted from the animation model to capture the accurate timing and deformation of the oropharyngeal structures during a swallowing motion. This figure shows tongue movement during a swallow motion captured by extracting the sequential meshes and it is repeated for all geometries of our model.

particular time instant, the number of vertices and faces are same in all the sequential meshes, only the position of the vertices are changed. Figure 3.5 show some of the sequential meshed generated for capturing the tongue motion over time for a normal swallow. This process is repeated for to generate sequential meshed for tongue, hard and soft palate, teeth, arytenoid, hyoid, jaw, thyroid, cricoid, epiglottis. By exporting the sequential meshes for all relevant objects in the animation scene, the clinically validates kinematics of swallowing events are recorded.

3.2.2 Coupled biomechanical model

Our biomechanical swallowing model of the oropharyngeal complex is built and simulated in ArtiSynth (`www.artisynth.org`), a biomechanical simulation toolkit [110] that supports combined multi-body and finite element simulation. The oropharyngeal complex is made of both soft and bony structures who undergo different type of deformation/movement depending of its tissue property during a swallowing motion. For example, bony tissue like jaw or hyoid bone undergo rigid transformations whereas the softer structures

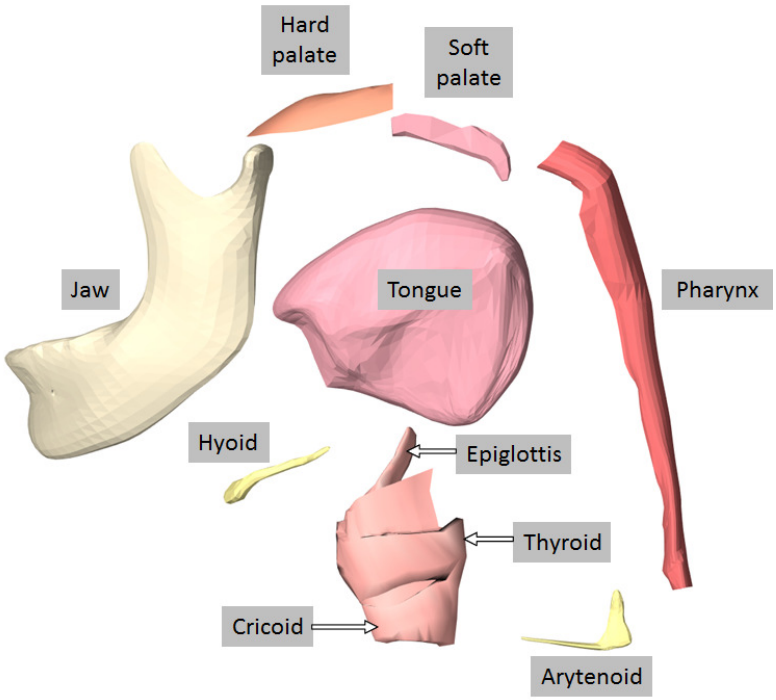

Figure 3.6: Different components of the 3D oropharyngeal biomechanical swallowing model.

like the tongue, undergoes significant nonrigid transformation. So it is not practical to simulate all the structures with rigid or nonrigid transformation. Figure 3.6 shows the simulated rigid bodies and FEMs in the model.

Building rigid bodies

Rigid bodies are implemented in ArtiSynth as dynamic components with six dimensional position, orientation state with corresponding velocity state with inertia. There is also a surface mesh associated with each rigid body describing its topology. A rigid body has 6 Degrees Of Freedom (DOF) which is described by its six dimensional *position* state and its *pose* is computed from its position and orientation with respect to world coordinates. The rigid bodies are created from the full 3D surface geometries of the bony anatomical structures of the oropharyngeal complex built in Section 3.1. A factory method used in ArtiSynth is used to create rigid bodies where the derived surface topologies are set as the surface mesh associated with the

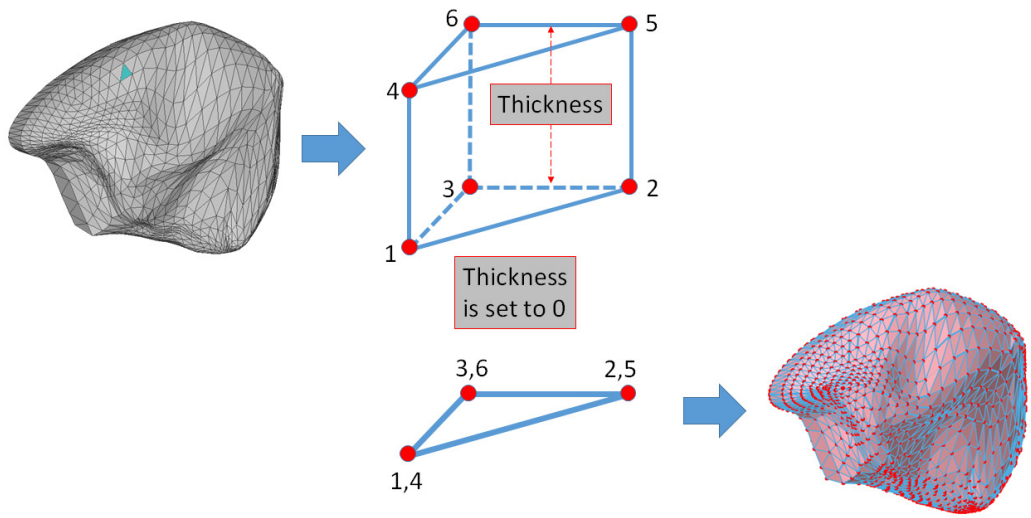

Figure 3.7: A surface is extruded along the normal of the triangular faces of the surface mesh creating FEM with 2 layer wedge element. The thickness which is the distance between the layers are set to 0 to superimpose one layer on top of the other.

rigid body. Uniform density is defined throughout from which mass and inertia properties are calculated.

Building finite element models

The general approach for generating a FE model is by dividing the domain into *elements* which are the cells or building blocks of the model. The vertices or corners of the elements are called *nodes*. The domain is a three-dimensional space occupied by the model and divided into small elements which accurately represent the model geometry. This elements allow to create local domains by approximating the system equations locally and the nodes act as the control points in the spatially discretized system. When the equation is solved, the solution is assumed to be smoothly interpolated across the elements based on values determined at the nodes. This discretization of the differential system is converted into an algebraic system where it can be linearized and solved iteratively.

Soft and deformable oropharyngeal structures are simulated as finite element models (FEM). The first step for generating a FEM is to build the

mesh topology i.e. node and element structure. The FEMs are generated from the surface meshes extracted in Section 3.1. Our model is intended to be driven by kinematics. So the FEMs are extruded to make a hollow FEMs to preserve the surface geometries. This makes it easier to drive the model kinematically with less computational complexity. A thin layer of elements are created along the normal direction by extruding the triangular faces of the surface mesh. As a result the triangular faces become two layer wedge elements with a defined thickness i.e. distance between the layers (see Figure 3.7). During extruding the triangular faces, the distance between the layers are set to zeros so two layers of FEM nodes are elements are superimposed on each other. As result the elements are inverted as the surface curvature becomes greater than total extruded thickness. This inversion of the element is mitigated by setting the boundary condition explicitly. What it means is the both position and velocity of the nodes will be controlled parametrically by applying this fixed boundary condition and turning the dynamic parameter to "false". After defining the surface topology, the material properties are defined as linear and different rendering properties are added to the model to make it look more realistic which is very important for it to be used in visualization application.

3.2.3 Adding kinematics

After developing the biomechanical model with rigid bodies and FEMs, kinematics are added to the model to mimic the oropharyngeal swallowing motion. The model was built from the geometries representing the first time instant of a swallow motion that is 0th time instant. Sequential surface topologies are extracted form the animations in Section 3.2.1 to capture the timing of swallowing events. The surface topologies were extracted for all the time frames starting from 0th to 108th time instant. These sequential meshes had same number of vertices and faces but different position in space capturing the deformation of the anatomical structure over time. The position of the FEM nodes over time were updated from the corresponding sequential mesh of that time instance to deform the FEM for emulating swallowing motion. The one to one correspondence between the vertices of the sequential meshes allowed to reliably propagate the swallowing kinematics into the model. 109 sequential meshes are loaded to simulation a swallowing motion of 3.18 second. Figure 3.8 shows different instances of our model emulating a normal swallow motion which is superimposed on the animation video. This

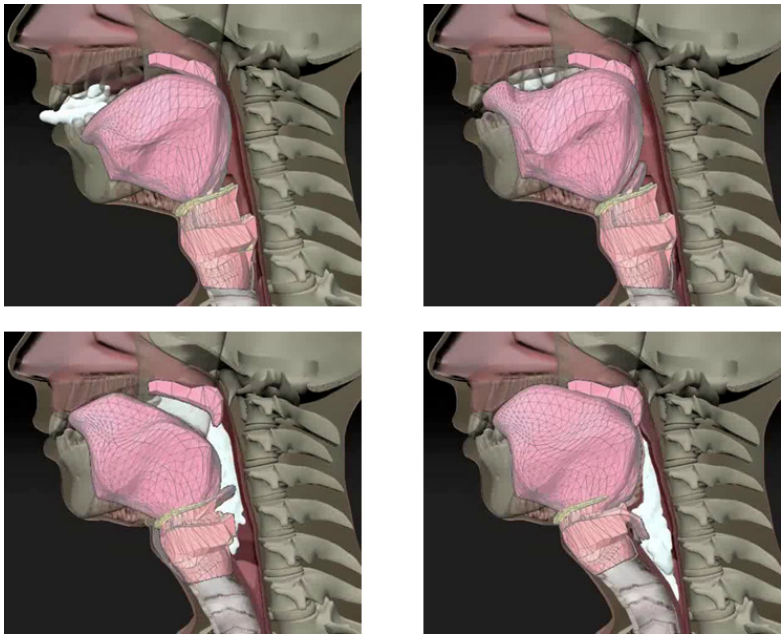

Figure 3.8: Kinematically driven biomechanical model superimposed on the normal swallowing video.

figure illustrate that kinematics of animations are propagated correctly into our model.

3.3 Results and Analysis

The VF allows the clinicians to access the swallowing functionality of a patients but for trainee clinicians, it is sometimes hard to comprehend the swallowing physiology from the VF. The animations helps the trainee clinicians' understanding of the swallowing physiology by illustrating the salient features more clearly. However, the animations lack realism as the bolus movements are animated not simulated. Furthermore, the animations are made to capture the swallowing motion from lateral plane. Using our biomechanical model, the motions can be simulated not animated. The advantage of simulating the motion not animating is that, it makes the model more interactive offering additional flexibility. With our model, the swallowing can be viewed from different viewpoints in full 3D allowing perspective visualization. This simulation can help incorporate the missing realism into

the training, which in turn will bridge the gap between the VF and training model. Figure 3.9 shows the kinematically driven model superimposed on the normal swallowing VF and animation.

The generated sequential meshes extracted for the animation scene are half cut surface representation as the animation model was half cut. However, the model components are full 3D models representing the first time instance of a swallow motion. So to update the position of the full 3D models with the half cut sequential meshes, the one-to-one property of the sequential meshes is applied. As the sequential meshed represent the deformation of the same object overtime, the number of vertices in each sequential mesh is same. During the creation of full 3D geometries (Figure 3.3) no new vertices were created only vertices of the mid sagittal cut plane were deleted. So a text file was generated for each time instance, starting for 0 to 108 only with the Cartesian coordinates of the vertices from the sequential meshes. The vertices of the left half of a object at the 0th time instance were updated with the positions of the vertices from the next time instance except for the vertices that were deleted when the mid-sagittal cut place was removed. For the other half, the X coordinate was multiplied by -1 to to mirror the Cartesian coordinates with respect to X axis. By doing so, the full object is updated with the position of the next half cut sequential mesh. Loading only the text file with vertices not the sequential surface meshes make the process more computationally efficient as it avoids unnecessary book keeping for each loaded mesh in the ArtiSynth. This process is repeated for each time frame and for each FEM components for simulating a swallowing motion. By doing so, we propagate the kinematics and accurate timings of swallow events to drive our coupled biomechanical model.

3.4 Summary

The synergy of oropharyngeal swallowing dynamics is simulated in this Chapter. Full 3D oropharyngeal model was built from surface geometries extracted from the animation model. Rigid body models for bony structures and FEMs for soft deformable structures of the oropharyngeal complex were generated from the surface geometries. This coupled biomechanical model was kinematically driven with accurate timing of swallowing events. This coupled model sets up the stage for further development where the model can be controlled dynamically by activating certain muscles. ArtiSynth supports a

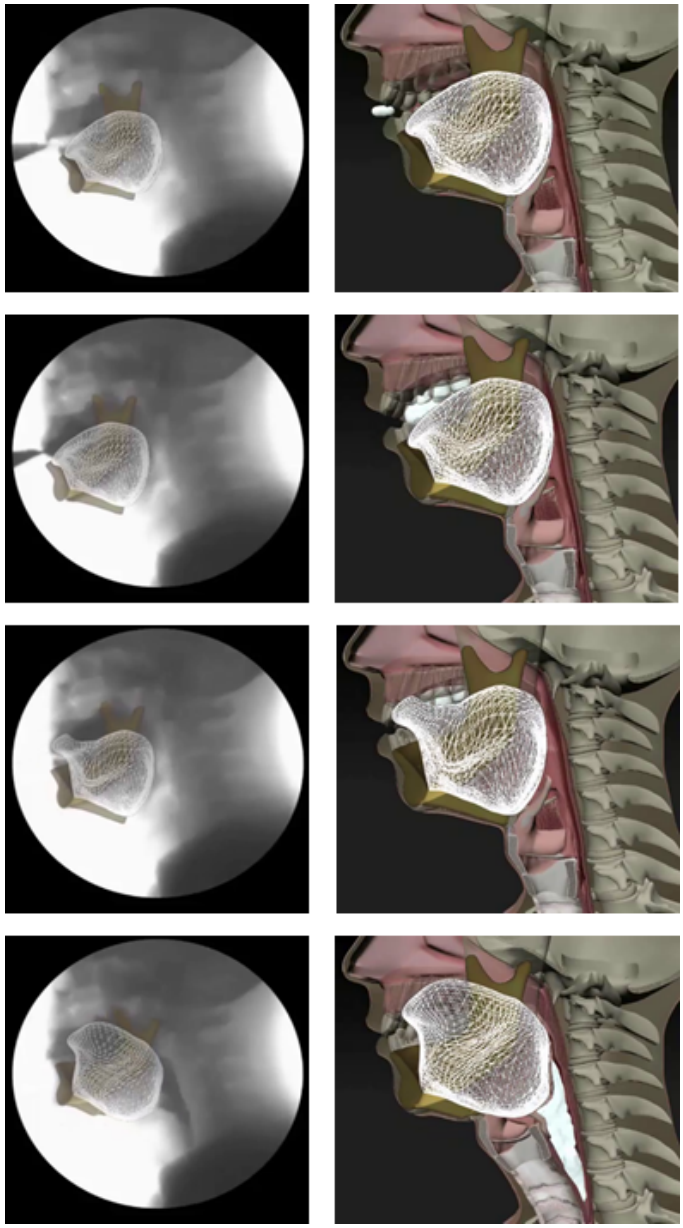

Figure 3.9: Our kinematically driven biomechanical model superimposed on videofluoroscopy (left column) and animation (right column) of a normal swallowing motion.

muscle driven FE model where the muscle fibres embedded in the model can be activated to follow a desired movement. It is possible to use the inverse modeling capability of ArtiSynth to estimate the virtual muscle activation from the kinematics of our implemented FE tongue for a normal and impaired swallow. This can give a deeper comprehension of the swallowing physiology from a neurological perspective and aid dysphagia diagnosis.

Chapter 4

Bolus Simulation

In Chapter 3, a biomechanical model of the oropharyngeal complex was developed from realistic geometries and accurate timing of swallowing events. In this Chapter, a fluid bolus is simulated inside the kinematically driven oropharyngeal model driven by the model kinematics. Section 4.1 describes the unified geometric skinning technique used to couple the airway-skin mesh with our oropharyngeal model. The airway-skin mesh represents upper airway which is deformed significantly by the movement of the oropharyngeal structures during a swallowing motion. Section 4.2 describes the Smoothed Particle Hydrodynamics (SPH) approach undertaken to simulate a fluid bolus inside the airway-skin mesh. The kinematics of the model geometry (including timings) characterized by changes in volume and shape, drive the coupled airway-skin that in turn mobilizes the simulated bolus. Boluses with standardized viscosity following National Dysphagia Diet Task Force specification [111] is simulated in Section 4.3.2. Finally, Section 4.4 discusses the implications of the bolus simulation and directions for future refinement.

4.1 Deformable Airway Model

Airway is the empty space starting at the tip of the tongue through the oropharynx and ending at the starting of the esophagus. This internal skin surface of the throat and mouth bounds the airway which covers hard and soft palate, tongue, uvula and pharynx. This internal skin is similar to to the external skin of the body but rather than enclosing other anatomical structures, it is enclosed by the surrounding structures. We call it the *airway-skin*. The esophageal part of the airway is not included in our model because we only simulate the oropharyngeal phase of swallowing motion.

The airway-skin describes the deformations of the empty space between the anatomical structures that are deformed (soft tissues like tongue) and translated (bony structures like hyoid) during a swallow motion. As a result, the size, shape and surface area of the airway are greatly influenced by the

movement of the surrounding structures during the swallowing motion. Thus modeling the airway-skin to incorporate the swallowing dynamics poses the following challenges:

- Our model is built as a mixture of rigid bodies and FEMs. So the airway-skin should be influenced by both type of dynamic components.
- The airway-skin changes its shape, size and volume during a swallowing motion. To incorporate the changes the airway-skin should deform at each time step with the underlying model dynamics.
- For simulating a swallow motion using the deforming airway-skin, a bolus is simulated inside the airway-skin. So the airway-skin is required to have watertight geometry and be able to bound the bolus throughout the swallowing motion.
- The bolus is transported from the tongue tip into the pharynx by the explicit force applied to the bolus by the deforming anatomies of the oropharyngeal complex. Thus the airway-skin should allow forces to be transmitted to the bolus, generated by the underlying model kinematics.

The main purpose of the airway-skin is to facilitate the simulation of bolus inside it (discussed in Section 4.2). In the following sections, we discuss our framework to generate a deformable airway-skin model to meet the challenges mentioned above and simulate a bouls inside it.

4.1.1 Airway geometry

The first step is to create the surface geometry of the airway-skin mesh that fits the model at the 0th time instant i.e. initiation of swallowing. Autodesk® Meshmixer®, a freely available tool for 3D modeling, is used to manually create the airway-skin mesh. The airway-skin is confined by the tongue surface and hard palate and progress posteriorly towards oropharynx covering parts of the pharynx. Figure 4.1 show the airway-skin mesh tailored to fit our oropharyngeal biomechanical at the 0th time instant.

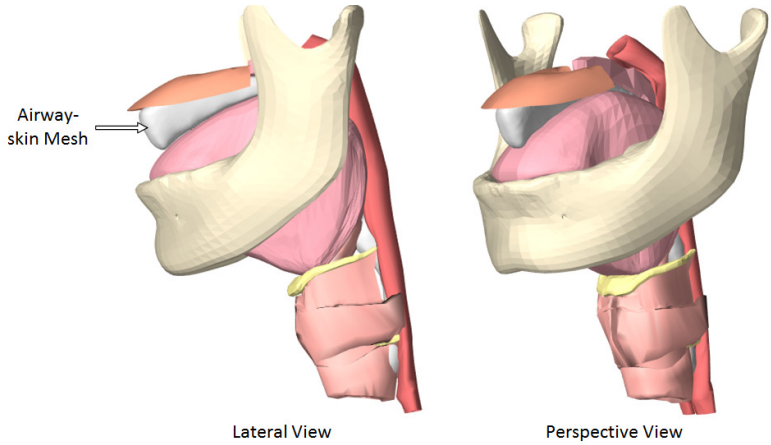

Figure 4.1: Airway-skin mesh coupled with the biomechanical model.

4.1.2 Deforming airway-skin with model dynamics

The airway-skin mesh is attached to the model using ArtiSynth's attachment mechanism. In ArtiSynth, different components, like surface meshes, rigid bodies and FEMs, can be attached by making the position q_a of an attached component to be a function of one or more master components q_m (details are given in [110]). The master component in this case are the dynamic components of the model i.e. FEMs or rigid bodies, and the attached component is the airway-skin mesh. The collective state of the attached component is given by:

$$q_a = f(q_m) \tag{4.1}$$

The relation between the velocity of the master component $\mathbf{u}_m$ and velocity of the attached component $\mathbf{u}_a$ is approximated by differentiating with respect to time.

$$\mathbf{u}_a = \mathbf{G}\mathbf{u}_m \tag{4.2}$$

where

$$\mathbf{G} \equiv \partial f / \partial \mathbf{q}_m \tag{4.3}$$

here $\mathbf{q}_m$ is the position the master component. ArtiSynth uses Equation 4.2 in each step to solve for all dynamic component velocities by applying Equation 4.1.

The airway-skin mesh is attached to underlying dynamic components based on Equation 4.1 by treating each vertex of the mesh as a virtual dynamic component. These virtual dynamic components are attached to one

or more dynamic components i.e. mater components. The master components in this case are 3-DOF FEM nodes and 6-DOF rigid body frames. The unified skinning method [112] is used to deform the airway-skin mesh with model dynamics. The position of each vertex of the airway-skin mesh, q_{as}, is given by:

$$q_{as} = q_{as0} + \sum_{i=1}^{M} w_i f_i\big(q_m, q_{m0}, q_{as0}\big) \tag{4.4}$$

where q_{as0} is the initial position of the airway-skin point, q_{m0} is the collective rest state of q_m, w_i is the skinning weight associated with the ith master component, and f_i is the corresponding blending function.

The bending function f_i for a FEM node is the its displacement from its initial position $\mathbf{q}_{i0}$ and is given by

$$f_i\big(\mathbf{q}_m, \mathbf{q}_{m0}, \mathbf{q}_{as0}\big) = \mathbf{q}_i - \mathbf{q}_{i0} \tag{4.5}$$

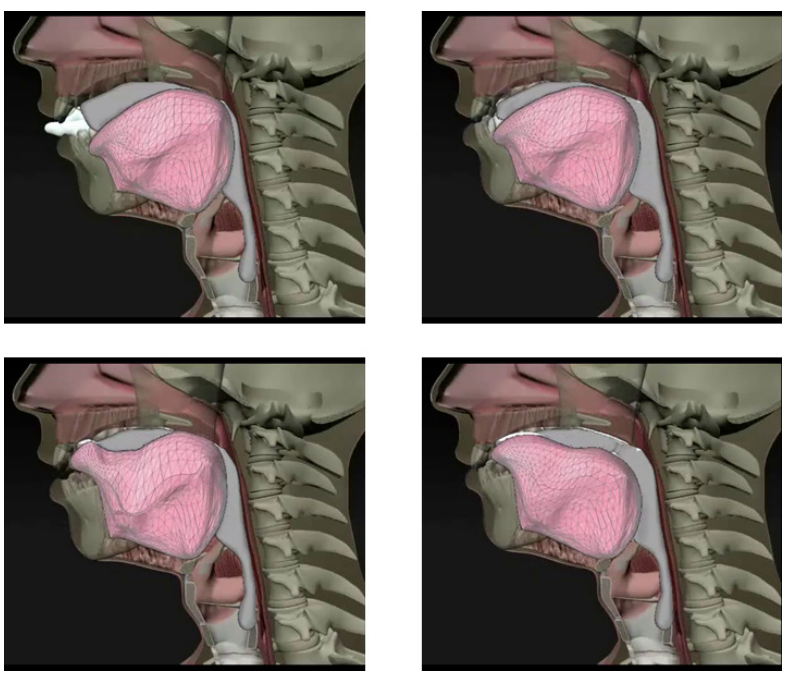

Figure 4.2: Deformable airway-skin model attached to the dynamic model components. The deformation of the airway-skin is influenced by the movement of surrounding anatomical structures during a swallowing motion.

When considering a rigid body as a master component, the blending function is given for linear and dual-quaternion linear blending. For linear blending

$$f_i\big(\mathbf{q}_m, \mathbf{q}_{m0}, \mathbf{q}_{as0}\big) = \hat{\mathbf{q}}_i \mathbf{q}_{as0} \hat{\mathbf{q}}_i{}^{-1} - \mathbf{q}_{as0} \tag{4.6}$$

where quaternion product $\mathbf{q} = \big(\hat{\mathbf{q}\mathbf{q}_0{}^{-1}}\big)$ is the relative control frame transform applied to the initial vertex location $\mathbf{q}_{as0}$. Considering the ith component, the blending function is given as

$$\hat{\mathbf{q}}_i = \mathbf{q}_i \mathbf{q}_{i0}{}^{-1} \tag{4.7}$$

Now for dual-quaternion linear blending f_i us expressed as

$$f_i\big(\mathbf{q}_m, \mathbf{q}_{m0}, \mathbf{q}_{as0}\big) = \tilde{\mathbf{q}}_i \mathbf{q}_{as0} \tilde{\mathbf{q}}_i{}^{-1} - \mathbf{q}_{as0} \tag{4.8}$$

where

$$\tilde{\mathbf{q}}_i = \frac{\mathbf{q}_i \mathbf{q}_{i0}{}^{-1}}{\| \sum_{j=1}^{M} w_j \mathbf{q}_j \mathbf{q}_{j0}{}^{-1} \|} \tag{4.9}$$

For more details on duel-quaternion blending please refer to [113]. The resulting airway-skin provides a bi-directional coupling that allows forces to be transmitted back and forth between the skin mesh and underlying dynamic components (see Figure 4.2).

4.2 Bolus Simulation Using SPH

Smoothed Particle Hydrodynamics (SPH) was designed to solve the hydrodynamic problems represented in the form of partial differential equations(PDE). These PDEs consists of field variables of the fluid (or solid) such as density, velocity, energy and so on. For obtaining analytical solutions for the PDEs, the problem domain is discretized at the beginning. After that, approximating of the values of the field functions and their derivatives at each point is assigned. This functional approximation is applied to the PDEs to formulate the ordinary differential equations in a discrete fashion with respect to time. Now these discretized ODEs are solved with conventional finite difference methods. The following list outline the key steps for obtaining analytical solutions for the set of PDEs using SPH. Mathematical formulation of these steps are discussed in details in the Appendix B.

1. **Meshfree representation:** If the problem domain is not represented with particles, it is described using a set of discrete arbitrarily distributed particles which are not connected by any computational mesh.

2. **Integral function representation:** In SPH methodology integral function representation is termed as kernel approximation which is used for approximating field function. This mathematically provides the necessary stability for SPH method. The integral representation behaves as a weak formulation as it has smoothing effect. Such weak formulation make the method robust as long as the numerical integration is performed correctly.

3. **Compact support:** The kernels are approximated further using particles and termed as particle approximation in SPH methodology. This approximations are achieved by substituting the integral representation of the field functions and its derivatives with summations of field values of the neighbouring particles in the support domain (the domain of influence or local domain). This approximation is very important because problems with large deformation requires high resolution simulations which means higher number of particles. With support domain, system matrices are sparse discretized to help reduce computation effort.

4. **Adaptive approximation:** In each time step, the compact support for the particle approximation method is calculated. Therefore, the local distribution of the particles contributes to particle approximation and it becomes adaptive. This adaptive approximations at the early stage of the field variable approximation allow arbitrary particle distribution and ensures that the SPH formulation can handle problems with large deformations.

5. **Lagrangian discretization:** The particle approximations are applied to the field functions in the PDEs to formulate a set of discretized ODEs with respect to time. This Lagrangian description allows the SPH method to have all the advantages of Lagrangian descriptions listed in Table 2.1.

6. **Dynamic solver:** To obtain the time history of the field variables for the particles, the discretized ODEs are solved using an explicit integration technique for achieving fast time stepping. To ensure stable

time integration, its important to select correct time step which can depend on the problem description.

The aforementioned features make the SPH method an attractive choice for simulating bolus. Detailed formulation for implementing SPH solver is discussed in Appendix B.

4.2.1 Artificial viscosity term

The viscosity of a simulated SPH fluid is modeled by a artificial viscosity term. Hydrodynamic simulation sometime include shock wave that develop nonphysical oscillations in the numerical results. Shock wave introduces a propagating disturbance in a fluid when a wave moves faster than the speed of sound in that fluid. Like ordinary waves shock wave carries energy and can propagate through a medium. The conservation of mass, momentum and energy equation requires simulation of energy transformation from kinetic form into heat form. This energy transformation can be physically represented as a form of viscous dissipation. This let to the idea of artificial viscosity term developed called von Neumann-Richtmyer artificial viscosity [114]. This von Neumann-Richtmyer artificial viscosity, Π_1 is a quadratic expression of velocity divergence, which is given by

$$\Pi_1 = \begin{cases} a_1 \Delta x^2 \rho (\nabla \cdot \mathbf{v})^2 & \nabla \cdot \mathbf{v} < 0 \\ 0 & \nabla \cdot \mathbf{v} \geq 0 \end{cases} \tag{4.10}$$

where a_1 is an adjustable non-dimensional constant.

By adding a liner viscosity term Π_2, the oscillation of the numerical results are further smoothed that are not damped by the quadratic artificial viscosity term.

$$\Pi_2 = \begin{cases} a_2 \Delta x c \rho \nabla \cdot \mathbf{v} & \nabla \cdot < 0 \\ 0 & \nabla \cdot \geq 0 \end{cases} \tag{4.11}$$

The above equitation introduces a new terms c, which is called the speed of sound and a_2 which is an adjustable non-dimensional constant. The combination of von Neumann-Richtmyer viscosity Π_1 and linear viscosity Π_2 are widely used for removing shock wave related oscillations in hydrodynamic simulation. Intuitively, the artificial viscosity term spreads the shock wave

over several cells and regularize the numerical instability caused by discontinuity. This term is added to the pressure term to help diffuse sharp variation in the flow and diffuse the energy of the high frequency term.

Monaghan and Gingold [107] also developed an artificial viscosity for SPH methods for simulating shocks and discontinuity. The detailed formulation for Monaghan artificial viscosity is given in Chapter 4 of [115]. In summary the Monaghan artificial viscosity Π_{ij} is given as

$$\Pi_{ij} = \begin{cases} \dfrac{-\alpha_\Pi \bar{c}_{ij}\phi_{ij} + \beta_\Pi \phi_{ij}^2}{\bar{\rho_{ij}}} & \mathbf{v}_{ij} \cdot \mathbf{x}_{ij} < 0 \\ 0 & \mathbf{v}_{ij} \cdot \mathbf{x}_{ij} \geq 0 \end{cases} \tag{4.12}$$

where

$$\phi_{ij} = \frac{h_{ij}\mathbf{v}_{ij} \cdot \mathbf{x}_{ij}}{\mid \mathbf{x}_{ij} \mid^2 + \varphi^2} \tag{4.13}$$

$$\bar{c}_{ij} = \frac{1}{2}\big(c_i + c_j\big) \tag{4.14}$$

$$\bar{\rho}_{ij} = \frac{1}{2}\big(\rho_i + \rho_j\big) \tag{4.15}$$

$$h_{ij} = \frac{1}{2}\big(h_i + h_j\big) \tag{4.16}$$

$$\mathbf{v}_{ij} = \mathbf{v}_i - \mathbf{v}_j \,\text{and}\, \mathbf{x}_{ij} = \mathbf{x}_i - \mathbf{x}_j \tag{4.17}$$

In the above equation α_Π and β_Π are constants whos values are set around 1. The viscosity associated with α_Π results in bulk viscosity and β_Π is similar to the von Neumann-Richtmyer artificial viscosity. c and v represent speed of sound and velocity respectively. When two particles are approaching each other, to prevent numerical divergence, φ is assumed to be $0.1h_{ij}$. The artificial viscosity given by Equation 4.12 is added to pressure terms in the SPH equations.

4.2.2 Artificial compressibility

In SPH formulation the particle motion is driven by pressure gradient. The particle pressure is calculated by the local particle density and internal energy through the equation of state. For the incompressible flows the equation of

state leads to extremely small time step which causes numerical instability (discussed in Section 4.2.3). An artificial compressibility term is introduced for simulating incompressible fluids with numerical stability. The concept of artificial compressibility assumes that every theoretically incompressible fluid is actually compressible. The artificial compressibility term is introduced to produce the time derivative of pressure. Monaghan [116] used the following equation to model free surface flow which is originally the equation of state of water:

$$p = B\left((\frac{\rho}{\rho_0})^{\gamma} - 1 \right) \tag{4.18}$$

where γ is set to be 7 empirically and ρ_0 is the reference density. B is a problem dependent parameter which sets a limit for the maximum change of density. Practically B is taken as the initial pressure [108]. In the Equation 4.18, 1 is subtracted to remove the boundary effect for free surface flow. Further this equation also shows that small change in the density results in a large variation of pressure.

The artificial compressibility can also be represented by the following relation

$$p = c^2 \rho \tag{4.19}$$

where c is speed of sound. Morris et al. [108] used this equation of state for modeling incompressible flows using SPH. The SPH simulation results presented in this thesis use this relation to enforce incompressibility.

The speed of sound is an important parameter for simulating a fluid using SPH formulation. For example, the actual speed of sound for water under standard pressure and temperature is $1480 m/s$. If this actual speed of sound is incorporated, a real fluid is approximated as an artificial fluid. Monaghan [116] described the density variation δ as

$$\delta = \frac{\Delta\rho}{\rho_0} = \frac{|\rho - \rho_0|}{\rho_0} = \frac{V_b^2}{c^2} = M^2 \tag{4.20}$$

where v_b is the fluid bulk viscosity and M is the Mach number which is a dimensionless quantity representing the ratio of flow velocity past a boundary to the speed of sound c in that medium. As the speed of the sound is large, the corresponding Mach number is very small. As a result, the density variation δ becomes negligible and to approximate a real fluid as an artificial incompressible fluid a much smaller speed of sound term in used. However, the speed of sound term should be large enough to make the behaviour of

the simulated fluid realistic and small enough that computation time step is computationally realistic (see Section 4.2.3). So the speed of sound should be selected in such a way that it balances the time step selection and the incompressible behaviour. Morris et al. [108] considered the balance of pressure, viscous force and body force to estimate the optimal value of the sound of speed term described by the following equation

$$c^2 = \max\left(\frac{v_b^2}{\delta}, \frac{\upsilon V_b}{\delta L}, \frac{FL}{\delta}\right) \tag{4.21}$$

where υ is the kinematic viscosity defined as $\upsilon = \mu/\rho$, F is the body force and L is the characteristic length scale. The speed of sound term was chosen carefully to maintain the stability of the simulation.

4.2.3 Time step selection

SPH formulation reduces the equations of fluid dynamics to a set of ODE of motion of the discrete particles. The discrete SPH equations are integrated with standard methods like Runge-Kutta (RK) method and so on. This step is computationally expensive which requires several evaluation of the force term at each time step.

The Courant–Friedrichs–Lewy (CFL) condition is a necessary condition for convergence while solving certain partial differential equations numerically by finite differences methods. The explicit time integration schemes are subject to the CFL condition for stability. The CFL condition states that a time step bigger than some computable quantity should not be taken. Which in other words mean that the time step must be kept small enough so that information has enough time to propagate through the space discretization. So the numerical simulation should include the physical domain of dependence, or the maximum speed of numerical propagation must exceed the maximum speed of physical propagation [95]. The CFL conditions requires the time step to be proportional to the smallest particle resolution which in SPH formulation is the smallest smoothing length. The time step Δt can be denoted as

$$\Delta t = \min\left(\frac{h_i}{c}\right) \tag{4.22}$$

Monaghan [116] suggested the following equation for selecting the time

step considering viscous dissipation $\Delta t_{c\nu}$ and external force Δt_f

$$\Delta t_{c\nu} = \min\left(\frac{h_i}{c_i + 0.6\big(\alpha_\Pi c_i + \beta_\Pi \max(\phi_{ij})\big)}\right) \tag{4.23}$$

$$\Delta t_f = \min\big(\frac{h_i}{f_i}\big)^{\frac{1}{2}} \tag{4.24}$$

where f is the magnitude of force per unit mass i.e. acceleration. It can be seen that Equation 4.23 is another representation of Equation 4.22 by adding the viscous force term. Typically time step is calculated taking the minimum of both of the time step terms using the following equation

$$\Delta t = \min\big(\lambda_1 \Delta t_{c\nu}, \lambda_2 \Delta t_f\big) \tag{4.25}$$

here λ_1 and λ_2 are coefficient which are empirically chosen to be 0.4 and 0.25 respectively.

Time step is estimated in this Thesis following the formulation of Morris et al. [108] considering viscous diffution

$$\Delta t = 0.125\frac{h^2}{\nu} \tag{4.26}$$

where ν is the kinematic viscosity defined by $\nu = \mu/\rho$.

4.2.4 Boundary treatment

Boundary treatment is an important consideration for SPH formulation. The particles near the boundary face a problem called *particle deficiency* which is due to truncated neighbourhood boundary. When a particles is near the boundary, only particles inside the boundary contributes to the summation of particle interaction even if that particles smoothing kernel expands beyond the boundary. Such assumptions lead to incorrect solution because on solid surfaces outside the boundary, all the field variable are not zero. For example, on the solid surface the velocity is zero but density do not necessarily reduce to zero. Monaghan [116] placed line of ghost particles on boundary which produces a highly repulsive force to the particles near the boundary. These ghost or dummy particles prevent the simulated SPH particles to penetrate the solid boundary emulating a solid surface. Some improvement are also proposed in simulating the dummy boundary particles.

To solve the particle deficiency problem, two different type of dummy particles are simulated (see Figure 4.3) which are called *type I* and *type II* particles. Type I particles are similar to the Monaghan type ghost particles which are located right on the solid boundary. The type II particles are located right outside the boundary. These two types of dummy particles are specially marked for contribution in the later summation on the SPH particles. For a simulated SPH particle i which is located within the distance κh_i from the boundary, a dummy particle is placed symmetrically on the outside of the boundary. So for a SPH particle i near the boundary, all the neighbouring particles within its influence are defined by radius κh_i can be divided into following three categories (see Figure 4.3):

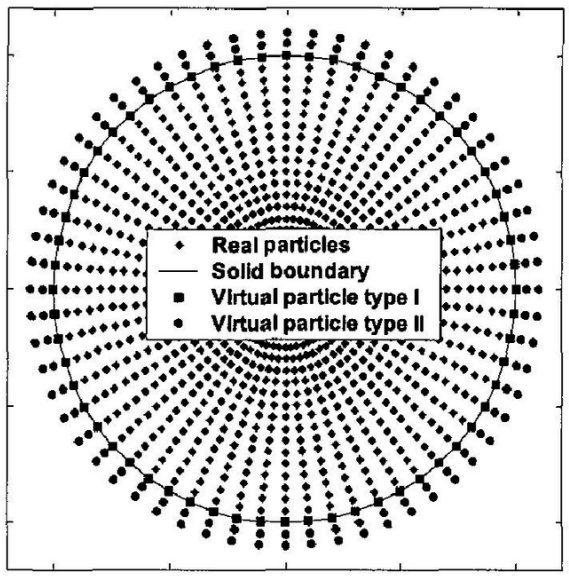

Figure 4.3: Illustration of real particles and the two types of virtual particles used for simulating the solid boundary. Adapted from [115].

1. **Interior particles:** All the SPH particles inside the neighbourhood of particle i. These particles are defined as $I(i)$.

2. **Boundary particles:** All the dummy particles simulated right on the solid boundary that are in the neighbourhood of particle i. These are the type I dummy particles denoted by $B(i)$. These type of particles take part in the kernel and particle approximation (see Appendix B

for detailed formulation) of the simulated SPH particles. The position and the physical variables of these dummy particles do not change in the simulation process. Furthermore, these particles apply repulsive boundary forces to prevent the SPH particles from penetrating the solid boundary. When a SPH particle is approaching a type I boundary particle, a force is applied pair-wisely along the centerline of these two particles. The force PB_{ij} is defined as

$$PB_{ij} = \begin{cases} D\left[(\frac{r_0}{r_{ij}})^{n_1} - (\frac{r_0}{r_{ij}})^{n_2}\right]\frac{x_{ij}}{r_{ij}^2} & (\frac{r_0}{r_{ij}}) \leq 1 \\ 0, & (\frac{r_0}{r_{ij}}) \geq 1 \end{cases} \tag{4.27}$$

where n_1 and n_2 are selected to be 12 and 4 respectively. D is a problem dependent parameter and chosen at the same scale as the square of the largest velocity. r_ij is the distance between the SPH particle and the boundary particle in question. The repulsive force is coordinated by r_0 which is defined as the cutoff distance. It effectively chosen to be equal to the initial particle spacing which means that if a SPH particle comes closer to the boundary than the initial particle spacing, the dummy particles would apply a repulsive force to establish a solid surface. Thus the choice of cutoff distance r_0 is important because if its chosen to be to large, some particles in the initial distribution may be subject to repulsive boundary condition. On the other hand, if the cut off distance r_0 is too small, the SPH particle may penetrate the solid boundary before even feeling the repulsive force.

3. **Exterior particles:** All the dummy particles simulated outside the solid boundary that are in the neighbourhood of particle i. These are the type II dummy particles denoted by $E(i)$ which can both be applied to treat solid boundaries and free surfaces. The dummy particles have the same density and pressure as the corresponding SPH particle with opposite velocity. The numerical tests [115] have shown that this treatment of the boundary is very stable and effective. It not only improves the accuracy of the SPH approximation in the boundary region, but also prevents the unphysical particle penetration outside the solid boundary.

In this Thesis, the SPH boundary particles are simulated as following the

Unified-semi-anatytic wall boundary conditions proposed by Ferrand et al [117].

As we drive our model kinematically, the SPH particles are only influenced by the movement of the OPAL structures, and not the other way around in which the SPH particles can apply forces back and influence the model dynamics. We are modeling the kinematic trajectories of the 3D surfaces as they move, rather than modeling the influence the fluid has on the dynamic structures.

4.3 Results and Analysis

The kinematically driven biomechanical model developed in Chapter 3 was build using ArtiSynth (www.artisynth.org) [110]. The SPH simulation is also performed using ArtiSynth with the formulation described in [118]. The SPH particles carry estimated physical quantities, e.g. velocity, density, pressure, by approximating values and derivatives of discrete samples of field quantities. These particles are analogous to particles occupying a fraction of the fluid domain and produce accurate results if the particles are dense i.e. high resolution.

4.3.1 Simulation of a stable bolus

The Navier-Stokes equations for a incompressible Lagrangian system can be written as:

$$\frac{D\mathbf{v}}{Dt} = -\frac{1}{\rho}\nabla p + \frac{1}{\rho}(\nabla \cdot \mu\nabla)\mathbf{v} + \mathbf{B}, \tag{4.28}$$

$$\frac{D\rho}{Dt} + \rho\nabla \cdot \mathbf{v} = 0, \tag{4.29}$$

where $\mathbf{v}$ is the velocity, ρ is the density, p is the pressure, μ is the Newtonian viscosity of the fluid and $\mathbf{B}$ is the body force per unit mass. We solve Equations 4.28 and 4.29 explicitly with an artificial speed of sound term using SPH approximations. Here the body force B is generated by the dynamics of the swallowing model i.e. movement of the tongue during swallowing. The force is propagated through the deforming boundaries of airway-skin mesh

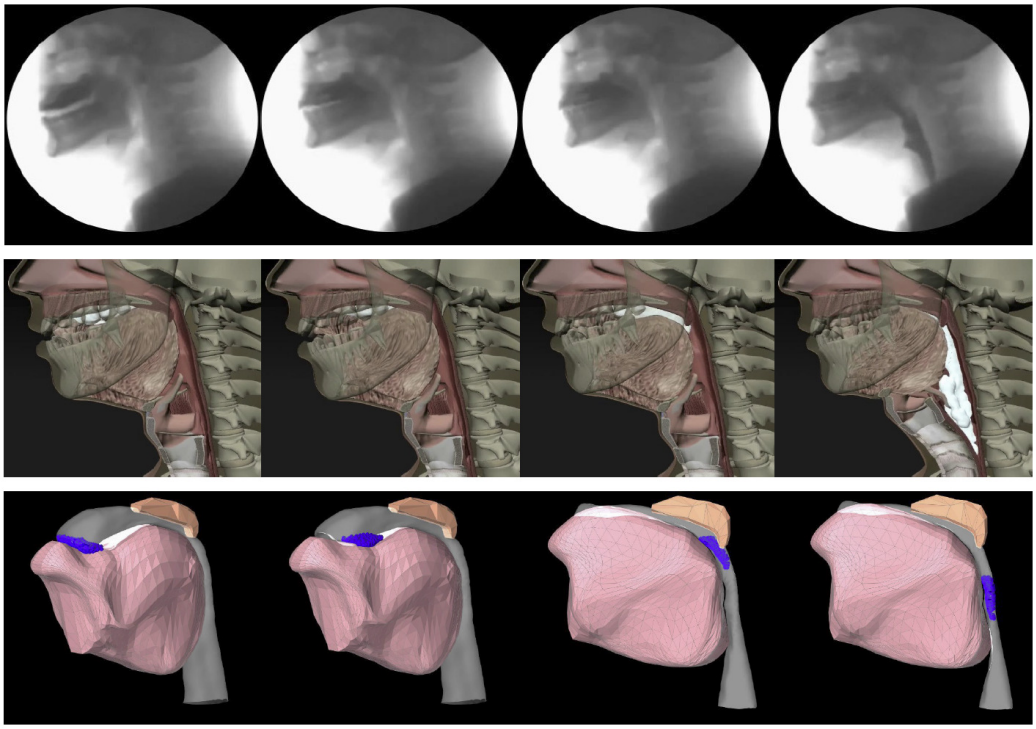

Figure 4.4: Comparing simulation results: Top row VF frames of a normal swallow, middle row 2D swallowing animation frames (bolus shown in white), and bottom row simulated SPH fluid bolus (in blue).

(discussed in Section 4.1) and is applied to the SPH particles simulated inside. Velocity, $\mathbf{v}$, of each particle is solved for each time step and the position of each particle is advanced accordingly.

The airway-skin mesh (derived in Section 4.1) acts as the boundary for the SPH formulation. SPH bolus particles are simulated inside the deforming airway-skin mesh. The boundary particles are simulated at the surface of the airway-skin mesh and the exterior particles are simulated outside the solid boundary of the surface of airway-skin mesh. These special particles enforces boundary conditions for the SPH simulation. These particles apply repulsive forces to the SPH particles that come closer to the boundary more than the initial inter-particle spacing. As a result the SPH particles move to represent the bolus movement with the deforming airway-skin mesh. The simulation is advanced using small time steps to maintain simulation stability.

Typically during a swallowing examination, patients are presented with

a 5-mL teaspoon of bolus. The simulated bolus was made to emulated the physical properties of a real bolus used during an MBS examination. The SPH particles are simulated with an initial inter-particle spacing of 2 mm with 621 fluid particles simulating about 5 mL of fluid inside the deforming airway-skin mesh. The viscosity μ, of the fluid was set to be 1000 centipoise(cP), similar to a thick fluid like honey with the density ρ initialized at 1000 kg/m^3. We applied a gravitation force from a superior to inferior direction, equivalent to someone swallowing in an upright position.

Figure 4.4 compares the instances of our simulation with the corresponding frames of VF and animation. The results show that our model is capable of simulating a bolus in a manner consistent with the input data and match the swallowing kinematics identified in the animations. The airway-skin was able to contain the bolus and allowed the model dynamics to apply forces on the SPH particles. Even though, we did not explicitly define a soft plate in this model, the airway skin provided the necessary boundary to restrict the fluid particles from entering the nasopharynx.

4.3.2 Simulating bolus with standardized consistencies

Diet adjustments are sometimes recommended for dysphagia patients to help maintain their nutritional needs. For instance, thinner liquids like water may be difficult to swallow safely if the patient has a delayed pharyngeal swallow or oral motor impairment [18]. Adjusting the diet by thickening the thin liquid may alleviate the swallowing impairment and minimize chances of aspiration. Clinical observations [119; 120] support the hypothesis that increase in bolus viscosity increase patient effort with positive effects on tongue base and pharyngeal wall movement in some dysphagic patients. It is presumed that increase in these clearance mechanisms are related to sensorimotor adaptations. We tested our model's capability of simulating fluid with different consistencies (i.e. viscosity) by simulating 4 boluses with different dynamic viscosity each representing standardized bolus consistency in context with dysphagia. The standardized bolus consistencies instituted by the National Dysphagia Diet [111] task force are as follows:

- Thin, 1050 centiPoise (cP)
- Nectar-like, 51–350 cP

- Honey-like, 351–1,750 cP
- Spoon-thick, >1,750 cP

We simulated each type of bolus with the same set of solid boundary motions provided by the airway-skin mesh. Qualitative observations indicate that the thinnest bolus (i.e. water-like) escapes the oral cavity with the greatest and the thickest one (i.e. spoon-thick) with the least velocity, and the intermediate ones follow the sequence. This result is intuitive since we expect our model to simulate significantly different bolus positions and track the mass of the bolus, when the viscosity of the fluid is changed for the same set of kinematics.

4.4 Summary

We demonstrated that our model is capable of simulating SPH bolus stably and is capable of simulating boluses with different viscosity. This sets up the ground work for investigating the influence of bolus on structural movement with a modeling based approach. Further refinement of our model will include simulation of aspiration risk related to abnormal changes in dynamic swallowing movement(s) for different volumes and viscosity. Our future directions will include development of models that predict the effect of targeted treatment(s) on the dynamic movement of swallowing structures and airway protection. Model development of normal swallowing and dysphagic patient specific impairment models are first steps toward this long range goal.

Chapter 5

Extending Standardized Dysphagia Training Materials

In the previous two Chapters, we developed a full 3D biomechanical model of the oropharyngeal complex (see Chapter 3) and simulated a fluid bolus driven by the kinematics of the model. This chapter discusses about the user study conducted in this Thesis. The study was deigned to assess, evaluate, quantify and gather feedback from the expert clinicians about the additional value our model can add to the clinician training for standardized dysphagia diagnosis. The first section of this chapter identifies the clinical collaborators who helped to carry out the user study. Following that, the two phase user study is discussed in details in the later sections. Finally, at the end of this chapter, the findings of the study, recommendation from the expert clinicians and concluding remarks are made.

5.1 Clinical Collaborators

Dr. Bonnie Martin-Harris from Medical University of South Carolina (MUSC), SC, USA provided the videofluoroscopy data used in the MBSImP™© online training platform as a part of our ongoing collaboration. We used this data to formulate our study design and conduct a pilot stusy. This data sharing met the minimal risk human ethics application criteria and thus an expedited review by the UBC Clinical Research Ethics Board(CREB) was conducted (UBC CREB number H15-02749).

5.2 Study Design

The study was divided into two major phases. During the first phase we contacted the SLPs from the local affiliated hospitals and asked to meet them for an interview. During this interviews, the SLPs were asked if extension

of the training materials for MBSImP™© i.e. additional 3D visualization can contribute to standardized training of dysphagia. Based on the feedback from the first phase we conduct a formal user study to access if enhanced visualization provided by 3D biomechanical models add value in clinician training for standardized dysphagia diagnosis. This user study met the minimal risk human ethics application criteria and thus expedited review by the UBC Behavioural Research Ethics Board (BREB) was conducted (UBC BREB number H15-02665).

5.3 Phase I- Interviewing the Stakeholders

The aim of this phase of the user study is to do a feasibility analysis of our developed biomechanical modeling approach for complementing the VF and animation video used in standardized dysphagia diagnosis training. The primary stakeholders are the Speech Language Pathologists. A series of interviews were conducted to collect feedback from SLPs to justify the feasibility analysis. All of the clinicians interviewed during this phase were registered MBSImP™© registered professionals which means after finishing the training, they passed the reliability testing with 80% or higher. The reason behind conducting the interviews were three fold.

1. To evaluate the effectiveness of current state-of-the-art dysphagia training.

2. To analyze the role of visualization in swallowing assessment examination.

3. To identify areas of swallowing continuum where biomechanical modeling can provide additional visualization and flexibility for assisting dysphagia training.

SLPs affiliated with St. Paul's Hospital, Vancouver, BC, Canada and Richmond Hospital, Richmond, BC, Canada was interviewed during the Phase-I of the study where we conducted series of interviews were conducted.

When we interviewed the SLPs, we asked the following question:

- When did you take MBSImP™© course?

- Why did you take this course?

- How does MBSImP™© help you professionally?
- What do you think was the most important part of the training?
- Do use the MBSImP™© 17 component grading system in your current practice?
- How has the training improved/changed/not-changed your practice?
- What swallowing impairments are easy to score?
- What swallowing impairments are hard to score?
- In your opinion, what type of visualization for training would help to better comprehend swallowing in order to evaluate dysphagia?
- What features did you wish existed in existing training system?
- What improvements would you love to have?

The first few questions were set to get an idea about SLP training. These questions helped us better understand the importance of swallowing impairment standardization and how state-of-the-art training is helping the SLPs follow the standardization in real practice. This discussion set up the stage for the discussion about the research question that "can additional visualization / tools add value to the training". While discussing about the following questions, we wanted their expert opinion to justify the need for additional visualization (3D perspective view) and flexibility (simulating different bolus consistencies) in dysphagia training. The feedback from the interviews are summarized under the following headings:

Standardized MBSS as a tool for swallowing assessment

All participating clinicians acknowledged that there are several techniques like MBS, FEES or bedside swallowing assessment for evaluating a dysphagic swallow. However, they also acknowledged that an MBS examination is preferred because it is standardized with the MBSImP™© protocol. After an MBS study is performed and scored using the MBSImP™© protocol, the SLPs recommend diet modification, tongue exercises and/or other procedures to alleviate the swallowing abnormality. The participating SLPs mentioned

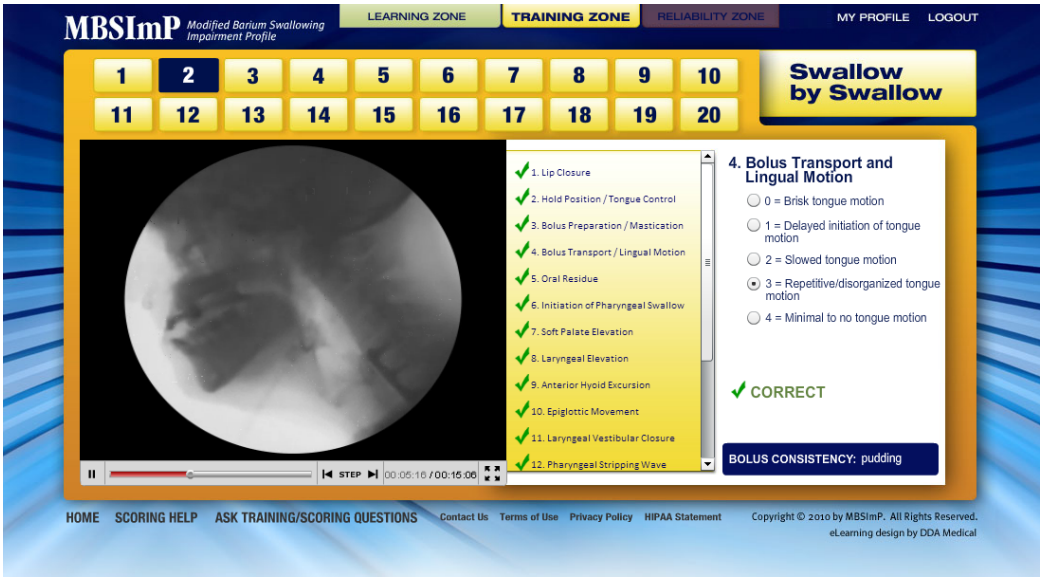

Figure 5.1: Example of videofluoroscopic and animated images used during MBSImP™© web-based training program. Image reproduced from MBSImP™© online training [76] with permission.

that such standardization helps them teach new SLPs about accessing different swallowing impairment. They also mentioned that MBSImP™© standardization makes it easier to communicate the patient swallow scores and enabled them to keep track of patient improvement quantitatively.

The clinicians were also asked about their experience with the MBSImP™© online training platform. Figure 5.1 shows the existing user interface of the online training. The participating clinicians registered for a seminar followed by the online course itself. The seminar is designed to give the trainee SLPs orientation about the MBSImP™© protocol. After that the SLPs started doing the formal online training followed by reliability testing. The participating clinicians appreciated the structured nature of the course and found that the swallowing animations used in training were able to illustrate the salient features of a swallow sufficiently to discern between a normal and impaired swallow. However, the participating clinicians also pointed out that sometimes the movement of the bolus and corresponding anatomical structures are not realistic. It is important to note that the bolus and structural movements in the animation are unrealistic as they are not bounded by the laws of physics even if they are fine tuned to match the VF of a patient swal-

low. They suggested that if the additional visualization provided with the VF during training were more realistic, it might contribute in the clinician training.

Most difficult physiologic swallowing component to score

The participating clinicians were asked to pick three components that they find easiest and hardest to score using current training protocol. The components the clinicians thought were easiest to score were: Component 1 - lip closure (Lip C), Component 2 - hold position/tongue control (HP), Component 9 - anterior hyoid motion (HM). The clinicians listed Component 4 - Bolus transport/lingual motion(BT), Component 5 Oral Residue, Component 13 - Pharyngeal Contraction (PC) as hardest to score. This line of questioning allowed a discussion to figure out why some components are easier to score and why some are not, and if the visualization used during the training contributed to it. Furthermore, this discussion set up the stage for addressing the need of additional visualization in the current MBSImP™© training protocol.

5.4 Phase II - User Study

The clinicians with MBSImP™© certification are required to have $\geq 80\%$ accuracy in training to be considered reliable. During field observations by our collaborators who instituted this protocol, it was found that some swallowing components are harder to score accurately than others. To identify the components with greatest level of difficulty we analyzed the MBSImP™© reliability test metrics in September 2015 [121]. This included 7441 test sessions 18328 individual component scores scored by 3461 trainees since the creation of the database in 2011. It was found that the physiologic components of the oral domain are most difficult to score. Furthermore, Component 4- Bolus Transport/Lingual Motion showed 55% accuracy in all test session making it the most difficult component to score.

The explanation behind this may be the oral phase of swallowing is largely controlled by voluntary movements of oropharyngeal muscle and structures. For example, tongue motion is largely controlled by voluntary motion which has a high variability among subject population. Due to such high variability the oral components are sometimes harder to score in a standardized

manner. On the other hand, although pharyngeal phase of swallow is more complicated and require intricate coordination, pharyngeal phase of swallow is largely controlled by involuntary muscle and structures. As a result, variability in patient population is lesser compared to that of oral components.

The state-of-the-art standardized dysphagia training module, MBSImP™©, includes videofluoroscopy (VF) and corresponding 2D animations of swallowing. However, during Phase I of the user study and the reliability data from MBSImP™© online training platform suggests that clinicians have most difficulty scoring oral components, particularly Component 4 – Bolus Transport/Lingual Motion, even though some pharyngeal components are often regarded as most complicated to comprehend. The training materials available as a aid for scoring the Component 4 and other oral components are captured from lateral mid-sagittal cut plane. So we concluded that training material itself might be a factor contributing to the complexity of scoring oral components.

5.4.1 Methodology

The goal of this study is to investigate if additional 3D visualizing during clinician training learning standardized dysphagia diagnosis, adds value in the training, and help the trainees to appreciate the swallowing anatomy and physiology in three dimension to better detail the physiologic characteristics contributing to dysphagia. So it is hypothesised that additional 3D visualization showing the movements of the oropharyngeal structures during a swallowing motion are likely to help clinicians understanding of swallowing dynamics and allow them to score more confidently following standardized dysphagia diagnosis protocol. We selected Component 4 as it has the lowest scoring accuracy to test in our user study. We wanted to know if our assumption that extending the training material by adding 3D perspective visualization can have positive impact and help the clinicians distinguish between different impairments of component 4.

Component 4 - Bolus Transport/Lingual Motion is evaluated at the onset of productive tongue movement to propel the bolus through the oral cavity. Component score definition for Bolus Transport/Lingual Motion are listed below:

(4–0) Brisk tongue motion – The movement of the tongue is brisk and timely without any hesitation that results in good bolus transport.

(4–1) Delayed initiation of tongue motion – To transport the bolus

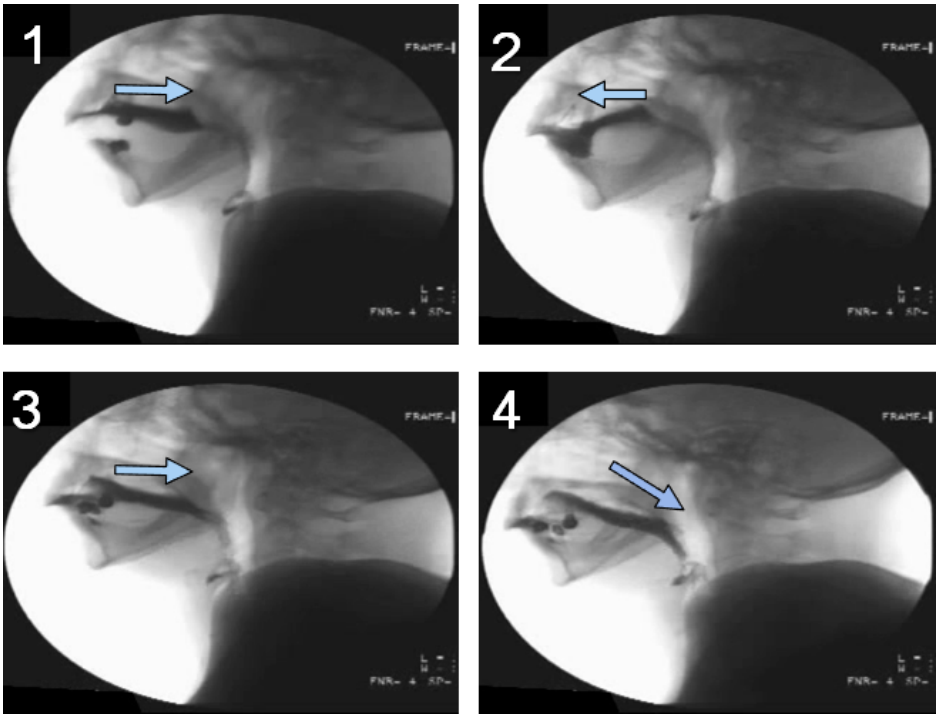

Figure 5.2: For a sore of 3 of Component 4, the tongue and the bolus moves back and fourth within the oral cavity before moving the bolus into the pharynx. On the other hand, if the bolus is slowly manipulated but progresses through the oral cavity in a single direction toward the pharynx, it is a score of 2 for Component 4.

through oral cavity, the patient requires multiple cues to initiate movement of the tongue. However, once initiated, the bolus progresses normally.

(4–2) Slowed tongue motion – The tongue motion is slow and weak. Despite the slow tongue movement, the tongue provides a productive posterior ward motion to propel the bolus through the oral cavity.

(4–3) Repetitive/disorganized motion – The tongue move back and forth moving the bolus anteriorly and posteriorly before transporting the bolus through oral cavity.

(4–4) Minimal to no tongue motion – There is minimal or no tongue motion despite cuing.

With respect to Component 4, a score of 0, 1 and 4 are usually apparent. This is because brisk, delayed or minimal tongue motion is usually easier

to identify. However, while differentiating between a score of 2 and 3, it is some what more difficult to discern between slowed and repetitive tongue motion (see Figure 5.2). This user study is aimed to evaluate if the additional visualization and flexibility provided by our 3D model can add value to the SLPs training learning standardized dysphagia diagnosis protocol. To evaluate the added value, we built an interface similar to the training zone for MBSImP™© online training platform and extended the existing training material available for scoring Component 4 - Bolus Transport/Lingual Motion. With the interface we performed a user study involving SLPs where they scored with the additional visualization provided for component 4.

We used our model to generate 3 different views from prospective 3D viewpoints for all five scores of Component – 4. These viewpoints were selected to enhance the salient feature of the individual components scores and were carefully selected and reviewed by our expert clinical collaborators.

5.4.2 Participant selection criteria

Study population for this study is was narrow due to the selection criteria and feasibility to conduct the study. We wanted to recruit SLPs with MBSImP™© experience for participation. So we contacted the SLP department of the major health-care facilities located Vancouver, BC, Canada. In the scope of this Thesis, only recruiting SLPs in the Vancouver was feasible for logistics issues. We advertised about the user study across health-care facilities in Vancouver, BC, Canada. We recruited participants from St. Paul's Hospital, Richmond Hospital, Lions Gate Hospital, GF Strong Rehabilitation Centre and Royal Columbian Hospital, and were able to recruit 8 participants. Although the there were limited number of participants in the user study, the expert opinion of the SLPs helped used evaluate if there was any additional value added to the training by the 3D views.

5.4.3 User interface

We built an interface that is similar to the existing "swallow by swallow" section in training zone of MBSImP™© protocol (see Figure 5.1). We included 10 MBS studies in the interface and asked the participants to score the first 4 components of the MBSImP™© for each of the 10 cases. The first 4 components are Component 1 – lip closure, Component 2 – tongue control during bolus hold, Component 3 – bolus preparation/mastication and Component

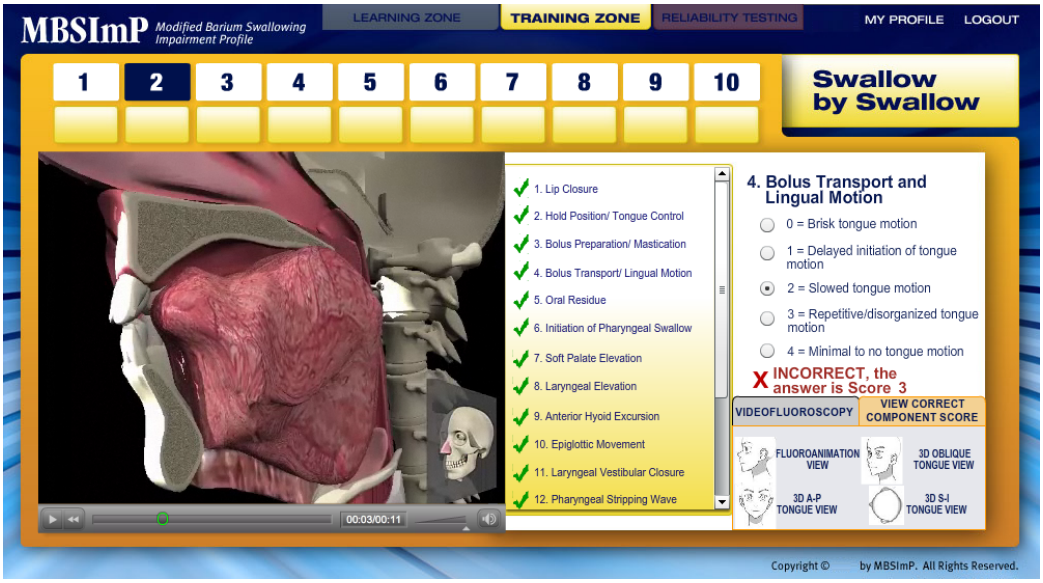

Figure 5.3: Additional 3D views to component the existing training materials for Component 4 was added to the new user interface built for the user study.

4 – bolus transport/lingual motion. While scoring Components 1 through 3, the participant had the option to review the 2D video correct component score animation in case of an incorrect score. This functionality is available in the existing training platform (see Figure 5.3). So the users had access to similar training materials when they were scoring the first 3 components. For component 4 Bolus transport/lingual motion, we included 3 different 3D views called 3D oblique tongue view, 3D A-P tongue view and 3D S-I tongue view in case of an incorrect score. Figure 5.4 shows the same instances of VF with the 3 additional 3D views added as an extension of training material available for scoring normal swallow motion for Component 4. Figure 5.5 makes the same comparisons for an impairment 4-3 (Repetitive/disorganized motion) without the bolus.

The study interface was designed in a way that the additional visualizations for Component 4 is only available when an incorrect score is selected. So if a participant scoreed all the components correctly he/she would not have been exposed to the additional 3D views. To make sure that clinicians are able to give feedback, an interview session was conducted after the participants completed their task and before they started completing the questionnaire. During the interview, the participant were shown different 3D

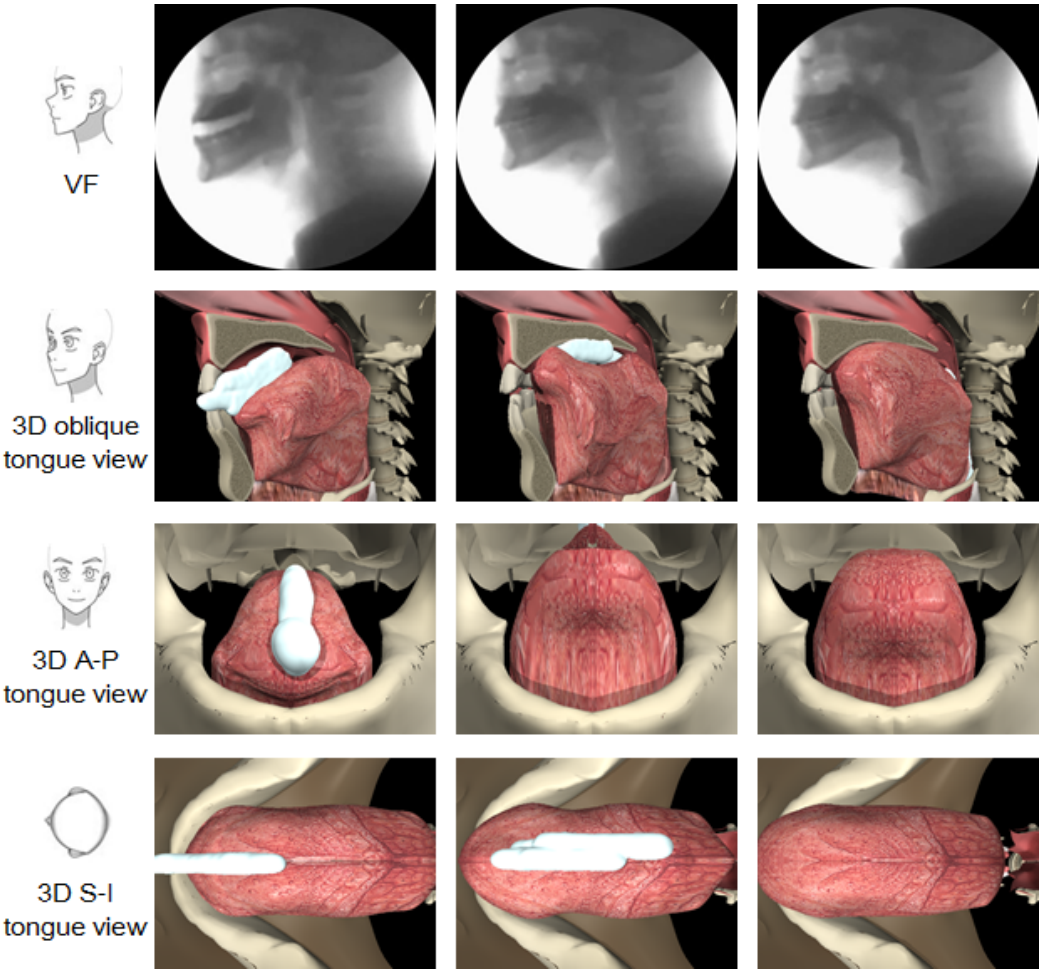

Figure 5.4: Top row: An MBS case for a patient with a score of 0- Brisk tongue motion tongue motion for Component 4 - Bolus Transport/Lingual Motion. The bottom three rows show 3D oblique tongue view, 3D A-P tongue view and 3D S-I tongue view respectively which was added to the training interface to extend the existing training material for scoring Component 4.

views and asked which view would help them identify the salient features to discern between different impairment of component 4. By doing so, we made sure that all the participants are exposed to the 3D views and be able to give us feedback on the views.

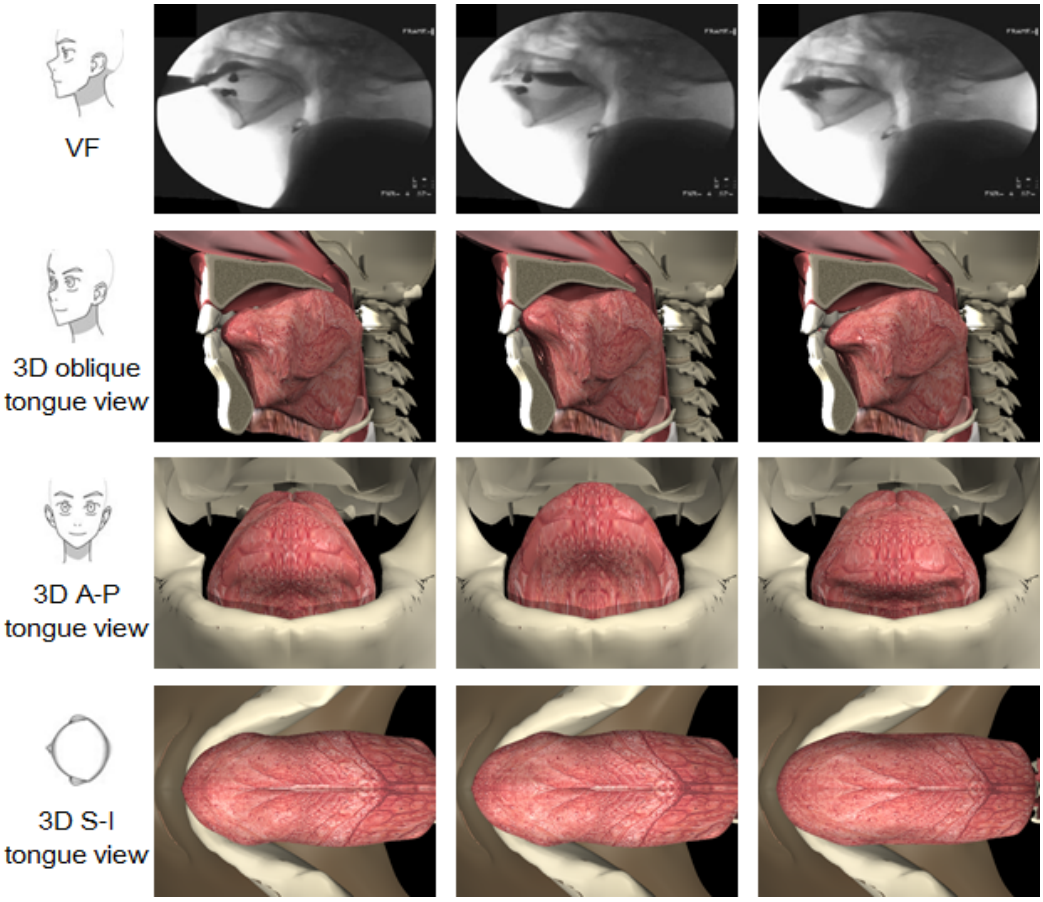

Figure 5.5: Top row: An MBS case for a patient with a score of 3- Repetitive/disorganized tongue motion for Component 4 - Bolus Transport/Lingual Motion. The bottom three rows show 3D oblique tongue view, 3D A-P tongue view and 3D S-I tongue view respectively which was added to the training interface to extend the existing training material for scoring Component 4.

Questionnaire

After finishing the study, the participants were asked to complete a questionnaire. The questionnaire is designed to identify if the additional visualization afforded by our model provided useful information to clinicians learning the standardized dysphagia diagnosis protocol. The questions were set up to access, record and quantify the response from the participants as they are the stakeholders as well as experts in the field.

The first part of the questionnaire consisted of questions about gender, age, years of experience as a SLP and affiliated hospital/health-care facility. We collected these information to help us analyze the data. Category type questions were set for indicating their gender. Ordinal questions were set for age and experience where the responses were recorded in categories. The age categories were set as 19–25, 26–60, 31–40, 41–50, 51–60 and 61 or above years. For experience, the categories were 0–3, 3–5 and more than 5 years of experience.

The next part of the questionnaire consisted of 6 Likert type questions [122] using a five point scale evaluation. A Likert scale is a sum of responses to several Likert items. A Likert item is a statement where the participant is asked to evaluate the statement with a quantitative value. The evaluation is usually subjective with level of agreement and disagreement with the statement. We used a typical five point Likert item with the following values to indicate the level of agreement and disagreement:

- SD – Strongly Disagree (1)
- D – Disagree (2)
- N – Neutral (3)
- A – Agree (4)
- SA – Strongly Agree (5)

We formulated the questions in a way to evaluate and record the clinicians response after they are exposed to 3D views provided by our model. These participating clinicians previously have undergone the standard training, so the questions were also set to see if they think these additional features could add value to the training. The questions set in the questionnaire are listed below:

Q1 I revisit the example videos in the MBSImP™© online training platform during my normal practice.

Q2 I find the example videos in the MBSImP™© online training platform useful.

Q3 I was able to easily switch between the different 3D views which were available for scoring Component 4 - Bolus Transport/Lingual Motion.

Q4 The 3D views available for scoring Component 4 - Bolus Transport / Lingual Motion, provided additional information that was not provided by the videos.

Q5 The 3D views were useful in differentiating between different impairments of Component 4 - Bolus Transport / Lingual Motion.

Q6 In my opinion, I think 3D views would be a helpful learning material for trainees.

5.5 Results and analysis

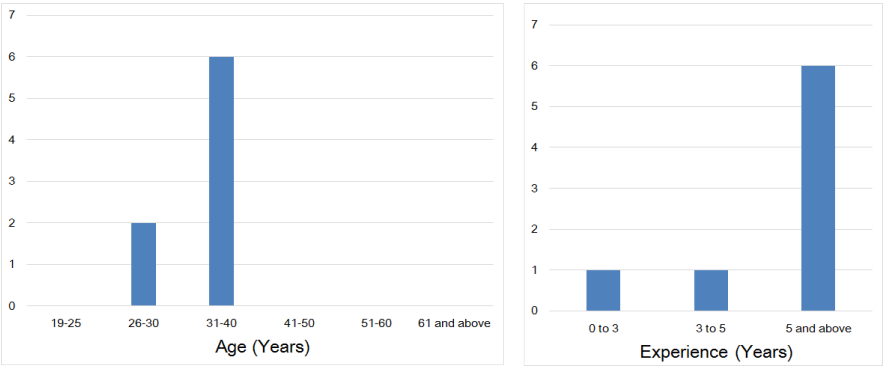

Figure 5.6: Variation of age and experience in the study population.

The aim of the user study was to gather feedback on adding features in the training zone that is provided by our 3D model. There were 8 participants in the study and all of them were women coincidentally. The participants were affiliated with health-care facilities/ hospital located in Vancouver, BC, Canada as listed in Section 5.4.2. Majority of the participating clinicians were aged between 31–40 (see Figure 5.6) and had more than 3 years of experience (see Figure 5.6). The following sections analyzes the

5.5.1 Questionnaire analysis

The next part of the questionnaire was the Likert scale questions which are separated into 3 groups for better analysis and visualization. Group I consisted of Q1 and Q2. In these questions we wanted to know if the participant

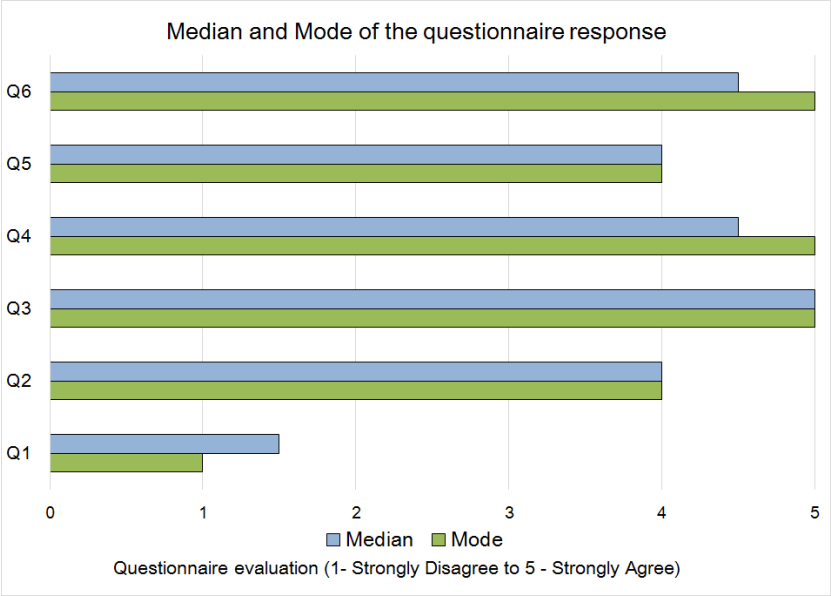

Figure 5.7: Median and Mode of the questionnaire response score for the study population (n=8).

revisit the training materials available in the existing system and find them useful. The average agreement for the first two question were respectively 2.375 and 4.33 out of 5. Group I questions identified the participants who are likely to be influenced by the additional training materials the most. The average agreement score in these questions implies that the participants are up to date about the training materials and can comment on if extension of training material is needed for enhancing the training.

Q3 is listed in Group II as it asks if the participant could switch between different views easily. This question is related to the user interface. Adding additional features to a interface sometimes adds complexity and have negative influence on the user experience. The response to this question helped us to evaluate if the added features introduces a level of complexity that has minimal impact on user experience. The average agreement score of this question is 5 out of 5 which means all participant strongly agree that they could switch between different views without having any negative impact on the user experience.

Group III consisted of Q4, Q5, Q6. These questions evaluated the participant's response about the usefulness of the additional 3D views. Q4 asked

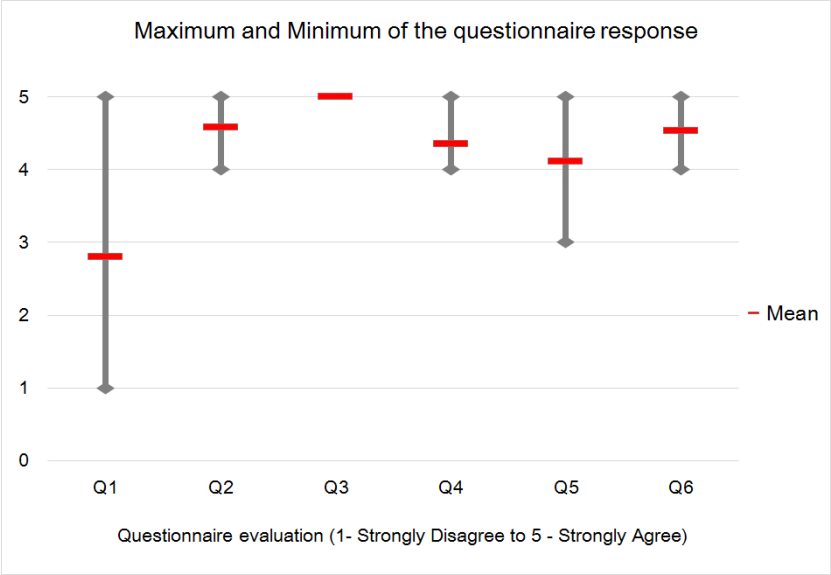

Figure 5.8: Range of the questionnaire response score with mean for the study population (n=8).

if the participant thought that the 3D views provided additional information to evaluate Component 4 and the next question asked if these additional information were useful. The average agreement score these questions were respectively 4.67 and 4.33 out of 5. The last question, Q6 asked the participants if they thought the 3D views would be an useful addition in the existing training system. The average agreement score for this questions was 4.375 out of 5 which means that the clinicians think that the participating clinicians believed that visualizing a swallowing motion in 3D cloud help the clinician training and contribute to extend the training materials available today.

Figure 5.7 shows the median and mode of the questionnaire response of the study population. Figure 5.8 shows the minimun and maximum of the questionnaire response of the study population. It can be seen that the responses for the Group III questions hold a high level of agreement score. This data from our pilot study support our initial assumption that adding 3D model in the standardized for that the additional visualization might be an useful extension for scoring and learning the standardized dysphagia diagnosis protocols.

5.5.2 Testimonial data

After the participants completed the questionnaire, they were asked if they wanted to give any additional feedback about the 3D views and their usefulness. Their testimonial data from the user study suggest the following:

Additional 3D views provide useful information

All the clinicians who participated in the study agreed the 3D view provided additional information about the swallowing swallowing dynamics. They also agreed that the additional information afforded by our 3D model can be useful for differentiating between the salient feature of Component 4; they agreed with an average agreement score of 4(see Figure 5.7). They reported that viewing the tongue movement in 3D form different perspective views points helped them to identify its direction of motion and provided them more detail about the physiology.

3D oblique tongue view is most useful for scoring Component 4

For scoring Component 4, the participating SLPs found the 3D oblique tongue view most useful. This view is similar to the mid-sagittal cut plane view only from a perspective viewpoint and with a full 3D model of tongue. In practice and training, the SLPs need to infer the tongue motion from 2D videofluoroscopic images. They mentioned that the 3D oblique tongue view allows them to view full tongue motion in a manner that is similar to looking inside the mouth of the patient during a swallowing motion. With this view, they agreed that they were able to more clearly discern between different tongue movement pattern descriptive of different Component 4 impairments.

After the 3D oblique tongue view, the participating SLPs thought that 3D A-P tongue view provided useful information. Even with a anterior-posterior VF scan, movement of the tongue tip is not readily visible. The existing training materials also do not illustrate the tongue tip motion clearly as it shows the swallowing from the midsagittal cut plane. The SLPs thought that the 3D S-I tongue view (see Figure 5.4 and 5.5) could provide more information identifying Component 5 - Oral Residue and other pharyngeal components which are best viewed from superior-anterior viewpoint.

3D views might be useful extension in MBSImP™© training

All the participating clinicians recommended with an average agreement score of 4.375 (see Figure 5.8) that 3D views can be a useful extension of the training materials for MBSImP™©. During the interview, we asked the experts to recommend which physiologic components of swallowing would benefit most from adding 3D extension to the existing training materials as additional scoring aid. After conducting a series of interviews with the participating SLPs, we discussed our findings and their recommendations with our clinical collaborator Dr. Bonnie Martin-Harris and her team at the Medical University of South Carolina (MUSC), Charleston, SC, USA. Dr. Martin-Harris and her team at MUSC instituted the MBSImP™© protocol and developed the existing training materials to help the clinicians score reliably following the standardized protocol. Dr. Martin-Harris agreed that the 3D views provided by our model might help extend the existing training materials and help the trainees clarify concepts about different component scores.

5.5.3 Recommendation

The participating SLPs from Vancouver, BC, Canada and Dr. Martin-Harris's team at MUSC recommended that the following components might also benefit from 3D extension of the existing training materials:

Component 15 – Tongue Base Retraction

Component 15 – Tongue base retraction is scored at the maximal retraction of the tongue base. Observations of tongue base retraction are made based on the presence and degree of bolus or air between the base of tongue and posterior pharyngeal wall (see Figure 5.9). It is view from a mid-sagittal plane provided by an MBS study. The retraction of the tongue base results in a "merging" of the base of the tongue with the posterior pharyngeal wall. So score of 0 to 4 are made judging the interaction between the base of the tongue and posterior pharyngeal wall. It is somewhat challenging to comprehend the interaction between these structures from 2D videos. Thus, the experts recommended 3D views might make significant difference if added to the existing training materials.

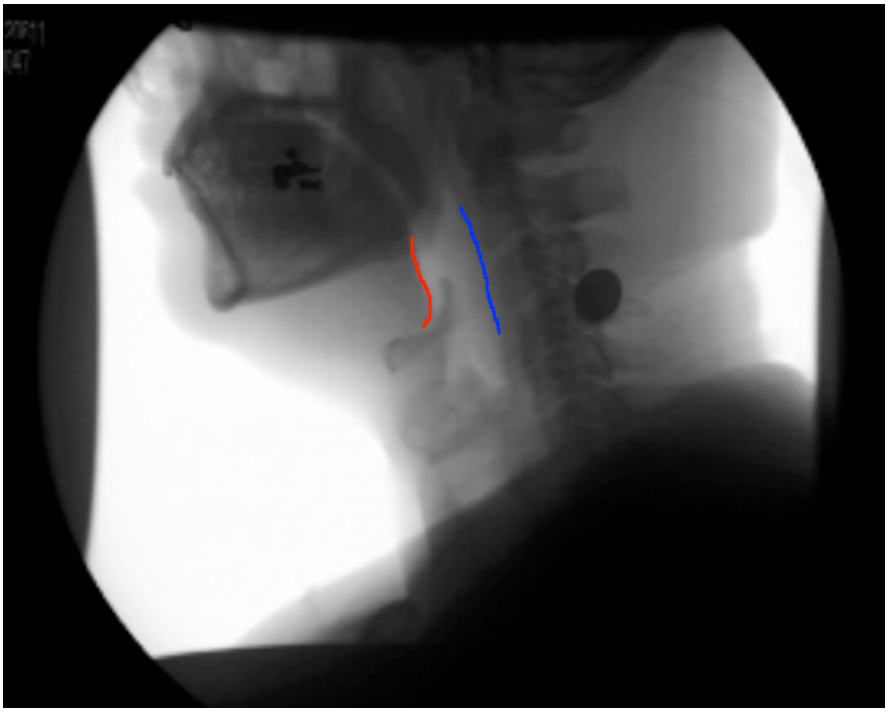

Figure 5.9: Observations of tongue base retraction are made based on the presence and degree of bolus or air between the base of tongue (outlined in red) and posterior pharyngeal wall (outlined in blue). VF image reproduced from MBSImP™© training module, with permission.

Component 8 – Laryngeal Elevation

Component 8 – Laryngeal Elevation is scored at the time the epiglottis reaches a horizontal position and it is scored just after initiation of hyoid motion which signals the onset of pharyngeal swallow. Hyoid excursion and the rise of the larynx sometimes cannot be visualized clearly in a VF and the animated illustrations in the existing training module. Furthermore, relative movement of thyroid cartilage, epiglottic petiole and arytenoid cartilages plays an important role when deciding between different scores of this component. So the experts suggested if the existing training materials are extended with 3D views to evaluate "minimal" to "partial" laryngeal elevation, the trainees will be able to comprehend the salient features pertinent to this component scores.

Component 13 – Pharyngeal Contraction

Component 13 – Pharyngeal Contraction is scored from a A-P view and this components is scored as a combination of pharyngeal shortening and stripping wave. For a score of 0 the pharyngeal shortening is symmetric and the contraction is complete. If there is unilateral bulging of one pharyngeal wall the score is 2 and for bilateral bulging of both pharyngeal walls the score is 3. For a case where the contraction is incomplete the score is 1. 3D views provided by our model can help determining the completeness of the pharyngeal contraction or the symmetry of the shortening of the pharynx, which cannot be easily seen from VF examples or the animated illustration captured from the AP view. The clinicians agreed that adding 3D views to the training of this component might have positive impact on the trainees understanding of this component.

5.6 Discussion

The pilot user study was conducted as a qualitative feasibility analysis to evaluate if the 3D perspective visualization provided by our model cab be an useful extension to the standardized training for dysphagia diagnosis. One limitation of this study was having small study population. We were limited by our resources so we only recruited SLPs in the greater Vancouver area with MBSImP™© certification. This limited our potential participant pool. However, to determine if scoring accuracy increases with 3D extension provided by our model, we would have to recruit more participants and compare their scoring efficiency of one group trained with and one group trained without the 3D extended visualization.

5.7 Summary

To summarize, we conducted a user study involving expert clinicians to investigate if the additional flexibility and visualization provided by our model can enhance the existing training materials for MBSImP™© protocol. This study involved building a training interface for adding the 3D extension to the existing training material, recruiting clinicians for participating in the study, analyzing data from the questioner and testimony. The result from the pilot data indicate that participating clinicians believe that the additional 3D

views are useful for identifying the salient features for differentiating between different swallowing impairments, such as direction, strength and timing of the tongue motion, and could be a useful addition to the current standardized MBSImP™© training system.

Chapter 6

Conclusions

To conclude, this chapter reviews and summarizes the contributions of this dissertation in terms of impact and potential application. It also acknowledges the remaining challenges and point towards the long term goals drawing on this research.

6.1 Impact and Potential Application

The contributions of this dissertation include a modeling frame work for generating a 3D biomechanical swallowing model from animated illustrations, a stable bolus simulation driven by the model kinematics and an extension of training materials used for standardized dysphagia training. For developing our model, we undertook participatory designing approach involving all stakeholders. The stakeholders in our case included the clinical educators who instituted standardized dysphagia diagnosis protocol and the Speech Language Pathologists who are learning/training/using the standardized protocol. We involved both type of stakeholders in our design process incorporated their feedback to produce what was needed to enhance the existing training materials. The contributions of this dissertation are summarized below:

Modeling of oropharyngeal swallowing motion

Oropharyngeal geometries are complex and consist of bony and soft anatomical structures. Generating a realistic swallowing model with accurate timing of swallowing event is a challenging task even with state-of-the-art imaging techniques; various research groups from different domains are trying to answer this challenge. We took a bottom up approach to build our model from the animation models used in clinician training. These animated illustrations are created by expert clinicians, using their knowledge about oropharyngeal

anatomy and observing real swallowing events using different imaging modalities. These animated illustrations are validated for clinicians training, thus these animations incorporate very important kinematic information of a swallowing motion.

We built a 3D biomechanical model of the oropharyngeal complex from realistic geometries derived from animated illustration used in clinician training. Sufficiently complex and realistic geometry is important for a biomechanical model to perform relevant and meaningful simulation. We generated rigid body models for bony structures and finite elements models for softer more deformable structures of the oropharyngeal complex. We coupled the rigid body and finite element models, and incorporated accurate and validated timing of swallowing events from the training materials available for standardized dysphagia diagnosis protocol to drive our model. With this approach we are able to bridge the gap between the 2D swallowing motion viewed in an MBS study and complement it with a more detailed 3D oropharyngeal swallowing model. For example, normally, in–vivo it is difficult to see the full dimension of tongue base retraction, supraglottic airway closure and particularly contraction of the pharynx, and cannot assume symmetry of movement from a lateral view. Our model allows for such detailed visualization and deeper comprehension of swallowing dynamics.

Simulating a bolus driven by model kinematics

Simulating a fluid bolus is a challenging computational fluid dynamics problem as it involves many level of complexity. The dynamics of the soft and bony oropharyngeal structures provide boundaries for the bolus which drives the bolus through the oral cavity. It is important to track the bolus to determine if there is any oral or pharyngeal residue, or to detect the presence of aspiration.

We used unified geometric skinning approach to incorporate the deformation of the upper airway during a swallow motion. This deforming airway mesh acted as the deforming boundary for the bolus simulations. We simulated a stable fluid bolus in the airway-skin driven by model dynamics to emulate oropharyngeal swallowing motion in our model. We demonstrated that our model can simulate a bolus in a manner consistent with the VF and animated illustrations used in standardized clinician training for dysphagia diagnosis. Being able to simulate a bolus driven by model dynamics could allow the clinicians to change the timings of the movements of oropharyngeal

structures to emulate a swallowing impairment, and visualize the resulting changes such as the bolus flow, presence of residue or aspiration. We also demonstrated that our model can simulate boluses with different viscosity by simulating standardized bolus consistencies used in clinical practice of dysphagia diagnosis. This marks our contribution by setting up the ground work for investigating the influence of bolus on structural movement with a biomechanical model based approach.

3D extension of training material for standardized dysphagia diagnosis

Our biomechanical swallowing model provides 3D perspective visualization that can be used as an extension of the standardized training materials currently used in MBSImP™© online training platform.

We conducted a pilot user study involving expert clinicians who are the intended users and stakeholders, to assess, evaluate, quantify and gather feedback about the additional value that our model might add to standardized dysphagia diagnosis. The pilot data from the user study indicate the following:

Firstly Visualization of swallowing motion in 3D from perspective viewpoints afforded by our model, can provide complementary information for scoring the most difficult physiologic component for standardized dysphagia diagnosis.

Secondly Perspective 3D visualisations afforded by our model might allows the clinician to understand, evaluate and quantify salient features specific to a particular swallowing impairment in more detail during standardized training.

Thirdly Extension of training materials in the existing system with 3D views provided by our model might improve the standardized training outcome.

6.2 Future Directions

This work sets up the ground for some promising research directions. Short term research directions for each contribution are discusses at the end of

corresponding chapters. Some potential long term research directions are listed as the following:

Transition from model space to patient space

In the scope of this Thesis, we build our model enforcing symmetry, because the aim of this work was to investigate the feasibility of using SPH to simulate a fluid bolus in a physics-based 3D model that is driven by kinematics derived from clinical data. Our model can be extended to allow for patient specific geometries and timings of swallowing events. With these patient specific inputs, our model could generate patient specific swallowing simulations which may lead to improved identification of physiologic treatment targets by testing the effectiveness of intervention strategies on the model rather than trial and error in-vivo testing.

Treatment alternative

A potential application for our oropharyngeal biomechanical model is as a tool for treatment planning and through quantitative analysis of trade-offs between treatment alternatives. For example, in case of head and neck cancer, sometime its required to do resection or reconstructive surgery. With accurate, validated, and patient-specific biomechanical models, the functional outcome of the surgery can be predicted. Alternative treatment pathways can be evaluated quantitatively to predict surgical effect on swallowing ability to choose the best surgical outcome in term of quality of life.

Muscle driven oropharyngeal model

ArtiSynth supports a muscle driven FE model where the muscle fibres embedded in the model can be activated to follow a desired movement. For the scope of this work, we drive our FE models kinematically. It is possible to use the inverse modeling capability of ArtiSynth to estimate the virtual muscle activation from the kinematics of our implemented FE tongue for a normal and different impaired swallow. This can give an enhanced understating of the swallowing physiology from a neurological perspective and aid dysphagia diagnosis.

To conclude, this dissertation has a presented a new frame work for generating biomechanical models by building surface geometries and extracting kinematics from animation models. We have applied our modeling frame

work to generate a 3D oropharyngeal model and simulated a fluid bolus driven by the model kinematics. We have applied 3D perspective visualization afforded by our model and are working toward extending the training materials for standardized dysphagia diagnosis. This work sets up the stage for enhancing the practice of medical pedagogy using biomechanical model for dysphagia diagnosis. The research has been carried out within an interdisciplinary team of clinicians and engineers across the world, and has lead to a number of ongoing collaborations and projects.

Appendix A

MBSImP™© scoring guideline

A.1 MBSImP™© Components, Scores, and Score Definitions

The MODIFIED BARIUM SWALLOW IMPAIRMENT PROFILE: MBSImP ™ ©
Components, Scores, and Score Definitions

ORAL Impairment

Component 1—Lip Closure
- 0 = No labial escape
- 1 = Interlabial escape; no progression to anterior lip
- 2 = Escape from interlabial space or lateral juncture; no extension beyond vermilion border
- 3 = Escape progressing to mid-chin
- 4 = Escape beyond mid-chin

Component 2—Tongue Control During Bolus Hold
- 0 = Cohesive bolus between tongue to palatal seal
- 1 = Escape to lateral buccal cavity/floor of mouth (FOM)
- 2 = Posterior escape of less than half of bolus
- 3 = Posterior escape of greater than half of bolus

Component 3—Bolus Preparation/Mastication
- 0 = Timely and efficient chewing and mashing
- 1 = Slow prolonged chewing/mashing with complete re-collection
- 2 = Disorganized chewing/mashing with solid pieces of bolus unchewed
- 3 = Minimal chewing/mashing with majority of bolus unchewed

Component 4—Bolus Transport/Lingual Motion
- 0 = Brisk tongue motion
- 1 = Delayed initiation of tongue motion
- 2 = Slowed tongue motion
- 3 = Repetitive/disorganized tongue motion
- 4 = Minimal to no tongue motion

Component 5 – Oral Residue
- 0 = Complete oral clearance
- 1 = Trace residue lining oral structures
- 2 = Residue collection on oral structures
- 3 = Majority of bolus remaining
- 4 = Minimal to no clearance

Location
- A = Floor of mouth (FOM)
- B = Palate
- C = Tongue
- D = Lateral sulci

Component 6—Initiation of Pharyngeal Swallow
- 0 = Bolus head at posterior angle of ramus (first hyoid excursion)
- 1 = Bolus head in valleculae
- 2 = Bolus head at posterior laryngeal surface of epiglottis
- 3 = Bolus head in pyriforms
- 4 = No visible initiation at any location

PHARYNGEAL Impairment

Component 7—Soft Palate Elevation
- 0 = No bolus between soft palate (SP)/pharyngeal wall (PW)
- 1 = Trace column of contrast or air between SP and PW
- 2 = Escape to nasopharynx
- 3 = Escape to nasal cavity
- 4 = Escape to nostril with/without emission

Component 8—Laryngeal Elevation
- 0 = Complete superior movement of thyroid cartilage with complete approximation of arytenoids to epiglottic petiole
- 1 = Partial superior movement of thyroid cartilage/partial approximation of arytenoids to epiglottic petiole
- 2 = Minimal superior movement of thyroid cartilage with minimal approximation of arytenoids to epiglottic petiole
- 3 = No superior movement of thyroid cartilage

Component 9—Anterior Hyoid Excursion
- 0 = Complete anterior movement
- 1 = Partial anterior movement
- 2 = No anterior movement

Component 10–Epiglottic Movement
- 0 = Complete inversion
- 1 = Partial inversion
- 2 = No inversion

Component 11—Laryngeal Vestibular Closure – Height of Swallow
- 0 = Complete; no air/contrast in laryngeal vestibule
- 1 = Incomplete; narrow column air/contrast in laryngeal vestibule
- 2 = None; wide column air/contrast in laryngeal vestibule

Component 12—Pharyngeal Stripping Wave
- 0 = Present - complete
- 1 = Present - diminished
- 2 = Absent

Component 13—Pharyngeal Contraction (*A/P VIEW ONLY*)
- 0 = Complete
- 1 = Incomplete (Pseudodiverticulae)
- 2 = Unilateral Bulging
- 3 = Bilateral Bulging

Component 14—Pharyngoesophageal Segment Opening
- 0 = Complete distension and complete duration; no obstruction of flow
- 1 = Partial distension/partial duration; partial obstruction of flow
- 2 = Minimal distension/minimal duration; marked obstruction of flow
- 3 = No distension with total obstruction of flow

Component 15—Tongue Base (TB) Retraction
- 0 = No contrast between TB and posterior pharyngeal wall (PW)
- 1 = Trace column of contrast or air between TB and PW
- 2 = Narrow column of contrast or air between TB and PW
- 3 = Wide column of contrast or air between TB and PW
- 4 = No visible posterior motion of TB

Component 16—Pharyngeal Residue
- 0 = Complete pharyngeal clearance
- 1 = Trace residue within or on pharyngeal structures
- 2 = Collection of residue within or on pharyngeal structures
- 3 = Majority of contrast within or on pharyngeal structures
- 4 = Minimal to no pharyngeal clearance

Location
- A = Tongue Base
- B = Valleculae
- C = Pharyngeal wall
- D = Aryepiglottic folds
- E = Pyriform sinuses
- F = Diffuse (>3 areas)

ESOPHAGEAL Impairment

Component 17—Esophageal Clearance Upright Position
- 0 = Complete clearance; esophageal coating
- 1 = Esophageal retention
- 2 = Esophageal retention with retrograde flow below pharyngo-esophageal segment (PES)
- 3 = Esophageal retention with retrograde flow through PES
- 4 = Minimal to no esophageal clearance

Appendix B

Formulation for SPH fluid simulation

This appendix discusses the basics of smoothed particle hydrodynamics (SPH) formulation, implementation will be discussed in details. The Navier–Stokes equations for a Lagrangian system are solved using methods described in [115] for simulating fluids using SPH methods. The SPH formulation is often divided into two major steps in literature [115]. The first step is integral representation and the latter one is particle approximation. The first step consists of integral representation of the function and the derivatives of the function. The integral representation of the function is further approximated by adding the values of the neighbouring particles. This makes the particle approximation of the function at discrete particle level whcih is the other step. These steps have been called as *kernel estimate* or *particle estimate* in the literature. In this Appendix kernel approximation and particle approximation will be used throughout to avoid confusion.

B.1 Integral representation of a function

The identity of the integral function $f(x)$ used in SPH formulation is represented as the following equation.

$$f(\mathbf{x}) = \int_{\Omega} f(\mathbf{x}')\partial(\mathbf{x}\text{-}\mathbf{x}')dx' \tag{B.1}$$

where f is a function of the position vector $\mathbf{x}$ in three dimension. Ω is the volume of the integral containing $\mathbf{x}$. The $\delta(\mathbf{x}\text{-}\mathbf{x}')$ term is the Dirac delta function given by

$$\delta(\mathbf{x} - \mathbf{x}') = \begin{cases} 1, & \mathbf{x} = \mathbf{x}' \\ 0, & \text{otherwise} \end{cases} \tag{B.2}$$

The Delta function makes the integral representation in Equation B.1 exact as long as the $f(\mathbf{x})$ is continuous in Ω. Now if the Delta function is replaced by a so called smoothing kernel function or smoothing function $W(\mathbf{x}-\mathbf{x}', h)$, equation (B.1) becomes

$$f(\mathbf{x}) = \int_{\Omega} f(\mathbf{x}')W(\mathbf{x}-\mathbf{x}', h)dx' \tag{B.3}$$

In the smoothing kernel function W, h represents the smoothing length defining the neighbourhood area or the area of influence of the function. As W is not a Dirac function rather an approximation, the integral representation in equation (B.3) called is termed as kernel approximation. In the SPH convention, the kernel operators is denoted by angle brackets $\langle\rangle$ (see [115]). Equation B.3 can be rewritten following the convention as

$$\langle f(\mathbf{x})\rangle = \int_{\Omega} f(\mathbf{x}')W(\mathbf{x}-\mathbf{x}', h)dx' \tag{B.4}$$

Some major properties or conditions of the smoothing function W are described in the following discussion.

1. *Unity* The first one is the unity condition or the normalization condition which simply state that the integration of the smoothing function provides unity (Equation B.5).

$$\int_{\Omega} f(\mathbf{x}')W(\mathbf{x}-\mathbf{x}', h)dx' = 1 \tag{B.5}$$

2. *Delta function property* The second condition (Equation B.6) ensures that if the smoothing length approaches zero, the smoothing function should satisfy the Dirac delta function condition.

$$\lim_{h\to 0} W(\mathbf{x}-\mathbf{x}', h) = \delta(\mathbf{x}\text{-}\mathbf{x}') \tag{B.6}$$

3. *Compact support* The dimension of the compact support is defined by the smoothing length h and a scaling factor κ

$$W(\mathbf{x}-\mathbf{x}', h) = 0, \text{ when } \mid \mathbf{x}-\mathbf{x}' \mid > \kappa h \tag{B.7}$$

here κ is a constant related to the smoothing function for point $\mathbf{x}$ that defines the smoothing area having non-zero values. The effective area is called the support domain of that point. This compact condition makes the integration domain Ω same as the support domain by localizing the integration over the entire problem domain. In other words this property transforms a SPH approximation from global operation into a localized operation. This leads to a set of sparse discretized system matrices which reduces the computational burden significantly.

4. *Positivity* At any point $\mathbf{x}'$ inside the support domain of $\mathbf{x}$ the smoothing function has a positive value, that is $W(\mathbf{x} - \mathbf{x}') \geq 0$. This is a important requirement to ensure a physically meaningful representation. For example, In hydrodynamic simulations negative value for the smoothing function can result in negative density and energy terms which leads to misrepresentation of the system.

5. *Decay* The value of the smoothing function should decrease with the increase of the distance away from the particle. In other words what it means is nearer particle should have a bigger influence on the concerned particle.

6. *Symmetry property* The smoothing function should be an even function. What it means is that particles at same distance should have equal effect on a given particle. However, this is not strictly enforced, and it is sometimes violated to provide higher consistency.

7. *Smoothness* The smoothing function should be sufficiently smooth. This so-called "smoothness" means that the kernel should be sufficiently continuous and smooth in order to insensitive to particle disorder and the errors in approximating the integral.

Any function having the above properties can be used as a SPH smoothing function and in literature many researchers have proposed different kind to kernel in order to achieve better approximation and computational efficiency. Some of such proposed kernels will be discussed in Section B.4.

The error of the SPH integral representation can be estimated roughly by expanding the smoothing function $\mid \mathbf{x} - \mathbf{x}' \mid > \kappa h$ from Equation B.7 and substituting the value in Equation B.4 which yields

$$\begin{aligned}\langle f(\mathbf{x})\rangle &= \int_{\Omega} [f(\mathbf{x}) + f'(\mathbf{x})(f(\mathbf{x}') - \mathbf{x}) + r((\mathbf{x}' - \mathbf{x})^2)W(\mathbf{x} - \mathbf{x}', h) \\ &= f(\mathbf{x}) \int_{\Omega} W(\mathbf{x} - \mathbf{x}', h) \\ &+ f(\mathbf{x}') \int_{\Omega} (\mathbf{x} - \mathbf{x}')W(\mathbf{x} - \mathbf{x}', h)d\mathbf{x}' + r(h^2)\end{aligned} \tag{B.8}$$

here r refers to the residual term. Now, the smoothing function W chosen to be a even function with respect to $\mathbf{x}$, therefore $(\mathbf{x} - \mathbf{x}')W(\mathbf{x} - \mathbf{x}', h)$ should be an odd function which will mean that

$$\int_{\Omega} (\mathbf{x} - \mathbf{x}')W(\mathbf{x} - \mathbf{x}', h)d\mathbf{x}' = 0 \tag{B.9}$$

Using the normalization condition (Equation B.5) and Equation B.9 the kernel approximation operator derived in Equation B.8 becomes

$$\langle f(\mathbf{x})\rangle = f(\mathbf{x}) + r(h^2) \tag{B.10}$$

From the above equation it can be seen the kernel approximation has a residual term with h^2 which means in the SPH method the kernel approximation has second order accuracy. However, if the smoothing function is not a even a function or the normalization condition in not satisfied; the kernel approximation might not be of second order accuracy (detailed discussion in [115]).

B.2 Integral representation of the derivative of a function

The integral representation of the derivative of the function is obtained by replacing $f(\mathbf{x})$ with $\nabla\cdot f(\mathbf{x})$ in the Equation B.4 which yields

$$\langle \nabla\cdot f(\mathbf{x})\rangle = \int_{\Omega} [\nabla\cdot f(\mathbf{x}')]W(\mathbf{x} - \mathbf{x}', h)d\mathbf{x}' \tag{B.11}$$

here the divergence is the integral operator with respect to the coordinates. Further, the term inside the integral operator gives

$$\begin{aligned}&[\nabla\cdot f(\mathbf{x}')]W(\mathbf{x}-\mathbf{x}',h)=\\&\nabla\cdot[f(\mathbf{x}')W(\mathbf{x}-\mathbf{x}',h)]-f(\mathbf{x}')\cdot\nabla W(\mathbf{x}-\mathbf{x}',h)\end{aligned}\tag{B.12}$$

Using the above equation to replace the term inside the integral operator, Equation B.11 becomes

$$\begin{aligned}\langle\nabla\cdot f(\mathbf{x})\rangle=&\int_{\Omega}\nabla\cdot[f(\mathbf{x}')W(\mathbf{x}-\mathbf{x}',h)]d\mathbf{x}'\\&-\int_{\Omega}f(\mathbf{x}')\cdot\nabla W(\mathbf{x}-\mathbf{x}',h)d\mathbf{x}'\end{aligned}\tag{B.13}$$

The first integral term of Equation B.13 can be converted to an integral over the whole surface S on the integration domain Ω with a unit vector $\overrightarrow{\mathbf{n}}$ which is normal to the surface S.

$$\begin{aligned}\langle\nabla\cdot f(\mathbf{x})\rangle=&\int_{S}f(\mathbf{x}')W(\mathbf{x}-\mathbf{x}',h)\cdot\overrightarrow{\mathbf{n}}dS\\&-\int_{\Omega}f(\mathbf{x}')\cdot\nabla W(\mathbf{x}-\mathbf{x}',h)d\mathbf{x}'\end{aligned}\tag{B.14}$$

The smoothing function for a point W has compact support (condition three Equation B.7) when the support domain is located within the problem domain (Figure B.1). For such points the surface integral becomes 0. Considering a point whose support domain intersects the problem domain, the smoothing function W is truncated at the boundary of problem domain (Figure B.2) making the surface integral nonzero. For such cases, modification should be made to remedy the boundary conditions. Nonetheless, for the points having a zero surface integral Equation B.14 becomes

$$\langle\nabla\cdot f(\mathbf{x})\rangle=-\int_{\Omega}f(\mathbf{x}')\cdot\nabla W(\mathbf{x}-\mathbf{x}',h)d\mathbf{x}'\tag{B.15}$$

The above equation shows that spatial gradient of a field function in SPH representation is calculated from the values of the function and the derivative

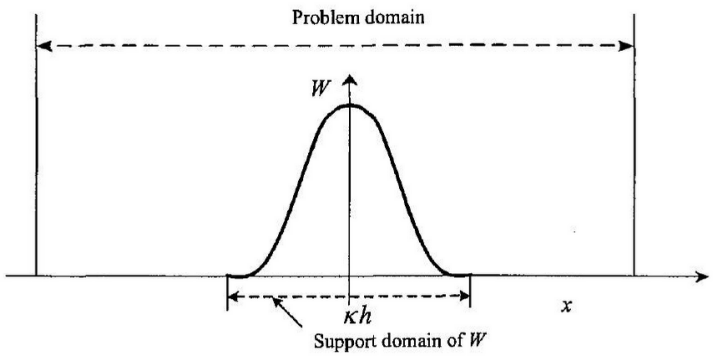

Figure B.1: The support domain of the smoothing function W and problem domain. The support domain is located within the problem domain. Therefore, the surface integral on the right hand side of Equation B.14 is zero. Adapted from [115]

.

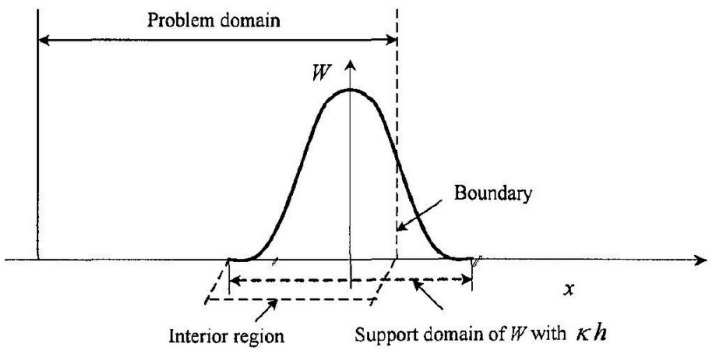

Figure B.2: The support domain of the smoothing function W and problem domain. The support domain intersects with the problem domain. Therefore, the smoothing function W is truncated by the boundary, and the surface integral on the right hand side of Equation B.14 is on longer zero. Adapted from [115]

.

of the smoothing function W, not the derivative of the function itself. This is significant because it reduces the consistency requirement on the assumed field functions for getting stable solution for the PDEs which is very similar to the weak form methods [123].

B.3 Particle approximation

After the kernel approximation (discussed in Section B.1 and B.2), another key operation in the SPH methodology is particle approximation. In this step the SPH kernel derived in Equation B.4 and B.15 are translated to discretized forms of summation over all the particles in the support domain.

A particle $j(=1,2,\ldots,N)$ with a support domain that has N number of particles, is chosen with mass m_j and density ρ_j. If the infinitesimal volume $d\mathbf{x}'$ in the integration function for particle j is replaced with finite volume of the particle ∇V_j, the mass can be written as $m_j = \nabla V_j \rho_j$. With these approximations in the continuous integral representation of $f(x)$ becomes the discretized particle approximation explained in the following derivation.

$$\begin{aligned} f(\mathbf{x}) &= \int_{\Omega} f(\mathbf{x}')W(\mathbf{x}-\mathbf{x}',h)dx' \\ &\equiv \sum_{j=1}^{N} f(\mathbf{x_j})W(\mathbf{x}-\mathbf{x_j},h)\nabla V_j \\ &= \sum_{j=1}^{N} f(\mathbf{x_j})W(\mathbf{x}-\mathbf{x_j},h)\frac{1}{\rho_j}(\rho_j \nabla V_j) \\ &= \sum_{j=1}^{N} \frac{m_j}{\rho_j} f(\mathbf{x}')W(\mathbf{x}-\mathbf{x_j},h) \end{aligned} \tag{B.16}$$

The particle approximation for a function at particle i can be written as the following

$$\langle f(\mathbf{x}_i)\rangle = \sum_{j=1}^{N} \frac{m_j}{\rho_j} f(\mathbf{x}_j)W_{ij} \tag{B.17}$$

where

$$W_{ij} = W(\mathbf{x}_i - \mathbf{x}_j, h) = W(|\mathbf{x}_i - \mathbf{x}_j|, h) \tag{B.18}$$

The particle approximation represented by Equation B.17 implies that the value of a function at particular particle is approximated using the average of that functions at all the particles in the support domain weighted by the smoothing function.

To use the particle approximation of the spatial derivative of the function, same assumptions like Equation B.16 can be made to achieve the following equation where the gradient of the smoothing function W is taken with respect to the particle j.

$$\langle \nabla \cdot f(\mathbf{x}) \rangle = -\sum_{j=1}^{N} \frac{m_j}{\rho_j} f(\mathbf{x}_j) \cdot \nabla W(\mathbf{x} - \mathbf{x}_j, h) \tag{B.19}$$

Now the particle approximation for a function at particle i, denoting the distance between particle i and j as r_{ij}, can be written as

$$\langle \nabla \cdot f(\mathbf{x}_i) \rangle = -\sum_{j=1}^{N} \frac{m_j}{\rho_j} f(\mathbf{x}_j) \cdot \nabla W_{ij} \tag{B.20}$$

where

$$\nabla_i W_{ij} = \frac{\mathbf{x}_i - \mathbf{x}_j}{r_{ij}} \frac{\partial W_{ij}}{\partial r_{ij}} = \frac{\mathbf{x}_{ij}}{r_{ij}} \frac{\partial W_{ij}}{\partial r_{ij}} \tag{B.21}$$

As $\nabla_i W_{ij}$ is taken with respect to particle i, the negative sign in Equation B.18 is removed in the following equation.

$$\langle \nabla \cdot f(\mathbf{x}_i) \rangle = \sum_{j=1}^{N} \frac{m_j}{\rho_j} f(\mathbf{x}_j) \cdot \nabla W_{ij} \tag{B.22}$$

This particle approximation of the derivative of a function stated that the value of the gradient of the function at a particular particle is approximated by averaging the value of the gradient of the function on all the particles in the neighbourhood or the support domain, weighted by the gradient of the smoothing function. The use of particle summations to approximate the integral makes the SPH method a meshfree method without the need of a background mesh for numerical integration. The particle approximation (Equation B.21) includes the mass and density of the particle in the formulation. This makes the SPH formulation convenient for hydrodynamic application because density is one of the key field variable for dynamic fluid flow problems. By substituting the the function $f(\mathbf{x})$ in Equation B.17 with density ρ the SPH approximation for the density function becomes

$$\rho_i = \sum_{j=1}^{N} m_j W_{ij} \tag{B.23}$$

which is referred as summation density approach which is commonly used to obtain density in a SPH simulation. This equation states that the density of a particle is weighted average of all the neighbouring particles in

Value of a function	Value of its derivatives
$\langle f(\mathbf{x}_i)\rangle = \sum_{j=1}^{N} \frac{m_j}{\rho_j} f(\mathbf{x}_j)\cdot W_{ij}$	$\langle \nabla\cdot f(\mathbf{x}_i)\rangle = \sum_{j=1}^{N} \frac{m_j}{\rho_j} f(\mathbf{x}_j)\cdot \nabla W_{ij}$
where	where
$W_{ij} = W(\mathbf{x}_i - \mathbf{x}_j, h) = W(\lvert\mathbf{x}_i - \mathbf{x}_j\rvert, h)$	$\nabla_i W_{ij} = \frac{\mathbf{x}_i - \mathbf{x}_j}{r_{ij}} \frac{\partial W_{ij}}{\partial r_{ij}} = \frac{\mathbf{x}_{ij}}{r_{ij}} \frac{\partial W_{ij}}{\partial r_{ij}}$

Table B.1: Particle approximation representation of the value of a function and its derivatives at particle i

Particle approximation representation of a field function and its derivatives for a given particle i can be summarized as in the following Table B.1, which explains the fundamental advantage of the SPH method; that is the derivatives of any function $f(\mathbf{x})$ can be found by differentiating the kernel rather than by using finite difference, finite volume or finite element expression calculated using the grid.

B.4 Choice of smoothing function

In SPH formulation, the choice of smoothing function is very important because it determines how effectively functional approximation is performed based on scattered nodes in the support domain without using a predefined grid that provides the connectivity of the nodes. This smoothing function is referred as smoothing kernel function, smoothing kernel or simply kernel in literature. Many researchers have proposed different kernel functions for optimal performance.

In the original paper Lucy [102] proposed a bell shaped curve as described

by the following equation as the smoothing function.

$$\begin{aligned} W(\mathbf{x}-\mathbf{x}', h) &= W(R, h) \\ &= \alpha_d \begin{cases} (1+3R)(1-R)^3 & R \leq 1 \\ 0 & R > 1 \end{cases} \end{aligned} \tag{B.24}$$

here R is the relative distance between two particles located at $\mathbf{x}$ and $\mathbf{x}'$, yielding $R = \frac{r}{h} = \frac{|\mathbf{x}-\mathbf{x}'|}{h}$. α_d satisfies the unity condition in all three dimensions having values $5/4h$, $5/\pi h^2$ and $105/16\pi h^3$ in one-,two- and three dimension respectively. Monaghan [101] in his seminal paper suggested to assume the smoothing function to be a Gaussian for simulating non-spherical stars.

$$W(R, h) = \alpha_d e^{-R^2} \tag{B.25}$$

where α_d is $1/\pi^{1/2}h$, $1/\pi h^2$ and $1/\pi^{3/2}h^3$ in one-,two- and three- dimentional space respectively.

Later on Monaghan and Lattamzio [124] defined a smoothing function based on the cubic splines popularly know as B-spline function. This function has been most widely used. Morris [125] introduced quartic splines to more closely approximate the Gaussian ensuring more stability. Johnson et al. [126] used a quadratic smoothing function as it could overcome the compressive instability problem which occurs in high velocity impact problems. More details about these smoothing functions can be found at Chapter 3 of [115].

B.5 SPH equation of motion

In the previous sections essential formulations and the smoothing functions for the SPH methods has been discussed for discretizing the PDEs. In this section some further modification in the formulation for these numerical procedures are made to facilitate dynamic fluid simulation. As discussed in 2.4.4, SPH describes the physical governing equations using an Lagrangian approach. In this section the SPH equations of motion will be derived based on such governing equations in Lagrangian form.

In a Lagrangian description, this control volume V will move with the fluid flow given that the mass of the fluids contained in V remains unchanged. Considering an infinitesimal fluid cell with control volume δV bounded by

control surface δS, which can be the differential volume dV and the differential surface dS. The conditions for selecting such infinitesimal fluid cell are (1) the cell is large enough that the continuum mechanics assumptions are valid and (2) the cell is small enough that fluid properties inside the cell can be regarded isotropic. This infinitesimal fluid cell can move along a streamline with vector velocity $\mathbf{v} = v_x, v_y, v_z$. In case of a Lagrangian control volume, the movement of fluids inside the control volume V changes the control surface S which again changes the control volume. So the change in the control volume ΔV due to the movement of dS over a Small time increment Δt can be written as

$$\Delta V = \mathbf{v}\Delta t \cdot \mathbf{n} dS \tag{B.26}$$

where $\mathbf{n}$ is the unit vector perpendicular to the surface dS.

The total volume change can be therefore calculated by integrating over the control surface S yielding

$$\Delta V = \int_S \mathbf{v}\Delta t \cdot \mathbf{n} dS \tag{B.27}$$

Applying the divergence theorem with a gradient operator ∇ after dividing the both sides of Equation B.27 by Δt, it becomes

$$\frac{\Delta V}{\Delta t} = \int_V \nabla \cdot \mathbf{v} dV \tag{B.28}$$

One of the condition of selecting a small enough infinitesimal fluid cell was that the fluid properties would be isotropic throughout. What it implies that if the entire control volume V is was considered as a small as the fluid cell volume δV, the fluid property would have been isotropic throughout δV. The following equation can be obtained with such assumptions

$$\frac{\Delta(\delta V)}{\Delta t} = (\nabla \cdot \mathbf{v}) \int_V d(\delta V) = (\nabla \cdot \mathbf{v})\delta V \tag{B.29}$$

Hence, the time rate of volume change for the infinitesimal fluid cell is found to be

$$\frac{D(\delta V)}{Dt} = (\nabla \cdot \mathbf{v})\delta V \tag{B.30}$$

Rearranging the above equation the velocity divergence is found to be

$$\nabla \cdot \mathbf{v} = \frac{1}{\delta V} \frac{D(\delta V)}{Dt} \tag{B.31}$$

The above equation physically interprets the velocity divergence as the time rate of volume change per unit volume.

Three fundamental conservation law govern the basic fluid dynamics equation. They are

1. Conservation of mass or the continuity equation
2. Conservation of momentum or the momentum equation
3. Conservation of energy or the energy equation

In the following sections, these governing equations in the Lagrangian form will be discussed for SPH method.

B.6 The continuity equation

The continuity equation is the law of conservation of mass. For a fluid cell of volume δV, the mass contained in the control volume is

$$\delta m = \rho \delta V \tag{B.32}$$

where m is the density and ρ is the density. According to the conservation of mass law, no mass can be created or destroyed. So the mass is conserved in the fluid cell and time rate of mass change is zero.

$$\begin{aligned} \frac{D(\delta m)}{Dt} &= \frac{D(\rho \delta V)}{Dt} = 0 \\ &= \delta V \frac{D\rho}{Dt} + \rho \frac{D(\delta V)}{Dt} = 0 \end{aligned} \tag{B.33}$$

which can be rewritten as

$$\frac{D\rho}{Dt} + \rho \frac{1}{\delta V} \frac{D(\delta v)}{Dt} = 0 \tag{B.34}$$

From the physical interpretation of velocity divergence (Equation B.31) and the above equation, the continuity equation in Lagrangian form can be obtained as

$$\frac{D\rho}{Dt} = -\rho \Delta \cdot \mathbf{v} \tag{B.35}$$

B.7 The momentum equation

The momentum equation is represented by Newton's second law. For an infinitesimal Lagrangian fluid cell, the net force acting on the cell is equal to the mass contained in the cell times acceleration if that fluid cell. The net force acting on the fluid cell includes body forces i.e. gravitational, magnetic and surface forces i.e. pressure, shear and normal stress. The surface force due to pressure p is imposed by the surrounding fluid cells and the shear and normal stress is the outcome of deformations and volume change respectively. The acceleration of the fluid cell with position vector $\mathbf{x} = (x, y, z)$ in three direction are Dv_x/Dt, Dv_y/Dt and Dv_z/Dt. Considering τ_{ij} as the stress in j direction acting on a plane perpendicular to i axis and the body force per unit mass in x direction is F_x, Newton's second law can be written as

$$\begin{aligned} m\frac{dv_x}{dt} =& \rho dxdydz\frac{dv_x}{dt} \\ =& -\frac{\partial p}{\partial x}dxdydz \\ &+ \frac{\partial \tau_{xx}}{\partial x}dxdydz + \frac{\partial \tau_{yx}}{\partial y}dxdydz + \frac{\partial \tau_{zx}}{\partial z}dxdydz \\ &+ F_x(\rho dxdydz) \end{aligned} \tag{B.36}$$

The equation of momentum in x direction becomes

$$\rho\frac{Dv_x}{Dt} = -\frac{\partial p}{\partial x} + \frac{\partial \tau_{xx}}{\partial x} + \frac{\partial \tau_{yx}}{\partial y} + \frac{\partial \tau_{zx}}{\partial z} + \rho F_x \tag{B.37}$$

Momentum equation in y and z direction have similar form like the above equation.

B.8 The energy equation

The energy equation is based on the first law of thermodynamics that is conservation of energy. The energy equation states that the time rate of energy change inside an infinitesimal fluid cell is the summation of (1) the work done by pressure multiplied by the volumetric strain and (2) the energy

dissipation due to the viscous shear forces.

$$\begin{aligned}\rho\frac{De}{Dt} &= p(\frac{\partial v_x}{\partial x}+\frac{\partial v_y}{\partial y}+\frac{\partial v_z}{\partial z}) \\ &+ \tau_{xx}\frac{\partial v_x}{\partial x}+\tau_{yx}\frac{\partial v_x}{\partial y}+\tau_{zx}\frac{\partial v_x}{\partial z} \\ &+ \tau_{xy}\frac{\partial v_y}{\partial x}+\tau_{yy}\frac{\partial v_y}{\partial y}+\tau_{zy}\frac{\partial v_y}{\partial z} \\ &+ \tau_{xz}\frac{\partial v_z}{\partial x}+\tau_{yz}\frac{\partial v_z}{\partial y}+\tau_{zz}\frac{\partial v_x}{\partial z}\end{aligned} \tag{B.38}$$

B.9 Navier-Stokes equations

Navier-Stokes equations are a set of partial differential equation using a Lagrangian description which states the conservation of mass, momentum and energy to govern dynamic fluid flow. The Navier-Stokes equations consists of the following set of equations.

1. The Continuity equation

$$\frac{D\rho}{Dt} = -\rho\frac{\partial \mathbf{v}^\beta}{\partial \mathbf{x}^\beta} \tag{B.39}$$

2. The momentum equation

$$\frac{D\mathbf{v}^\alpha}{Dt} = \frac{1}{\rho}\frac{\partial \sigma^{\alpha\beta}}{\partial \mathbf{x}^\beta} \tag{B.40}$$

3. The energy equation

$$\frac{De}{Dt} = \frac{\sigma^{\alpha\beta}}{\rho}\frac{\partial \mathbf{v}^\alpha}{\partial \mathbf{x}^\beta} \tag{B.41}$$

In the above equations α and β are used to denote the coordinate system where the summation in the equations are taken over repeated indices. σ is the total stress tensor which is expressed as

$$\sigma^{\alpha\beta} = -p\delta^{\alpha\beta} + \tau^{\alpha\beta} \tag{B.42}$$

here p is the isotropic pressure and τ is the viscous stress.

B.10 Particle approximation of density

In SPH method density determines the particle distribution and smoothing length evaluation. There are two major approaches to evolve density using SPH mehtod. The first approach is *summation density* where SPH approximation is directly applied to density itself. Following such approach, density ρ for a particle i can be written in the form of

$$\rho_i = \sum_{j=1}^{N} m_j W_{ij} \tag{B.43}$$

where N number of particles reside in the support domain of i, m_j is the mass associate with particle j and W_{ij} is the smoothing function of particle i evaluated at particle j which has an unit of inverse of volume. So this equation states that the density of a particle is approximated by averaging the densities of the particles in the support domain.

There is another approach for approximating the density which is called *continuity density* approach. If SPH approximation is applied to only to the velocity divergence part in the continuity equation (B.39), it becomes

$$\frac{D\rho_i}{Dt} = -\rho_i \sum_{j=1}^{N} \frac{m_j}{\rho j} \mathbf{v}_j^{\beta} \cdot \frac{\partial W_{ij}}{\partial \mathbf{b}_i^{\beta}} \tag{B.44}$$

Density can also be approximated using continuity density by applying the following identity to place the density term inside the gradient operator

$$-\rho \frac{\partial \mathbf{v}^{\beta}}{\partial \mathbf{x}^{\beta}} = -\Big(\frac{\partial(\rho \mathbf{v}^{\beta})}{\partial \mathbf{x}^{\beta}} - \mathbf{v}^{\beta} \cdot \frac{\partial \rho}{\partial \mathbf{x}^{\beta}}\Big) \tag{B.45}$$

If the SPH approximation is only applied at every gradient and to the velocity at the second term in the right hand side of the Equation B.46, the continuity density equation becomes

$$\frac{D\rho_i}{Dt} = \sum_{j=1}^{N} m_j \mathbf{v}_{ij}^{\beta} \cdot \frac{\partial W_{ij}}{\partial \mathbf{x}_i^{\beta}} \tag{B.46}$$

where $\mathbf{v}_{ij}^{\beta} = \left(\mathbf{v}_i^{\beta} - \mathbf{v}_j^{\beta}\right)$ which introduces velocity difference into the discrete particle approximation. Equation B.46 shows that the time rate of density

change of particle is dependent on relative velocity between the particle and the other particles in the support domain weighted by the gradient of the smoothing function.

There are comparative advantages and disadvantages of both approach which depended on the application. General fluid continuity problems without discontinuities like shock-waves can be simulated with the simulation density approach. On other hand for simulating phenomena with strong discontinuity e.g. explosion, high velocity impact, the continuity density approach produces better results.

B.11 Particle approximation of momentum

Momentum can be approximated using SPH formulation like density was in the last section. This approximation is achieved by directly applying SPH particle approximation concepts to the gradients of the momentum equation (Equation B.40).

$$\frac{D\mathbf{v}_i^\alpha}{Dt} = \frac{1}{\rho_i}\sum_{j=1}^{N} m_j \frac{\sigma_j^{\alpha\beta}}{\rho_j}\frac{\partial W_{ij}}{\partial \mathbf{x}_i^\beta} \tag{B.47}$$

By defining different identities different formulations for approximating momentum can be achieved which over various advantages for simulating different type of problems. One frequently used formulation of momentum defines the following identity

$$\sum_{j=1}^{N} m_j \frac{\sigma_i^{\alpha\beta}}{\rho_i\rho_j}\frac{\partial W_{ij}}{\partial \mathbf{x}_i^\beta} = \frac{\sigma_i^{\alpha\beta}}{\rho_i}\left(\sum_{j=1}^{N}\frac{m_j}{\rho_j}\frac{\partial W_{ij}}{\partial \mathbf{x}_i^\beta}\right) \tag{B.48}$$

which yields

$$\frac{D\mathbf{v}_i^\alpha}{Dt} = \sum_{j=1}^{N} m_j \frac{\sigma_i^{\alpha\beta}+\sigma_j^{\alpha\beta}}{\rho_i\rho_j}\frac{\partial W_{ij}}{\partial \mathbf{x}_i^j} \tag{B.49}$$

The above formulation takes advantage of the summation representation which in term reduces error arising from the particle inconsistency problem (Chapter 3 of [115]).

B.12 Particle approximation of energy

For Newtonian fluids the viscous shear stress τ is proportional to the shear strain ε with dynamic viscosity μ.

$$\tau^{\alpha\beta} = \mu\varepsilon^{\alpha\beta} \tag{B.50}$$

where

$$\varepsilon^{\alpha\beta} = \frac{\partial \mathbf{v}^{\beta}}{\partial \mathbf{x}^{\alpha}} + \frac{\partial \mathbf{v}^{\alpha}}{\partial \mathbf{x}^{\beta}} - \frac{2}{3}(\nabla\cdot \mathbf{v})\delta^{\alpha\beta} \tag{B.51}$$

Separating isotropic pressure and the viscous stress in energy equation (Equation B.41), it becomes

$$\frac{De}{Dt} = -\frac{p}{\rho}\frac{\partial \mathbf{v}^{\beta}}{\partial \mathbf{x}^{\beta}} + \frac{\mu}{2\rho}\varepsilon^{\alpha\beta}\varepsilon^{\alpha\beta} \tag{B.52}$$

To evaluate the internal energy e in the above equation, the pressure work is derived following SPH formulations. The continuity density equation (Equation B.46) at particle i can be approximated as

$$-\frac{p}{\rho}\frac{\partial \mathbf{v}_i^{\beta}}{\partial \mathbf{x}_i^{\beta}} = \frac{p_i}{\rho_i^2}\sum_{j=1}^{N} m_j \mathbf{v}_{ij}^{\beta}\cdot \frac{\partial W_{ij}}{\partial \mathbf{x}_i^{\beta}} \tag{B.53}$$

Considering the following identity

$$-\frac{p}{\rho}\frac{\partial \mathbf{v}^{\beta}}{\partial \mathbf{x}^{\beta}} = -\frac{\partial}{\partial \mathbf{x}^{\beta}}\left(\frac{p\mathbf{v}^{\beta}}{\rho}\right) + \mathbf{v}^{\beta}\frac{\partial}{\partial \mathbf{x}^{\beta}}\left(\frac{p}{\rho}\right) \tag{B.54}$$

if considered for particle i, using SPH approximation the above identity becomes

$$-\frac{p}{\rho}\frac{\partial \mathbf{v}_i^{\beta}}{\partial \mathbf{x}_i^{\beta}} = \sum_{j=1}^{N} m_j \frac{p_j}{\rho_j^2}\mathbf{v}_{ij}^{\beta}\cdot \frac{\partial W_{ij}}{\partial \mathbf{x}_i^{\beta}} \tag{B.55}$$

summing Equation B.53 and B.55 yields

$$-\frac{p}{\rho}\frac{\partial \mathbf{v}_i^{\beta}}{\partial \mathbf{x}_i^{\beta}} = \frac{1}{2}\sum_{j=1}^{N} m_j \left(\frac{p_i}{\rho_i^2} + \frac{p_j}{\rho_j^2}\right)\mathbf{v}_{ij}^{\beta}\cdot \frac{\partial W_{ij}}{\partial \mathbf{x}_i^{\beta}} \tag{B.56}$$

So the SPH formulation for internal energy evaluation (Equation B.52) for a particle i with N number of particles in its support domain becomes

$$\frac{De_i}{Dt} = \frac{1}{2}\sum_{j=1}^{N} m_j \left(\frac{p_i}{\rho_i^2} + \frac{p_j}{\rho_j^2}\right)\mathbf{v}_{ij}^{\beta}\frac{\partial W_{ij}}{\partial \mathbf{x}_i^{\beta}} + \frac{\mu_i}{2\rho_i}\varepsilon_i^{\alpha\beta}\varepsilon_i^{\alpha\beta} \tag{B.57}$$

Bibliography

[1] K. Matsuo and J. B. Palmer, "Anatomy and physiology of feeding and swallowing: normal and abnormal," *Physical medicine and rehabilitation clinics of North America*, vol. 19, no. 4, pp. 691–707, 2008. → page 1

[2] B. Bloem, A. Lagaay, W. Van Beek, J. Haan, R. Roos, and A. Wintzen, "Prevalence of subjective dysphagia in community residents aged over 87." *Bmj*, vol. 300, no. 6726, pp. 721–722, 1990. → page 1, 2

[3] S. Lindgren and L. Janzon, "Prevalence of swallowing complaints and clinical findings among 50–79-year-old men and women in an urban population," *Dysphagia*, vol. 6, no. 4, pp. 187–192, 1991. → page 1, 2

[4] G. Pugliese and D. A. Lichtenberg, "Nosocomial bacterial pneumonia: an overview," *American journal of infection control*, vol. 15, no. 6, pp. 249–265, 1987. → page 1

[5] C. S. Bryan and K. L. Reynolds, "Bacteremic nosocomial pneumonia: Analysis of 172 episodes from a single metropolitan area 1, 2," *American Review of Respiratory Disease*, vol. 129, no. 5, pp. 668–671, 1984. → page 1

[6] R. Wenzel, "Hospital-acquired pneumonia: overview of the current state of the art for prevention and control," *European Journal of Clinical Microbiology and Infectious Diseases*, vol. 8, no. 1, pp. 56–60, 1989. → page 1

[7] T. J. Marrie, H. Durant, and C. Kwan, "Nursing home-acquired pneumonia: A case-control study," *Journal of the American Geriatrics Society*, vol. 34, no. 10, pp. 697–702, 1986. → page 1

[8] O. Ekberg, S. Hamdy, V. Woisard, A. Wuttge-Hannig, and P. Ortega, "Social and psychological burden of dysphagia: its impact on diagnosis

and treatment," *Dysphagia*, vol. 17, no. 2, pp. 139–146, 2002. → page 1

[9] J. Penman and M. Thomson, "A review of the textured diets developed for the management of dysphagia," *Journal of Human Nutrition and Dietetics*, vol. 11, no. 1, pp. 51–60, 1998. → page 2

[10] Y. Noh, M. Segawa, K. Sato, C. Wang, H. Ishii, J. Solis, A. Takanishi, A. Katsumata, and Y. Iida, "Development of a robot which can simulate swallowing of food boluses with various properties for the study of rehabilitation of swallowing disorders," in *Robotics and automation (ICRA), 2011 IEEE international conference on*. IEEE, 2011, pp. 4676–4681. → page 3, 30

[11] J. Remmers, E. Sauerland, A. Anch *et al.*, "Pathogenesis of upper airway occlusion during sleep," *Journal of Applied Physiology*, vol. 44, no. 6, pp. 931–938, 1978. → page 3

[12] D. Friberg, T. Ansved, K. Borg, B. Carlsson-Nordlander, H. LARSSON, and E. Svanborg, "Histological indications of a progressive snorers disease in an upper airway muscle," *American journal of respiratory and critical care medicine*, vol. 157, no. 2, pp. 586–593, 1998. → page 3

[13] R. JOHN KIMOFF, E. Sforza, V. Champagne, L. Ofiara, and D. Gendron, "Upper airway sensation in snoring and obstructive sleep apnea," *American journal of respiratory and critical care medicine*, vol. 164, no. 2, pp. 250–255, 2001. → page 3

[14] D. Friberg, B. Gazelius, T. Hökfelt, and B. Nordlander, "Abnormal afferent nerve endings in the soft palatal mucosa of sleep apnoics and habitual snorers," *Regulatory peptides*, vol. 71, no. 1, pp. 29–36, 1997. → page 3

[15] "Omnibus survey: caseloads for speech-language pathologists, american speech-language-hearing association and others," rockville, MD: ASHA, 2000. → page 4

[16] T. M. Kidder, S. E. Langmore, and B. J. Martin, "Indications and techniques of endoscopy in evaluation of cervical dysphagia: comparison

with radiographic techniques," *Dysphagia*, vol. 9, no. 4, pp. 256–261, 1994. → page 4

[17] B. Martin-Harris, M. B. Brodsky, Y. Michel, D. O. Castell, M. Schleicher, J. Sandidge, R. Maxwell, and J. Blair, "MBS measurement tool for swallow impairment–MBSImP: establishing a standard," *Dysphagia*, vol. 23, no. 4, pp. 392–405, 2008. → page 4, 15, 23, 31

[18] J. A. Logemann and J. A. Logemann, "Evaluation and treatment of swallowing disorders," 1983. → page 5, 72

[19] B. Martin-Harris, Y. Michel, and D. O. Castell, "Physiologic model of oropharyngeal swallowing revisited," *Otolaryngology-Head and Neck Surgery*, vol. 133, no. 2, pp. 234–240, 2005. → page 5

[20] I. J. Cook, W. J. Dodds, R. O. Dantas, M. K. Kern, B. T. Massey, R. Shaker, and W. J. Hogan, "Timing of videofluoroscopic, manometric events, and bolus transit during the oral and pharyngeal phases of swallowing," *Dysphagia*, vol. 4, no. 1, pp. 8–15, 1989. → page 5

[21] F. McConnel, D. Cerenko, and M. Mendelsohn, "Manofluorographic analysis of swallowing." *Otolaryngologic Clinics of North America*, vol. 21, no. 4, pp. 625–635, 1988. → page 5

[22] R. Olsson, J. Castell, D. Castell, and O. Ekberg, "Solid-state computerized manometry improves diagnostic yield in pharyngeal dysphagia: simultaneous videoradiography and manometry in dysphagia patients with normal barium swallows," *Abdominal imaging*, vol. 20, no. 3, pp. 230–235, 1995. → page 5

[23] W. J. Dodds, "The physiology of swallowing," *Dysphagia*, vol. 3, no. 4, pp. 171–178, 1989. → page 6

[24] S. M. Shaw and R. Martino, "The normal swallow: muscular and neurophysiological control," *Otolaryngologic clinics of North America*, vol. 46, no. 6, pp. 937–956, 2013. → page 8

[25] E. R. Blonsky, J. A. Logemann, B. Boshes, and H. B. Fisher, "Comparison of speech and swallowing function in patients with tremor disorders and in normal geriatric patients: a cinefluorographic study," *Journal of Gerontology*, vol. 30, no. 3, pp. 299–303, 1975. → page 8, 10

[26] ""hyoglossus" by image:gray1019.png modiefied by uwe gille via wikimedia commons," https://commons.wikimedia.org/wiki/File:Hyoglossus.png#/media/File:Hyoglossus.pngviaWikimediaCommons, accessed: 2015-07-14. → page 8

[27] ""mouth illustration–otis archives" by duncan kenneth winter via wikimedia commons," https://commons.wikimedia.org/wiki/File:Mouth_illustration-Otis_Archives.jpg#/media/File:Mouth_illustration-Otis_Archives.jpg, accessed: 2015-07-14. → page 8

[28] W. Pommerenke, "A study of the sensory areas eliciting the swallowing reflex," *American Journal of Physiology–Legacy Content*, vol. 84, no. 1, pp. 36–41, 1928. → page 9

[29] J. Robbins, G. Gensler, J. Hind, J. Logemann, A. Lindblad, D. Brandt, H. Baum, D. Lilienfeld, S. Kosek, D. Lundy *et al.*, "Can thickened liquids or chin-down posture prevent aspiration?" 2008. → page 9

[30] J. A. Logemann, B. R. Pauloski, L. Colangelo, C. Lazarus, M. Fujiu, and P. J. Kahrilas, "Effects of a sour bolus on oropharyngeal swallowing measures in patients with neurogenic dysphagia," *Journal of Speech, Language, and Hearing Research*, vol. 38, no. 3, pp. 556–563, 1995. → page 9

[31] B. Martin-Harris, M. B. Brodsky, Y. Michel, F.-S. Lee, and B. Walters, "Delayed initiation of the pharyngeal swallow: normal variability in adult swallows," *Journal of Speech, Language, and Hearing Research*, vol. 50, no. 3, pp. 585–594, 2007. → page 9

[32] W. J. Dodds, E. T. Stewart, and J. A. Logemann, "Physiology and radiology of the normal oral and pharyngeal phases of swallowing." *AJR. American journal of roentgenology*, vol. 154, no. 5, pp. 953–963, 1990. → page 9, 10

[33] F. Mcconnel, "Analysis of pressure generation and bolus transit during pharyngeal swallowing," *The Laryngoscope*, vol. 98, no. 1, pp. 71–78, 1988. → page 10

[34] W. G. Pearson Jr, S. E. Langmore, B. Y. Louis, and A. C. Zumwalt, "Structural analysis of muscles elevating the hyolaryngeal complex," *Dysphagia*, vol. 27, no. 4, pp. 445–451, 2012. → page 10

[35] "Human physiology: Digestion," https://humanphysiology2011.wikispaces.com/13.+Digestion, accessed: 2015-07-14. → page 11

[36] T. J. Humphries and D. O. Castell, "Pressure profile of esophageal peristalsis in normal humans as measured by direct intraesophageal transducers," *The American journal of digestive diseases*, vol. 22, no. 7, pp. 641–645, 1977. → page 11

[37] R. K. Goyal and B. W. Cobb, "Motility of the pharynx, esophagus and esophageal sphincters," *Physiology of the gastrointestinal tract*, vol. 1, pp. 359–391, 1981. → page 11

[38] N. De Vincentis, R. Lenti, C. Pona, A. Lococo, R. Crisci, G. Coloni, I. Flutsch, and G. Mariani, "Scintigraphic evaluation of the esophageal transit time for the noninvasive assessment of esophageal motor disorders," *J Nucl Med Allied Sci*, vol. 28, pp. 137–142, 1984. → page 12

[39] B. Martin, J. Logemann, R. Shaker, and W. Dodds, "Coordination between respiration and swallowing: respiratory phase relationships and temporal integration," *Journal of Applied Physiology*, vol. 76, no. 2, pp. 714–723, 1994. → page 12

[40] M. S. Klahn and A. L. Perlman, "Temporal and durational patterns associating respiration and swallowing," *Dysphagia*, vol. 14, no. 3, pp. 131–138, 1999. → page 12

[41] S. Jafari, R. A. Prince, D. Y. Kim, and D. Paydarfar, "Sensory regulation of swallowing and airway protection: a role for the internal superior laryngeal nerve in humans," *The Journal of physiology*, vol. 550, no. 1, pp. 287–304, 2003. → page 12

[42] N. R. BLEACH, "The gag reflex and aspiration: a retrospective analysis of 120 patients assessed by videofluoroscopy," *Clinical Otolaryngology & Allied Sciences*, vol. 18, no. 4, pp. 303–307, 1993. → page 12

[43] G. Mann and G. J. Hankey, "Initial clinical and demographic predictors of swallowing impairment following acute stroke," *Dysphagia*, vol. 16, no. 3, pp. 208–215, 2001. → page 13

[44] A. R. Maccarini, A. Filippini, D. Padovani, M. Limarzi, M. Loffredo, and D. Casolino, "Clinical non-instrumental evaluation of dysphagia," *Acta otorhinolaryngologica italica*, vol. 27, pp. 299–305, 2007. → page 14

[45] P. Linden and A. Siebens, "Dysphagia: predicting laryngeal penetration." *Archives of Physical Medicine and Rehabilitation*, vol. 64, no. 6, pp. 281–284, 1983. → page 14

[46] "Fluoroscope," https://commons.wikimedia.org/wiki/File:Fluoroscope.jpg#/media/File:Fluoroscope.jpg, accessed: 2015-07-14. → page 14

[47] J. B. Palmer, K. V. Kuhlemeier, D. C. Tippett, and C. Lynch, "A protocol for the videofluorographic swallowing study," *Dysphagia*, vol. 8, no. 3, pp. 209–214, 1993. → page 15, 21

[48] K. Kuhlemeier, P. Yates, and J. Palmer, "Intra-and interrater variation in the evaluation of videofluorographic swallowing studies," *Dysphagia*, vol. 13, no. 3, pp. 142–147, 1998. → page 15, 21

[49] B. Martin-Harris, J. A. Logemann, S. McMahon, M. Schleicher, and J. Sandidge, "Clinical utility of the modified barium swallow," *Dysphagia*, vol. 15, no. 3, pp. 136–141, 2000. → page 16

[50] G. Ramsey, J. Watson, R. Gramiak, and S. Weinberg, "Cinefluorographic analysis of the mechanism of swallowing 1," *Radiology*, vol. 64, no. 4, pp. 498–518, 1955. → page 16

[51] O. Ekberg and S. V. Sigurjónsson, "Movement of the epiglottis during deglutition," *Gastrointestinal radiology*, vol. 7, no. 1, pp. 101–107, 1982. → page 16

[52] "Fiberoptic Endoscopic Evaluation of Swallowing (FEES): Evaluate the pharyneageal stage of swallowing and diagnose dysphagia." http://www.videostroboscopy.com/flexible_scope.html, accessed: 2015-07-14. → page 17

[53] S. E. Langmore, S. M. Kenneth, and N. Olsen, "Fiberoptic endoscopic examination of swallowing safety: a new procedure," *Dysphagia*, vol. 2, no. 4, pp. 216–219, 1988. → page 16

[54] "View of the glottis as seen during laryngoscopy." https://commons.wikimedia.org/wiki/File:Larynx_endo_2.jpg, accessed: 2015-07-14. → page 18

[55] "Anatomical parts seen during laryngoscopy by alan hoofring." → page 18

[56] S. E. Langmore, "Endoscopic evaluation of oral and pharyngeal phases of swallowing," *GI Motility online*, 2006. → page 18

[57] ""achalasia ems" by jc petit," https://en.wikipedia.org/wiki/File:Achalasia_EMS.jpg#/media/File:Achalasia_EMS.jpg, accessed: 2015-07-14. → page 19

[58] J. E. Pandolfino and P. J. Kahrilas, "Aga technical review on the clinical use of esophageal manometry," *Gastroenterology*, vol. 128, no. 1, pp. 209–224, 2005. → page 19

[59] "Ultrasound images of the tongue nevit dilmen," https://upload.wikimedia.org/wikipedia/commons/e/ee/Ultrasound_Scan_ND_110201103913_1047580.jpg, accessed: 2015-07-14. → page 20

[60] T. H. Shawker, B. Sonies, M. Stone, and B. J. Baum, "Real-time ultrasound visualization of tongue movement during swallowing," *Journal of Clinical Ultrasound*, vol. 11, no. 9, pp. 485–490, 1983. → page 20

[61] T. H. Shawker, B. C. Sonies, and M. Stone, "Soft tissue anatomy of the tongue and floor of the mouth: an ultrasound demonstration," *Brain and language*, vol. 21, no. 2, pp. 335–350, 1984. → page 20

[62] T. Shawker, B. Sonies, and M. Stone, "Sonography of speech and swallowing," *Ultrasound annual*, pp. 237–260, 1984. → page 21

[63] J. Benson and D. Tuchman, "Other diagnostic tests used for evaluation of swallowing disorders," *Disorders of Feeding and Swallowing in Infants and Children: Pathophysiology, Diagnosis and Treatment (1st edn). San Diego: Singular*, pp. 201–9, 1994. → page 21

[64] B. C. Sonies, G. Chi-Fishman, and J. L. Miller, "Ultrasound imaging and swallowing," in *Normal and Abnormal Swallowing*. Springer, 2003, pp. 119–138. → page 21

[65] J. A. Cichero and B. E. Murdoch, *Dysphagia: foundation, theory and practice*. John Wiley & Sons, 2006. → page 21

[66] F. E. Ardakani, "Evaluation of swallowing patterns of the tongue using real-time b-mode sonography," *J Contemp Dent Pract*, vol. 7, no. 3, pp. 67–74, 2006. → page 21

[67] W. Chih-Hsiu, H. Tzu-Yu, C. Jiann-Chyuan, C. Yeun-Chung, and L. Shiann-Yann, "Evaluation of swallowing safety with fiberoptic endoscope: comparison with videofluoroscopic technique," *The Laryngoscope*, vol. 107, no. 3, pp. 396–401, 1997. → page 21, 22

[68] M. Sitton, J. Arvedson, A. Visotcky, N. Braun, J. Kerschner, S. Tarima, and D. Brown, "Fiberoptic endoscopic evaluation of swallowing in children: feeding outcomes related to diagnostic groups and endoscopic findings," *International journal of pediatric otorhinolaryngology*, vol. 75, no. 8, pp. 1024–1031, 2011. → page 21, 22

[69] S. Périé, L. Laccourreye, A. Flahault, V. Hazebroucq, S. Chaussade, and J. L. S. Guily, "Role of videoendoscopy in assessment of pharyngeal function in oropharyngeal dysphagia: comparison with videofluoroscopy and manometry," *The Laryngoscope*, vol. 108, no. 11, pp. 1712–1716, 1998. → page 21, 22

[70] J. A. Logemann, A. W. Rademaker, B. R. Pauloski, Y. Ohmae, and P. J. Kahrilas, "Normal swallowing physiology as viewed by videofluoroscopy and videoendoscopy," *Folia phoniatrica et logopaedica*, vol. 50, no. 6, pp. 311–319, 1998. → page 21, 22

[71] "Translating research into practice (TRIP)-II. fact sheet. agency for health quality research." → page 22

[72] B. Martin-Harris and B. Jones, "The videofluorographic swallowing study," *Physical medicine and rehabilitation clinics of North America*, vol. 19, no. 4, pp. 769–785, 2008. → page 22, 23

[73] G. J. Bours, R. Speyer, J. Lemmens, M. Limburg, and R. De Wit, "Bedside screening tests vs. videofluoroscopy or fibreoptic endoscopic evaluation of swallowing to detect dysphagia in patients with neurological disorders: systematic review," *Journal of advanced nursing*, vol. 65, no. 3, pp. 477–493, 2009. → page 22

[74] L. Perry and C. P. Love, "Screening for dysphagia and aspiration in acute stroke: a systematic review," *Dysphagia*, vol. 16, no. 1, pp. 7–18, 2001. → page 22

[75] R. Martino, G. Pron, and N. Diamant, "Screening for oropharyngeal dysphagia in stroke: insufficient evidence for guidelines," *Dysphagia*, vol. 15, no. 1, pp. 19–30, 2000. → page 22

[76] "Modified barium swallow impairment profile. northern speech services." https://www.mbsimp.com/, accessed: 2015-07-14. → page 23, 24, 31, 77

[77] J. Cooper and V. Taqueti, "A brief history of the development of mannequin simulators for clinical education and training," *Quality and Safety in Health Care*, vol. 13, no. suppl 1, pp. i11–i18, 2004. → page 29

[78] "Resusci Anne via Wikimedia Commons," https://commons.wikimedia.org/wiki/File:Resusci_Anne.jpg, accessed: 2015-09-22. → page 29

[79] "The newer version of "harvey" mannequin along with it's base via wikimedia commons," https://commons.wikimedia.org/wiki/File:Harvey_new.jpg, accessed: 2015-09-22. → page 29

[80] A. Grenvik and J. Schaefer, "From resusci-anne to sim-man: the evolution of simulators in medicine," *Critical care medicine*, vol. 32, no. 2, pp. S56–S57, 2004. → page 29, 30

[81] M. S. Gordon, "Cardiology patient simulator: development of an animated manikin to teach cardiovascular disease," *The American journal of cardiology*, vol. 34, no. 3, pp. 350–355, 1974. → page 30

[82] D. Gillies and C. Williams, "An interactive graphic simulator for the teaching of fibrendoscopic techniques," in *Eurographics*, vol. 1987, 1987, pp. 127–138. → page 30

[83] B. Bray, C. R. Schwartz, D. L. Weeks, and S. Kardong-Edgren, "Human patient simulation technology: perceptions from a multidisciplinary sample of health care educators," *Clinical Simulation in Nursing*, vol. 5, no. 4, pp. e145–e150, 2009. → page 30

[84] E. M. Benadom and N. L. Potter, "The use of simulation in training graduate students to perform transnasal endoscopy," *Dysphagia*, vol. 26, no. 4, pp. 352–360, 2011. → page 30

[85] S. Lin, J. Chen, P. Hertz, and P. J. Kahrilas, "Dynamic reconstruction of the orophanryngeal swallow using computer based animation," *Computerized medical imaging and graphics*, vol. 20, no. 2, pp. 69–75, 1996. → page 31

[86] I. Scholten and A. Russell, "Learning about the dynamic swallowing process using an interactive multimedia program," *Dysphagia*, vol. 15, no. 1, pp. 10–16, 2000. → page 31

[87] "Oculus Rift via Wikimedia Commons," https://en.wikipedia.org/wiki/Oculus_Rift, accessed: 2015-07-14. → page 32

[88] "A screenshot from the 3DiTeams game, player is percussing chest Source: Duke University Human Simulation and Patient Safety Center via Wikimedia Commons," https://commons.wikimedia.org/wiki/File:3DiTeams_percuss_chest.JPG, accessed: 2015-07-14. → page 32

[89] "Oculus Rift," https://www.oculus.com/en-us/, accessed: 2015-07-14. → page 33

[90] "Sony's Project Morpheus," https://www.playstation.com/en-gb/explore/ps4/features/project-morpheus/, accessed: 2015-07-14. → page 33

[91] "Flexible endoscopy training with the Simbionix GI Mentor™," http://surgery.uthscsa.edu/jcsi/images/gimentor.jpg, accessed: 2015-07-14. → page 33

[92] C. Williams, J. Baillie, D. Gillies, D. Borislow, and P. Cotton, "Teaching gastrointestinal endoscopy by computer simulation: a prototype for colonoscopy and ercp," *Gastrointestinal endoscopy*, vol. 36, no. 1, pp. 49–54, 1990. → page 34

[93] F. H. Harlow, J. E. Welch *et al.*, "Numerical calculation of time-dependent viscous incompressible flow of fluid with free surface," *Physics of fluids*, vol. 8, no. 12, p. 2182, 1965. → page 35

[94] O. C. Zienkiewicz and R. L. Taylor, *The finite element method: Solid mechanics*. Butterworth-heinemann, 2000, vol. 2. → page 36

[95] J. D. Anderson and J. Wendt, *Computational fluid dynamics*. Springer, 1995, vol. 206. → page 36, 66

[96] H. U. Mair, "Review: hydrocodes for structural response to underwater explosions," *Shock and Vibration*, vol. 6, no. 2, pp. 81–96, 1999. → page 37

[97] D. J. Benson, "Computational methods in lagrangian and eulerian hydrocodes," *Computer methods in Applied mechanics and Engineering*, vol. 99, no. 2, pp. 235–394, 1992. → page 37, 38

[98] C. Hirt, A. A. Amsden, and J. Cook, "An arbitrary lagrangian-eulerian computing method for all flow speeds," *Journal of Computational Physics*, vol. 14, no. 3, pp. 227–253, 1974. → page 37, 38

[99] J. O. Hallquist *et al.*, "Ls-dyna theory manual," *Livermore software Technology corporation*, vol. 3, 2006. → page 38

[100] G. Liu, K. Lam, and C. Lu, "Computational simulation of sympathetic explosion in a high performance magazine," in *Proc. of 3rd Weapon Effects Seminar, Singapore*, 1998, pp. 65–75. → page 38

[101] R. A. Gingold and J. J. Monaghan, "Smoothed particle hydrodynamics: theory and application to non-spherical stars," *Monthly notices of the royal astronomical society*, vol. 181, no. 3, pp. 375–389, 1977. → page 39, 110

[102] L. B. Lucy, "A numerical approach to the testing of the fission hypothesis," *The astronomical journal*, vol. 82, pp. 1013–1024, 1977. → page 39, 109

[103] J. Monaghan, "Smoothed particle hydrodynamics and its diverse applications," *Annual Review of Fluid Mechanics*, vol. 44, pp. 323–346, 2012. → page 39

[104] S. Li and W. K. Liu, "Meshfree and particle methods and their applications," *Applied Mechanics Reviews*, vol. 55, no. 1, pp. 1–34, 2002. → page 39

[105] M. Sonomura, H. Mizunuma, T. Numamori, H. Michiwaki, and K. Nishinari, "Numerical simulation of the swallowing of liquid bolus," *Journal of Texture Studies*, vol. 42, no. 3, pp. 203–211, 2011. → page 40

[106] S. J. Cummins and M. Rudman, "An sph projection method," *Journal of computational physics*, vol. 152, no. 2, pp. 584–607, 1999. → page 40

[107] J. Monaghan and R. Gingold, "Shock simulation by the particle method sph," *Journal of computational physics*, vol. 52, no. 2, pp. 374–389, 1983. → page 40, 64

[108] J. P. Morris, P. J. Fox, and Y. Zhu, "Modeling low reynolds number incompressible flows using sph," *Journal of computational physics*, vol. 136, no. 1, pp. 214–226, 1997. → page 40, 65, 66, 67

[109] G. Hopkin, "Neonatal and adult tongue dimensions," *The Angle orthodontist*, vol. 37, no. 2, pp. 132–133, 1967. → page 47, 48

[110] J. E. Lloyd, I. Stavness, and S. Fels, "Artisynth: a fast interactive biomechanical modeling toolkit combining multibody and finite element simulation," in *Soft tissue biomechanical modeling for computer assisted surgery*. Springer, 2012, pp. 355–394. → page 49, 59, 70

[111] "National dysphagia diet: Standardization for optimal care." *National Dysphagia Task Force. American Dietetic Association.*, 2002. → page 57, 72

[112] I. Stavness, C. A. Sánchez, J. Lloyd, A. Ho, J. Wang, S. Fels, and D. Huang, "Unified skinning of rigid and deformable models for anatomical simulations," in *SIGGRAPH Asia 2014 Technical Briefs*. ACM, 2014, p. 9. → page 60

[113] L. Kavan, S. Collins, J. Žára, and C. O'Sullivan, "Geometric skinning with approximate dual quaternion blending," *ACM Transactions on Graphics (TOG)*, vol. 27, no. 4, p. 105, 2008. → page 61

[114] J. VonNeumann and R. D. Richtmyer, "A method for the numerical calculation of hydrodynamic shocks," *Journal of applied physics*, vol. 21, no. 3, pp. 232–237, 1950. → page 63

[115] G.-R. Liu and M. B. Liu, *Smoothed particle hydrodynamics: a meshfree particle method*. World Scientific, 2003. → page 64, 68, 69, 101, 102, 104, 106, 110, 116

[116] J. J. Monaghan, "Simulating free surface flows with sph," *Journal of computational physics*, vol. 110, no. 2, pp. 399–406, 1994. → page 65, 66, 67

[117] M. Ferrand, D. Laurence, B. Rogers, D. Violeau, and C. Kassiotis, "Unified semi-analytical wall boundary conditions for inviscid, laminar or turbulent flows in the meshless sph method," *International Journal for Numerical Methods in Fluids*, vol. 71, no. 4, pp. 446–472, 2013. → page 70

[118] A. K. Ho, L. Tsou, S. Green, and S. Fels, "A 3d swallowing simulation using smoothed particle hydrodynamics," *Computer Methods in Biomechanics and Biomedical Engineering: Imaging & Visualization*, vol. 2, no. 4, pp. 237–244, 2014. → page 70

[119] E. M. Bisch, J. A. Logemann, A. W. Rademaker, P. J. Kahrilas, and C. L. Lazarus, "Pharyngeal effects of bolus volume, viscosity, and temperature in patients with dysphagia resulting from neurologic impairment and in normal subjects," *Journal of Speech, Language, and Hearing Research*, vol. 37, no. 5, pp. 1041–1049, 1994. → page 72

[120] P. J. Kahrilas, S. Lin, J. Chen, and J. A. Logemann, "Oropharyngeal accommodation to swallow volume," *Gastroenterology*, vol. 111, no. 2, pp. 297–306, 1996. → page 72

[121] R. Hazelwood, M. Farazi, K. Humphries, S. Fels, and B. Martin-Harris, "Standardized mbss assessment clinician training patterns," dysphagia Research Society (DRS), 2016 (Accpeted). → page 78

[122] R. Likert, "A technique for the measurement of attitudes." *Archives of psychology*, 1932. → page 85

[123] G.-R. Liu, *Meshfree methods: moving beyond the finite element method*. Taylor & Francis, 2009. → page 106

[124] J. J. Monaghan and J. C. Lattanzio, "A refined particle method for astrophysical problems," *Astronomy and astrophysics*, vol. 149, pp. 135–143, 1985. → page 110

[125] J. P. Morris, "A study of the stability properties of sph," *arXiv preprint astro-ph/9503124*, 1995. → page 110

[126] G. R. Johnson, R. A. Stryk, and S. R. Beissel, "Sph for high velocity impact computations," *Computer methods in applied mechanics and engineering*, vol. 139, no. 1, pp. 347–373, 1996. → page 110